ERUPTIVE VARIATIONS DURING THE EMPLACEMENT OF CERRO PINTO DOME COMPLEX, PUEBLA, MEXICO

by Brian William Zimmer

A Thesis

Submitted in Partial Fulfillment

Of the Requirements for the Degree of

Master of Science

In Geology

Northern Arizona University

May, 2007

Approved:

_____
Nancy R. Riggs, Ph.D., Chair

_____
Gerardo Carrasco-Nuñez Ph.D.

_____
Michael Ort Ph.D.

_____
Wendell Duffield Ph.D.

ABSTRACT

ERUPTIVE VARIATIONS DURING THE EMPLACEMENT OF CERRO PINTO DOME COMPLEX, PUEBLA, MEXICO

Brian William Zimmer

Cerro Pinto is a Pleistocene rhyolite dome complex located in the eastern Trans-Mexican Volcanic Belt. The complex is composed of four tuff rings and four domes that were emplaced in three distinct eruptive stages marked by changes in vent location and eruptive character. During Stage I, vent clearing produced a 1.5 km diameter tuff ring that was then followed by emplacement of two domes of approximately the same volume (~ .2 km^3). After a brief hiatus in activity, Stage II began with the explosive formation of a second tuff ring to the north of the original ring that was ~ 2.0 km in diameter. Subsequent Stage II eruptions produced two smaller tuff rings within the northern tuff ring as well as a small dome that was mostly destroyed by vulcanian eruptions. The final stage, Stage III, involved the emplacement of a final dome within the southern tuff ring.

Cerro Pinto's eruptive history includes sequences that follow simple rhyolite-dome models, in which a pyroclastic phase is followed immediately by effusive dome emplacement. Some aspects, however, such as the occurrence of explosive reactivation and explosive dome destruction, are not well documented in rhyolitic structures originating from small, isolated magma chambers. These events are more commonly associated with polygenetic structures, such as stratovolcanoes or calderas, in which new pulses of magma initiate reactivation. A comparison of major and trace element geochemistry with surrounding silicic centers suggests that Cerro Pinto was produced by a small, isolated magma chamber. The compositional variation of the erupted material at

Cerro Pinto is minimal, suggesting that there were no additional pulses of magma responsible for the complex behavior of the volcano.

The variations in eruptive nature seen at Cerro Pinto are related to both phreatomagmatic activity and the presence of an irregularly shaped magma chamber that was zoned with respect to volatiles. The rising magma encountered small amounts of ground or surface water that initiated the eruption, while the irregular shape of the chamber may have allowed for at least two separate accumulations of volatiles in the upper portions of the magma chamber. Isolated rhyolite domes are rare and are not currently viewed as prominent volcanic threats, but their ability to explosively reactivate and collapse must be taken into account when making hazard assessments.

ACKNOWLEDGEMENTS

Thanks go to…
Nancy Riggs – For guidance, patience, faith, and friendship.
Michael Ort – For advice, inspiration, critical thinking, and shop talk.
Wendell Duffield – For showing me how it's done and friendly, practical advice.
Gerardo Carrasco-Nuñez – For welcoming me in Mexico, XRF analyses, help with field interpretations and tons of logistical support (i.e. Finding a 97' Toyota Corolla radiator while I was stranded in Oriental).
Mike Ketterer – For help with the ICPMS analyses.
Friday Lunch Clubbe – For having a sense of humor and a healthy portion of sympathy.
My parents Chris and Larry Zimmer - For unwavering love and support.
And finally to Christyanne who has provided constant love and kindness as we walk this life together.

TABLE OF CONTENTS

LIST OF TABLES

LIST OF FIGURES

LIST OF PLATES

CHAPTER I

INTRODUCTION

Rhyolite domes have long been considered simple, monogenetic structures with only localized hazard implications. Most documented rhyolite domes follow a single, predictable evolutionary path that includes an initial pyroclastic phase followed by the effusive emplacement of dome lava (Swanson et al., 1989; Duffield et al., 1995). Recent work suggests that the evolution of isolated rhyolite domes can be more complex, involving reactivation, vent migration, sector collapse, and significant changes in eruptive style (Riggs and Carrasco-Nuñez, 2004). This divergence from traditional rhyolite dome growth has direct implications in the analysis of existent dome systems as well as for hazard assessments related to eruptions that produce rhyolite domes.

This study describes and interprets the emplacement sequence of Cerro Pinto, a rhyolite dome complex located in east-central Mexico. The dome complex is likely less than 70 ka in age, but is heavily dissected by erosional drainages, providing excellent exposures to study the differences between simple dome growth, as described above, and more complex dome growth. Cerro Pinto has the volume and chemistry of a simple dome, but eruptive styles more commonly associated with polygenetic structures. Compositional variations (e.g. dissolved H_2O, crystallinity, vesicularity, and chemistry) within ascending magmas greatly affect the style of eruptions (Sparks, 1997; Newhall and Melson, 1983).

At Cerro Pinto, products from various eruptive styles are well preserved and analyses of these deposits have allowed for the reconstruction of the entire emplacement sequence.

Location

Cerro Pinto dome complex is located in the eastern Trans-Mexican Volcanic Belt, approximately 150 km east of Mexico City in the state of Puebla (Fig. 1.1). The study area is approximately 35 km^2 and lies within the Serdán-Oriental intermontane basin. This basin is bordered by andesitic and dacitic stratovolcanoes to the east and west and by Los Humeros caldera to the north. The small village of Miravalles is located less than 5 km to the west of Cerro Pinto and the larger town of Oriental (pop. ~ 30,000) is 8 km to the northwest.

Regional Setting

Trans-Mexican Volcanic Belt

The Trans-Mexican Volcanic Belt is approximately 1000 km long, extending from the Pacific coast to the Gulf of Mexico, between the 19^{th} and 20^{th} north latitude parallels (Fig 1.1) and contains over 8000 volcanoes ranging from large stratovolcanoes and calderas to minor domes and cinder cones (Ferriz and Mahood, 1984). Volcanism in the region includes sub-alkaline, alkaline, and calc-alkaline rock suites with compositions ranging from basaltic to rhyolitic (Marquez et al., 1999a).

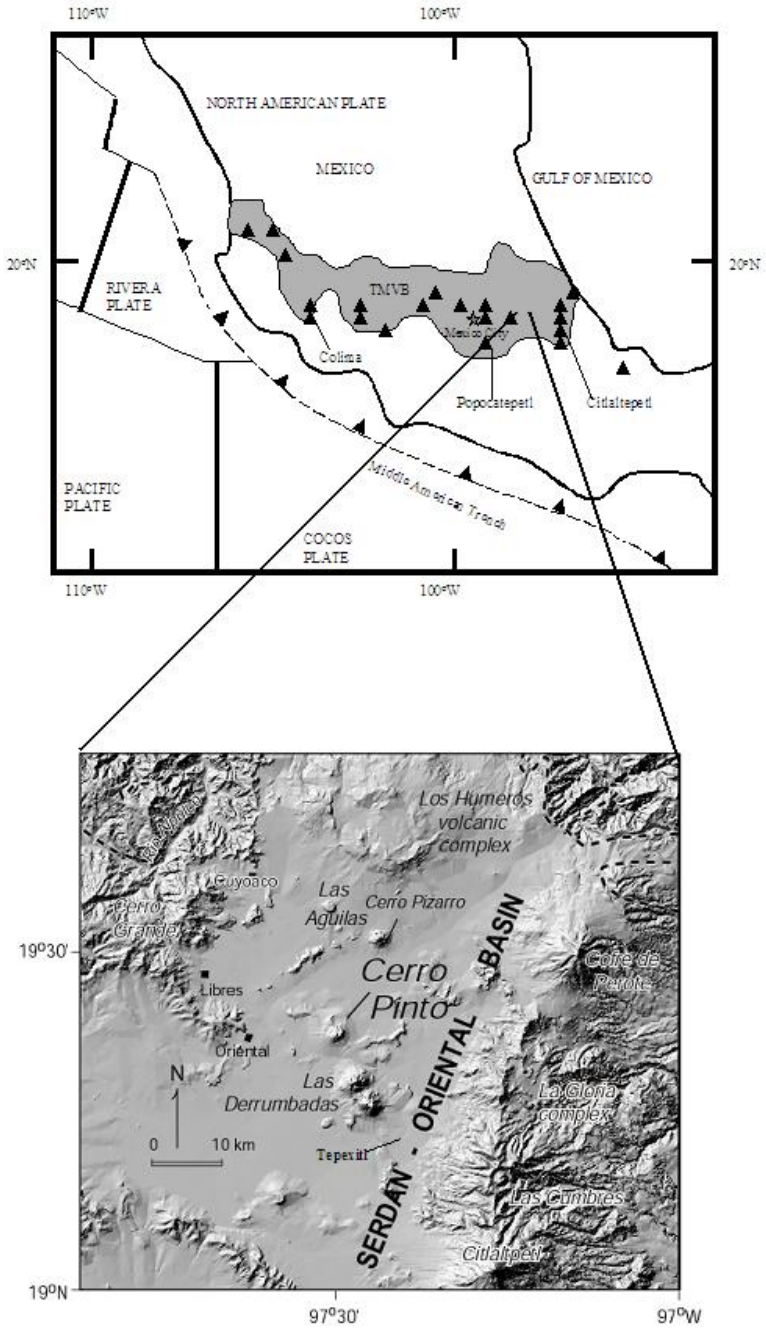

Figure 1.1. Location of Cerro Pinto and the Trans-Mexican Volcanic Belt in relation to the Cocos and Rivera plates. Note the increasing distance from the trench to the volcanic belt moving east (after Siebert and Carrasco-Nuñez, 2002, and Riggs and Carrasco-Nuñez, 2004).

Volcanism within the Trans-Mexican Volcanic Belt is related, at least in part, to the subduction of the Pacific Cocos and Rivera plates beneath the North American plate at the Middle American Trench, located approximately 50 km off Mexico's western coast (Fig. 1.1; Luhr, 1997). Unlike typical volcanic arcs, where the trench and arc are roughly parallel, the Middle American Trench is offset from the orientation of the volcanic front of the Trans-Mexican Volcanic Belt by 15-20 degrees (Maldonado-Sanchez and Schaff, 2005). Consequently, the distance from trench to volcanic front within the belt ranges from 150 to 400 km (Siebert and Carrasco-Nuñez, 2002). The average dip of the subducting plates is around 20 degrees, with a major hinge located 70 km inland from the trench. At this hinge, the subducting plates appear to level out until 270 km inland. There the plates begin dipping ~20 degrees again (Manea et al., 2005).

Many volcanoes within the belt, both polygenetic and monogenetic, are aligned N-S, generally younging to the south (Marquez et al., 2001). This trend in age, while certainly not universal, is prevalent and is driven by magma accumulation beneath the lower crust and migration along N-S-oriented rifts, based on a two-layer crustal-stretching model composed of a brittle and a ductile layer (Marquez et al., 2001; Fig 1.2). The finer details of how the subduction in the west and the extension in the east are correlated with volcanoes within the volcanic belt are strongly debated and include a pure subduction model (Maldonado-Sanchez and Schaaf, 2005), an unrooted mantle plume model (Marquez et al., 1999b; Verma, 1999), and a model suggesting that advection of the asthenosphere is produced by the subducting Cocos and Rivera plates (Wallace and Carmichael, 1999; Marquez and DeIgnacio, 2002**;** Siebe et al., 2004**;** Manea et al., 2005).

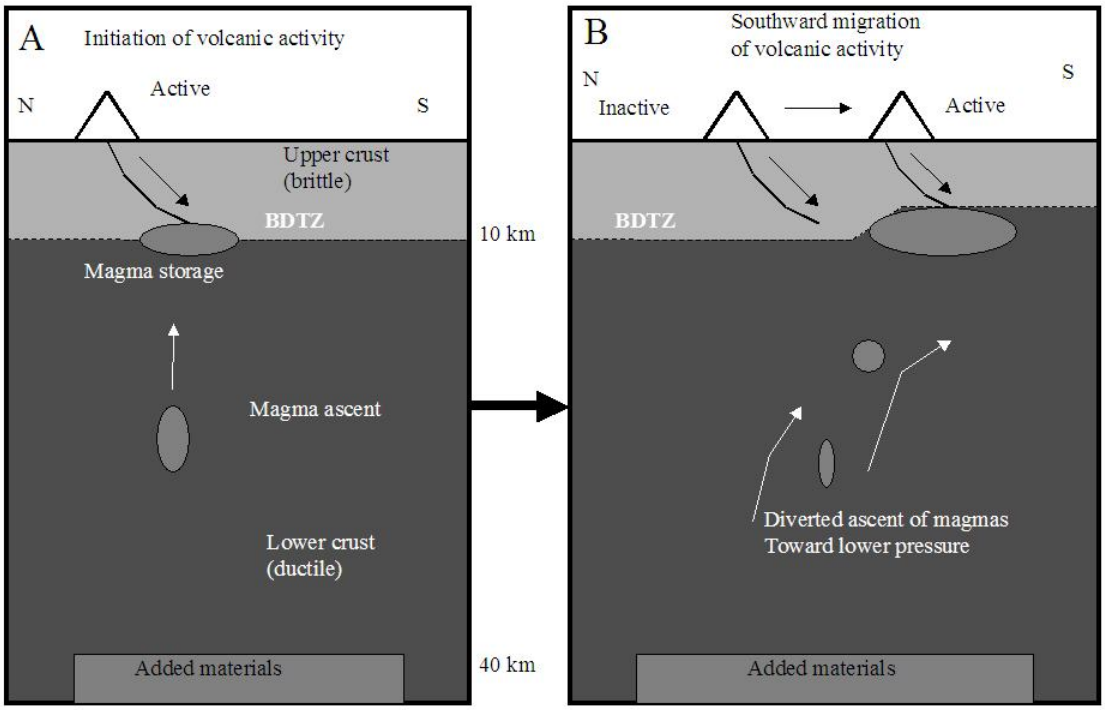

Figure 1.2. Idealized cross-sectional representation of the N-S trend of volcanism. From A to B there has been extension and shallowing of the brittle / ductile transition zone (BDTZ). Decoupling causes the southward diversion of magma which is then stored at the BDTZ. Magma can ascend along the normal faults giving rise to volcanic activity. (After Marquez et al., 2001)

Serdán-Oriental Basin

The Serdán-Oriental basin is located on the Mexican High Plain (Altiplano) in the eastern Trans-Mexican Volcanic Belt (Fig. 1.1). Stratovolcanoes and calderas that are Miocene to Holocene in age surround the 15,000 km^2 basin, while the interior is home to a number of Quaternary domes, tuff rings, calderas, and maars (Carrasco-Nuñez et al., 1997). Prominent rhyolitic volcanoes within the Serdán-Oriental basin include Cerro Pinto (the subject of this study), Cerro Pizarro, Las Derrumbadas, and Los Humeros caldera (Siebe et al., 1995). Small mafic volcanoes are also common in the Serdán-Oriental basin and

include isolated scoria and lava cones and maars (Riggs and Carrasco-Nuñez, 2004). Volcanism has been occurring in the eastern Mexican Volcanic Belt since at least Miocene time and volcanism tends to young to the south (Carrasco-Nuñez et al., 1997).

The Serdán-Oriental basin is a hydrologic basin that receives as much as 1000 mm of precipitation each year (McConnell, 2004). Surface water is generally scarce due to the prevalence of highly permeable volcanic rock deposits. However, the basin is home to two large saltpans and a number of young maar volcanoes that erupted into fluvial, lacustrine, or playa settings (e.g. Tepexitl maar), indicating that the region has had high-level aquifers over the past 100 ka. Groundwater is abundant today in the water-bearing Cretaceous limestone units that underlie much of the basin (McConnell, 2004).

Tectonic trends within the Serdán-Oriental basin are not uniform. The basin marks the contact between differing structural lineation trends. Folds and overthrusts in the bedrock in the region trend NW-SE, but younger volcanism associated with the emplacement of the Pico de Orizaba-Cofre de Perote range occurs along lineaments oriented NE-SW to N-S (Campos-Enríquez and Garduno Monroy, 1987).

Regional Basement Material

The regional basement is predominately Cretaceous limestone that was folded during the Laramide Orogeny and intruded by small plutons of granodiorite, monzonite, and syenite during Oligocene and Miocene times (Yañez and Garcia, 1982). The basement beneath

Cerro Pinto also includes Tertiary volcanic deposits, which include andesite, basaltic andesite, and basalt (Campos-Enríquez and Garduno-Monroy, 1987).

Cerro Pinto Dome Complex

Cerro Pinto is an isolated volcanic complex composed of four domes and four tuff rings. The dome complex covers approximately 35 km^2, with tephras covering more than 220 km^2 (Garcia-Banda, 1984). The four domes have a combined volume of approximately 0.5 km^3. Geochemical and petrologic analyses, discussed in Chapter V, show that Cerro Pinto is chemically uniform throughout the complex, but significant petrologic differences exist from one volcanic structure to the next. $^{40}Ar/^{39}Ar$ dating of sanidine from juvenile pumice fragments collected in the northern part of the complex (location NR5-1; Plate 1) has returned a date of 62 +/- 8 ka (Lisa Peters, personal communication, 2006; Appendix B).

Cerro Pinto is distinctly shaped, like the number 8, with two large adjacent tuff rings aligned north-south (Fig 1.3). The southern tuff ring encircles the three largest domes (Fig. 1.4) while the northern tuff ring encircles a smaller dome and two partial tuff rings (Fig. 1.5). Cerro Pinto is bordered to the northeast and southwest by Cretaceous limestone hills. In the ~ 60 ka since its emplacement, tephra deposits have been only partially cemented and are poorly consolidated in many locations. Consequently, Cerro Pinto is heavily dissected by steep-sided drainages that provide excellent exposures of tephra deposits.

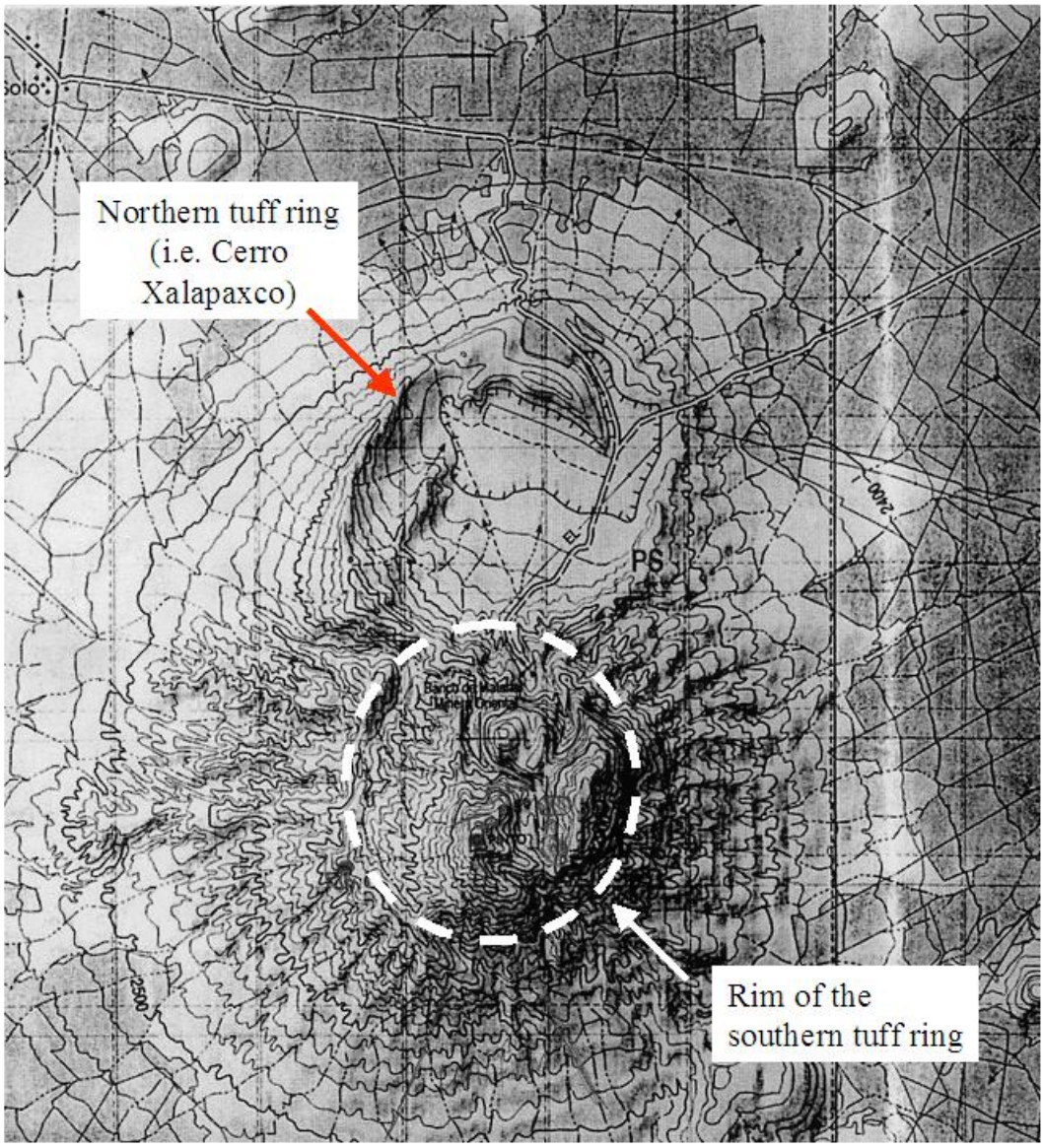

Figure 1.3. Shaded relief map of Cerro Pinto. Siebe and others (1995) identify the northern tuff ring as Cerro Xalapaxco. Contour interval is 20m.

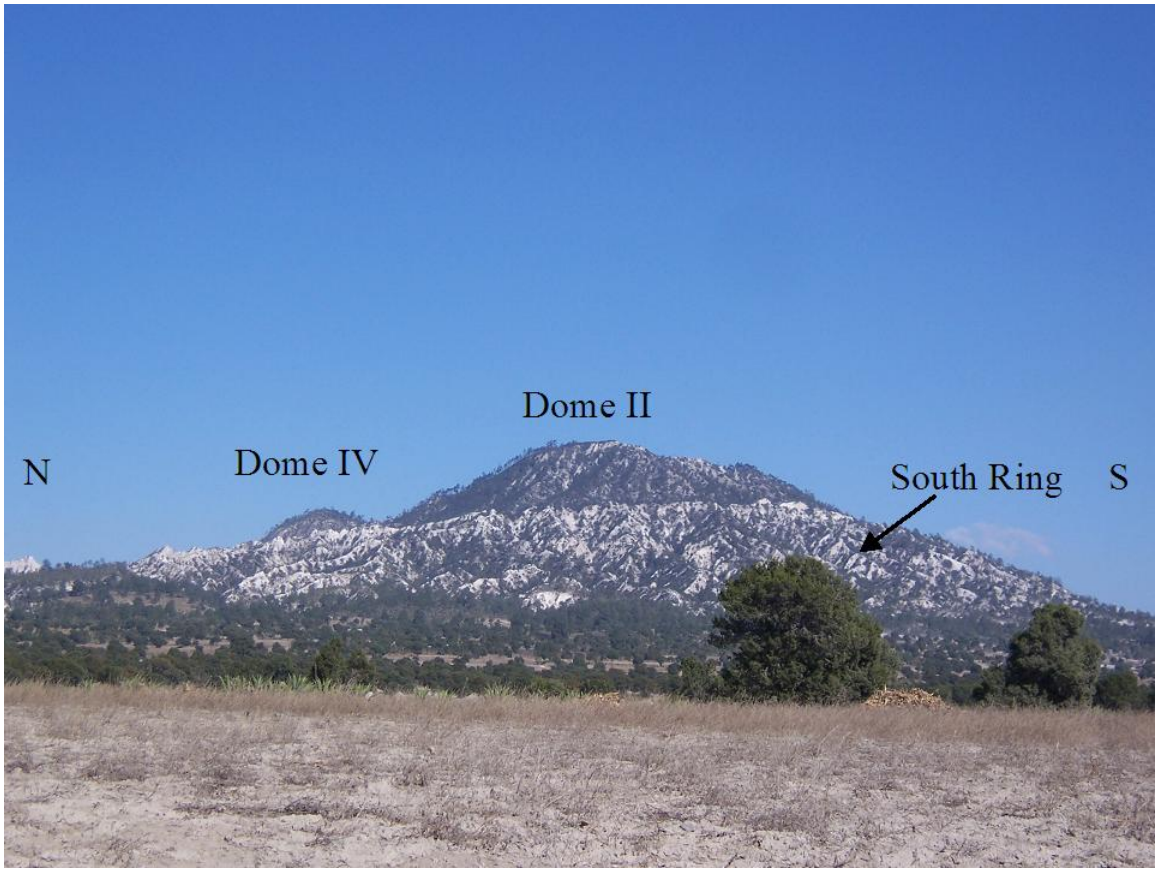

Figure 1.4. View of Cerro Pinto from the west. The northern tuff ring is just left (north) of this photo and Dome III is located directly behind Dome II in this picture.

Cerro Pinto is a multi-phase dome system whose history includes oscillations between explosive and effusive emplacement, dome collapse, and phreatomagmatic interactions between ground water and magma. Within the Serdán-Oriental Basin, silicic domes have reactivated due to the influxes of new batches of magma, events that are easily identified by the presence of polymodal chemistry (Las Derrumbadas; Siebe and Verma, 1988; Cerro Pizarro; Riggs and Carrasco-Nuñez, unpublished data, 2006). However, multi-phase eruptions from a single, isolated batch of magma are not well understood.

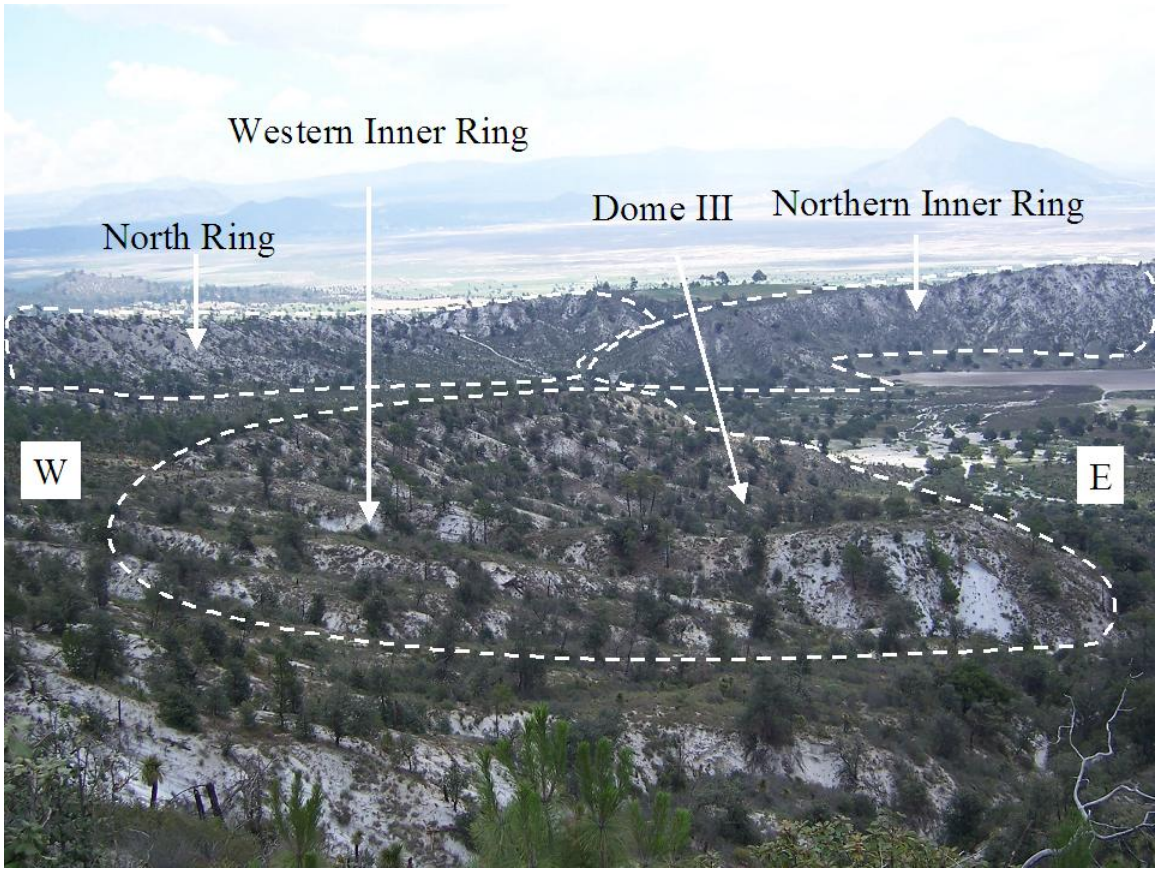

Figure 1.5. View looking into the northern tuff ring from the south. Northern inner ring edge is ~1,600 m away.

The Serdán-Oriental Basin contains a number of isolated silicic domes (e.g. Cerro Pizarro, Las Derrumbadas, and Cerro Pinto) that have eruptive histories that appear to be more complex than a single monogenetic eruption. Cerro Pinto has both the uniform chemistry of a monogenetic structure and the eruptive variations commonly associated with polygenetic volcanism. This thesis describes the evolution of Cerro Pinto dome complex and illustrates how and why Cerro Pinto diverges from traditional rhyolite dome models.

Statement of Problem

This project initially had two goals, 1) to describe and map the deposits of Cerro Pinto and 2) to determine the evolutionary history of the complex. To meet these goals, the entire complex was mapped in detail and many stratigraphic sections were produced. While completing the first two goals it became increasingly apparent that Cerro Pinto's history is considerably more complex than would be predicted for a simple rhyolite dome and necessitates further explanation. By comparing Cerro Pinto's evolution with other known silicic dome evolutions and modeled dome behaviors, I have been able to determine the probable magmatic and environmental variables that led to the Cerro Pinto's multi-staged emplacement history.

Previous Work

Currently, no published works have focused on the evolution of Cerro Pinto, although it has been of peripheral interest to two regional studies within the Serdán-Oriental basin. Garcia-Banda (1984) compared Cerro Pinto to Cerro Pizarro and the Tepeyahualco flows originating from Los Humeros caldera based on geochemistry and petrology. Garcia-Banda's study documented high-silica rhyolite with a relative enrichment of Rb and depletions of Sr and Zr at Cerro Pinto. An unspecified method of isotopic dating suggested an age of 0.405 +/- 0.142 ma for the dome complex with a late-stage steam explosion occurring at 0.172 +/- 0.06 ma (Garcia-Banda, 1984). This implies that the dome complex had a thermal lifespan of over 225 ka.

Siebe et al. (1995) mentioned Cerro Pinto in a regional field trip guide. In this publication, the Cerro Pinto dome complex was broken down into two separate structures, Cerro Xalapaxco and Cerro Pinto (Fig. 1.3). The term xalapaxco is a Nahautl (Aztec language) word meaning vessel or container made of sand. When the vessel contains water, it is called an axalapaxco. Across the Trans-Mexican Volcanic Belt, tuff rings, maars, and tuff cones are referred to as xalapaxco or axalapaxco depending on whether a lake exists within the crater (Abrams and Siebe, 1994). Cerro Xalapaxco simply refers to the dry northern tuff ring of Cerro Pinto. Siebe et al. (1995) suggested that Cerro Xalapaxco, the northern tuff ring, was emplaced by a strictly magma-driven eruption prior to the emplacement of the Cerro Pinto domes.

Terminology

Certain terms in this paper have been used in different ways in the literature and are defined here to avoid confusion. The term “tuff ring” is used for any circular or semi-circular deposit of pyroclastic tephra originating from a single vent produced from a phreatomagmatic eruption. At Cerro Pinto the definition is expanded to include rings of tephra without any apparent phreatomagmatic influence. “Grain-flow deposits” are talus deposits that were produced during active growth of the lava domes and were emplaced, at least in part, by grain flow. The term “outsized clast” refers to any clast more than five times the average grain size for any deposit. Outsized clasts can include blocks or bombs, but the term does not imply any particular process. “Stony rhyolite” is volcanogenic material that is poorly vesiculated and devitrified. An “isolated dome” is a lava dome whose evolution was not associated with any other prominent volcanic features (e.g.

stratovolcano, caldera, or a large dome field) and that was sourced from a single, relatively small magma chamber that gave rise to no other volcanoes.

CHAPTER II

SILICIC LAVA DOMES

Silicic (rhyolite to andesite) lava domes are emplaced in three primary geologic settings; 1) as part of larger volcanic features such as calderas and stratovolcanoes (e.g. South Sister Volcano, Oregon; Scott, 1987; Mt Unzen, Japan; Nakada et al., 1995; Novarupta, Alaska; Houghton et al., 2004), 2) as part of dome fields (e.g. Inyo Domes, California; Swanson et al., 1989; Taylor Creek, New Mexico; Duffield et al., 1995), and 3) as single, isolated volcanic structures (Cerro Pizarro, Mexico; Riggs and Carrasco-Nuñez, 2004). Some domes are emplaced by small batches (<50 km^3) of homogeneous magma and have minimal variation in major element compositions over the course of the eruption (e.g., Scott, 1987). Larger batches of magma (>500 km^3) can give rise to fields of compositionally similar domes, such as those of the Taylor Creek Rhyolite (Duffield and Dalrymple, 1990), although, more often than not, large batches of magma produce heterogeneous deposits due to compositional zoning of the magma chamber (Fisher and Schmincke, 1984). Occasionally, silicic domes with variable geochemistry are produced by small, heterogeneous magma chambers or by magma mixing from the influx of a new batch of magma (Siebe and Verma, 1988).

Although domes are generally effusive, nearly all types of domes are prone to explosive episodes (Fink and Anderson, 2000). Newhall and Melson (1983) note that, because variations in whole-rock SiO_2 and magma supply rate show no systematic relation to the timing or character of an eruption, these particular controls on eruptive behavior cannot

be well constrained. However, the compositional characteristics of magmas (e.g. crystallinity, vesicularity, and volatile content) can be well constrained in isolated domes because most of the eruptive products are deposited relatively close to the vent in a single continuous sequence. In this way, isolated domes can be effective analogs for larger volcanoes when looking at the compositional characteristics associated with variations in eruptive character.

Current Dome Models

The umbrella term “silicic domes” includes the sub-population “rhyolitic domes”. The dome models that follow are in reference to rhyolite domes, but can commonly be applied to silicic domes. While it is important to note the similarities that rhyolite domes can have with other silicic domes, it must also be clear that rhyolite domes have unique eruptive characteristics and they can not be lumped in with silicic domes in general. Behaviors of silicic domes are not necessarily common to rhyolitic domes. In the literature, rhyolitic domes are considered simple, monogenetic volcanic features (Christiansen and Lipman, 1966; Swanson et al., 1989; Duffield et al., 1995) with small hazard potential. From previously well-studied dome systems, such as Inyo Dome chain in California (Miller, 1985; Manley and Fink, 1987), the Taylor Creek Rhyolite, New Mexico (Duffield et al., 1995), and the Glass Mountain Rhyolite, California (Metz and Bailey, 1993) three basic models explain different aspects of rhyolitic dome emplacement and their internal structures.

The first of these models, based primarily on work by Duffield et al. (1995), explains the unidirectional progression of eruption style during rhyolitic dome emplacement. This model was developed to explain the emplacement of the Taylor Creek Rhyolite, but it can be applied to other simple rhyolite domes. The second model discusses the transition from closed to open system degassing and the correlated change from explosive to effusive eruptions. The third model discusses internal structures and textures common to simple rhyolite domes. These models are not mutually exclusive and when combined give a good general picture of rhyolite dome growth.

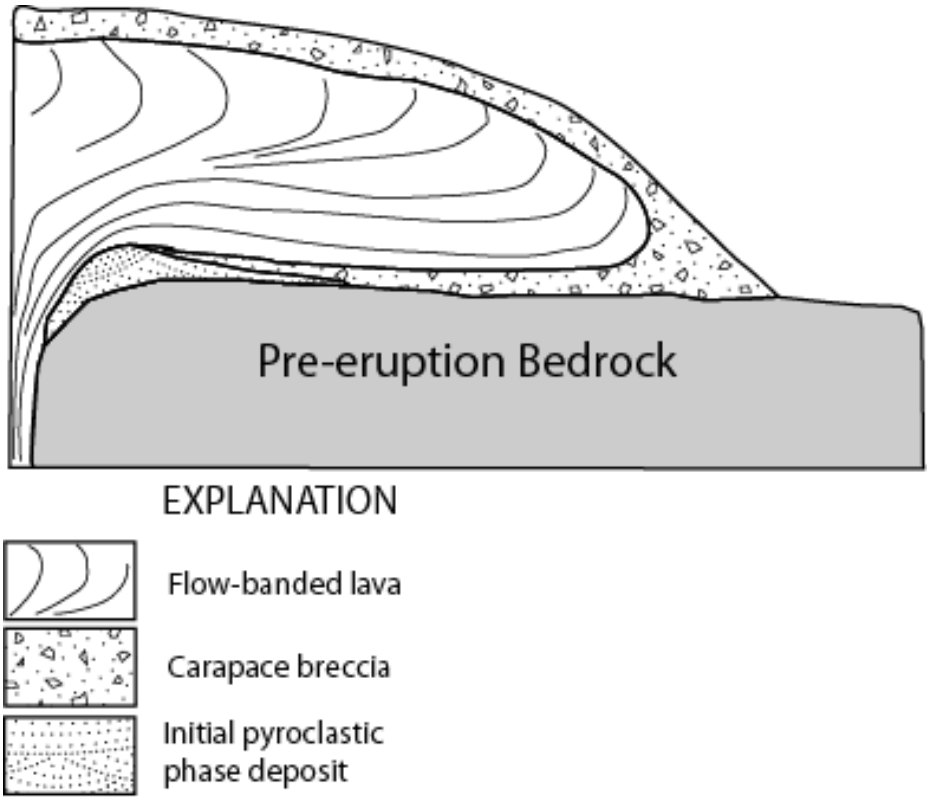

Figure 2.1. Cross-section of an idealized simple rhyolite dome. The relative volumes of the three main constituents may vary greatly from one dome to the next. At Cerro Pinto, the initial pyroclastic deposits are much more voluminous than suggested in this model. (After Duffield and Dalrymple, 1990).

Simple Dome Growth Model

According to Duffield et al. (1995), nearly all rhyolitic magma eruptions begin with an explosive pyroclastic phase during which vent opening occurs. These eruptions produce pyroclastic-fall, -flow, and -surge deposits that can be tens of meters thick. Eruptions can be initiated by interactions with groundwater or through exsolution of volatiles during magma ascent (Manley and Fink, 1987). When volatile-rich magmas are exposed to near-surface pressures, gas exsolution can occur at rates efficient enough to explosively eject overlying material, which is commonly local bedrock (Fisher and Schmincke, 1984). Consequently, basal tephra beds are typically higher in lithic clast concentrations than higher beds (Schroeder, 1996). Tephra deposits are typically nonwelded, but can become welded or agglutinated in areas proximal to the vent (Duffield et al., 1995).

The pyroclastic / vent-clearing phase is followed by the quiet effusion of magma, producing either a lava dome or a lava flow. The type of volcanic feature produced, whether tuff ring, tuff cone, maar, dome, coulee, or lava flow, is related to numerous morphological and compositional variables including topography, extrusion rate, crystallinity, gas content, dissolved H_2O concentration, temperature, and chemistry (Fink and Griffiths, 1998). Duffield et al. (1995) suggest that during the growth of lava domes, flow-generated envelopes of breccia form around a flow-foliated coherent lava core and can be overrun by the advancing flow, much like a tractor tread, resulting in a basal breccia beneath the coherent lava (Fig. 2.1). According to this model, once effusive activity ceases, there is little likelihood of reactivation at the same vent because of the blocking of the conduit by cooled igneous rock. With larger magma bodies where

additional magma rises into the region, it is likely that vent migration will be to a nearby area of structural weakness (e.g. faults, fractures, joints), beginning a new emplacement sequence.

Transition from Explosive to Effusive Eruption

According to the simple dome growth model, rhyolite domes make a one-time transition from an explosive pyroclastic phase to the slow effusion of dome lava. The primary cause for this transition is a change in the style of degassing of the extruding magma. Explosive eruptions are produced by "closed-system" degassing in which the rapid, coupled ascent of gas and lava leads to the shallow release of dissolved volatiles (Mangan et al., 2004). If the rate of magma ascent exceeds the rate at which volatiles can exsolve, a state of super saturation and gas disequilibrium within the melt is reached and can result in explosive fragmentation and ejection of juvenile material (Cashman et al., 2000).

In contrast, effusive eruptions are associated with "open-system" degassing in which the gas and melt ascend at different rates, allowing for the diffusion of gasses through the conduit walls (Cashman et al., 2000). The efficient removal of volatiles through conduit walls reduces the explosive potential of extruding magma (Wallace and Anderson, 2000). While ascent rate is paramount in the change from closed to open-system degassing, recent studies have noted feedback relations among magma viscosity, vesicularity, crystallization, and gas loss (Anderson et al., 1995; Sparks, 1997; Barmin et al., 2002).

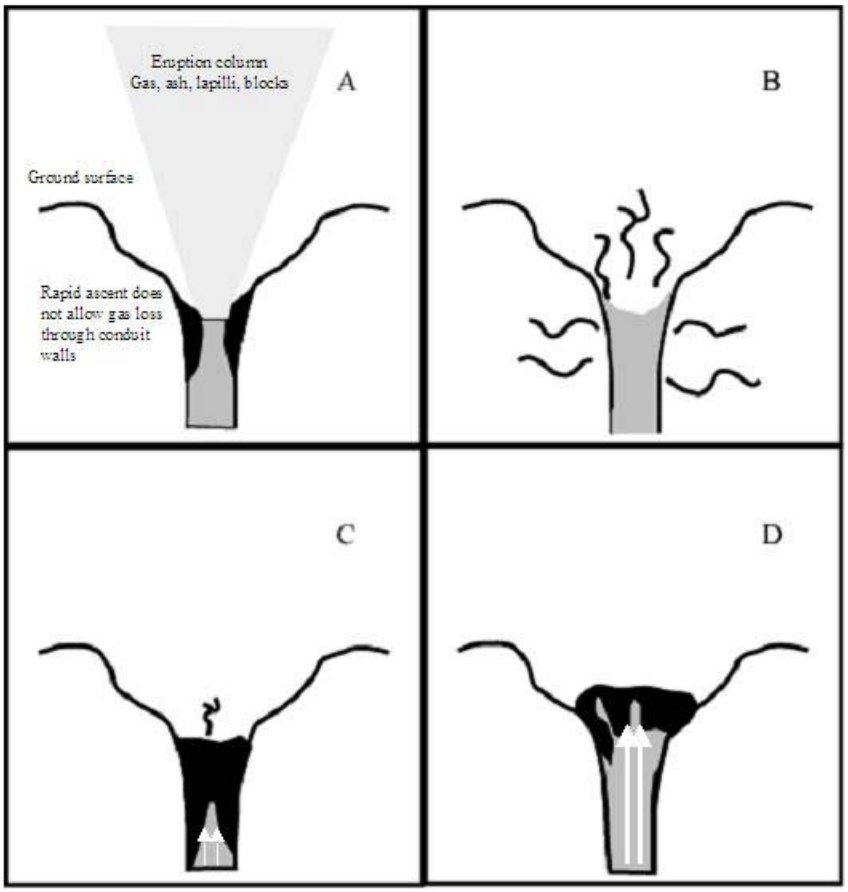

Figure 2.2. Gray zones represent hot, mobile magma while black represents solidified magma. This figure illustrates the shift from closed to open system degassing. A) In closed-system degassing, rapid, coupled ascent of gases and melt leads to disequilibrium and explosive eruption. B) In open-system degassing, efficient decoupling of volatiles and melt during ascent permits permeable flow and gas loss through the conduit walls and vent. Degassed, dense magma accumulates along the conduit walls. C) The accumulation of cooled lava eventually seals off the vent while gas-rich magma continues to push up from below. D) Cap rock solidification removes the pathway for gas to escape. When gas exsolution exceeds the capacity of the system to passively degas, pressure builds and vulcanian eruptions often occur. (Figure adapted from Adams et al., 2006).

Ascending magma that degasses efficiently becomes more viscous, but is still fluid and undergoes vesicle collapse along the conduit margins while the melt continues to rise rapidly through the center of the conduit, sustaining explosive pyroclast generation (Adams et al., 2006). Eventually, the accumulating viscous magma plugs the conduit, blocking the rise of the still-volatile-rich underlying melt. The underlying volatile-rich melt is the driving force that slowly pushes the degassed, but still-fluid plug up and out of the conduit, forming a coherent lava dome (Adams et al., 2006; Fig. 2.2)

Model for Internal Dome Structures

Research drilling at the Inyo Domes, CA (Manley and Fink, 1987; Swanson et al., 1989) and in-depth textural studies at Taylor Creek, NM (Duffield et al., 1995) and Fortymile Canyon, NV (Christiansen and Lipman, 1966) have shown certain internal structures to be common among rhyolite domes and flows. Christiansen and Lipman (1966) were the first to identify the basic stratification of a rhyolite lava flow (Fig. 2.3). This includes a breccia envelope, seen at the upper and lower margins of the flow and produced by the "tractor tread" advance of silicic magmas described by Nakada et al. (1995) and Duffield et al. (1995). A second envelope of vitrophyre surrounds the coherent foliated lava core. The glassy texture is a result of low levels of nucleation and crystal growth due to the high viscosity of rhyolite lava flows and to the accelerated cooling rate along these outer margins (Christiansen and Lipman, 1966). Internal temperatures of larger lava flows can remain hot for years, allowing for devitrification and more extensive crystal growth within the flow core (Manley and Fink, 1987).

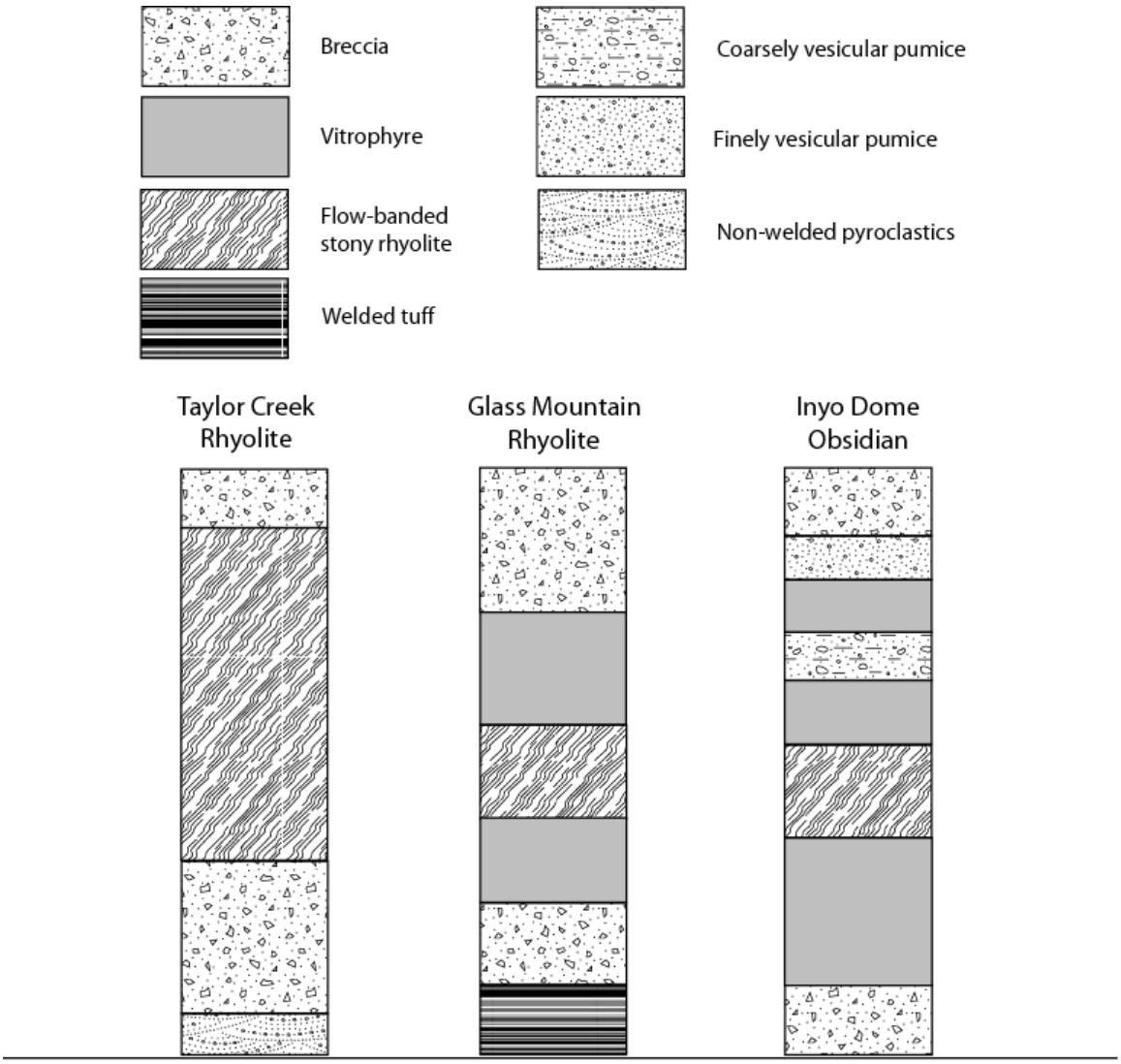

Figure 2.3. Cross-section view of idealized rhyolite domes showing variations in internal structures compared to the simple rhyolite dome model represented by the Taylor Creek Rhyolite. Internal structures at Glass Mountain include an inner vitrophyre envelope as well as welding of the underlying pyroclastic deposits. At Inyo dome, the upper part of the vitrophyre envelope is interrupted by a coarsely vesicular pumice zone attributed to migrating vapor that becomes trapped beneath the upper hardened crust of the flow where tensile cracks can no longer aid in the migration of volatiles through the highly viscous magma (Manley and Fink, 1987). (Modified from Schroeder, 1996).

Manley and Fink (1987) expanded on this basic model for the internal structures of domes by breaking the upper vitrophyre into two distinct zones differentiated by patterns in vesicularity. These zones are identified as finely vesicular pumice and coarsely vesicular pumice. The finely vesicular pumice forms at the flow surface where even small vesicles remain uncollapsed due to the low overlying pressure. The coarsely vesicular pumice is found lower in the flow and contains vesicles produced by localized increases in vapor pressure from the accumulation of gas migrating through microfractures within the cooling lava (Fink and Manley, 1987).

Dome Model Application

Endogenous dome growth following the simple dome growth model has been seen both in dome fields (Inyo Domes, CA; Swanson et al., 1989; Taylor Creek Rhyolite, NM; Duffield et al., 1995) and in domes associated with rhyolitic to andesitic stratovolcanoes and calderas (Glass Mountain Rhyolite, CA; Metz and Bailey, 1993; Lascar Volcano, Chile; Matthews et al., 1997). At stratovolcanoes, where domes are typically andesitic to dacitic, individual episodes of dome growth mirror the simple dome growth model, but the total progression is repeated many times and is complicated by the episodic explosive removal of domes and the high rates of magma recharge (Mt. Unzen, Japan; Nakada et al., 1995). Explosive activity usually occurs within a year of dome extrusion (Newhall and Melson, 1983).

Silicic domes, especially those associated with stratovolcanoes, are known to reactivate, sometimes with predictable regularity (e.g. Mount St. Helens, Washington (1980-1987)

and Santiaguito, Guatemala (1922-2000); Barmin et al., 2002; Lascar volcano, Chile; Matthews et al., 1997). In the Serdán-Oriental basin, two isolated rhyolitic domes were reactivated due to the influx of new magma. Las Derrumbadas has polymodal geochemistry ranging from andesite to rhyolite, implying multiple phases of reactivation (Siebe and Verma, 1988). Cerro Pizarro is composed of only high-silica rhyolite, but chemistry shows bimodal distributions separated in age by ~ 100 ka, suggesting reactivation by a secondary batch of magma (Carrasco-Nuñez and Riggs, unpublished data).

Dome growth associated with larger volcanic structures is more complicated than isolated rhyolite dome growth because of the commonality of explosive or gravitational dome collapse from the injection of new magma. Gravitational dome collapse and explosive reactivation can occur at isolated rhyolite domes, but these events are apparently less common, at least as documented. Isolated rhyolite domes are susceptible to phreatomagmatic explosions and subsequent dome-collapse events as well. However, the smaller volumes of these structures allow them to cool more quickly and reduces the overall time span in which phreatomagmatism is likely to occur. Gravitational dome collapse is most likely to occur at stratovolcanoes where domes are often extruded on steeply dipping topography as opposed to the relative stability of flat-lying bedrock.

Phreatomagmatism

Phreatomagmatism is any volcanic activity that results from the interaction between magma or lava and ground water or surficial water such as seawater, fluvial systems, or

lake water (Morrissey et al., 2000**).** Eruptions of this nature are driven by the rapid volumetric expansion of flash-vaporized water after contacting magma or hot lava. The magma-to-water ratio is responsible for the efficiency, explosivity, and type of structure produced by the eruption (Lorenz, 1986; Fig. 2.4).

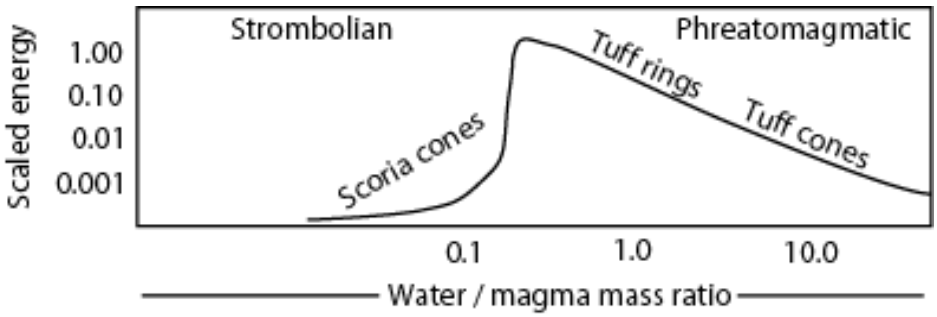

Figure 2.4. Relative energy and associated structures produced by increased water/magma ratios. (Modified from Wohletz and Sheridan, 1979).

Phreatomagmatism can produce various types of eruptions, including surtseyan, vulcanian, and phreatoplinian. Phreatoplinian eruptions are long-duration eruptions that are similar to plinian eruption except that their deposits are generally finer grained. When water-to-magma ratios and magma recharge rates are high, surtseyan eruptions, with their unique "cock's tail" jet of ash and steam, are commonly produced (Morrissey et al., 2000). When the water to magma ratio is low, as in the percolation of meteoric water through a hot lava dome, brief but highly explosive vulcanian eruptions (Heiken and Wohletz, 1987) or periodic episodes of dome collapse can be initiated (Yamasato et al., 1998; Matthews and Barclay, 2004).

Deposits produced by phreatomagmatism contain accretionary lapilli and higher concentrations of angular lithic clasts than strictly magma-driven eruptions. Angular clast edges indicate fragmentation instead of abrasion (Morrissey et al., 2000). Phreatomagmatic deposits also contain high quantities of glass shards and crystals. Under a scanning electron microscope or a binocular microscope, glass shards produced by phreatomagmatic eruptions are commonly blocky, platy, or spherical in shape with grooves and scratches on the surface, depending on transport mechanism (Heiken and Wohletz, 1985)**.** During transport by pyroclastic surge or pyroclastic flow, the planar edges of blocky and platy pyroclasts are chipped and rounded. Fallout pyroclasts tend to be more angular, but still have conchoidal fractures where the glass was broken during ejection. Because of the interactions of lava and water or water vapor, volcanic glass produced by phreatomagmatic eruptions is more likely to undergo significant hydrothermal alteration when compared to glass produced by primarily magma-driven eruptions (Morrissey et al., 2000).

Tuff Rings

Tuff rings are small, monogenetic volcanoes that range in diameter from a few hundred meters to about 3 km and can have rim thicknesses of over 100 m (Vespermann and Schmincke, 2000). They are produced by the explosive interaction of magma with surface or ground water in small quantities (Sheridan and Wohletz, 1983). These shallow, phreatomagmatic eruptions give tuff rings their distinctive shape by producing wide craters that are subsequently mantled by pyroclastic deposits, accentuating the

topography (Fisher and Schmincke, 1984). Subsidence surrounding the vent can also lead to accentuated ring-shaped topography (Lorenz, 1970).

The primary mechanism for tuff ring emplacement is through phreatomagmatic surges, although at Cerro Pinto, dry pyroclastic eruptions also produced tuff rings. According to Vespermann and Schmincke (2000), basaltic tuff rings are usually produced when the magma/water volume ratio is about 1:1. Additional water produces tuff cones while less water produces scoria cones (Fig. 2.4). Many factors in addition to water/magma ratios can affect the morphology of a volcano, including magmatic chemistry, volatile content, eruption rate, wind speed and direction, and pre-existing topography.

Surge, Flow, and Fallout Deposits

Fallout Deposits

Tephra can be deposited by pyroclastic flow, pyroclastic surge, or fallout. Each depositional mechanism is indicative of associated processes at the vent during the eruption. Fallout deposits are produced when an eruption creates a sustained eruption column in which pyroclasts are entrained in rising plumes of hot gas before gradually cooling and falling back to the ground. Fallout deposits are well sorted due to the gradual cooling of a volcanic plume as it moves away from the vent. As the clasts within the plume cool, they lose their buoyancy and particles of similar size and mass fall out concurrently. Some fall deposits can be normally or reversely graded as a response to fluctuations in eruptive intensities at the vent.

The dispersion of fallout pyroclasts is directly related to the energy of the eruption, vent morphology, clast size, wind speed and direction, and any involvement of external water (Houghton et al., 2000). Ideally, fallout deposits should be distributed radially, but the aforementioned variables often lead to fallout deposits being concentrated to one side of a volcano. Bombs and blocks tend to follow ballistic paths from the point of ejection to the point of impact while smaller clasts can be suspended in the air by convection cells and transported farther away from source. If fine volcanic ash is ejected high enough and reaches the high winds of the stratosphere, it can circulate around the globe and not settle back to Earth for years.

Pyroclastic Density Currents

As summarized by Wilson and Houghton (2000), the term “pyroclastic density current” is an umbrella term that spans an entire spectrum of gravity-controlled, laterally moving mixtures of pyroclasts and gas. These flows range from dense pyroclastic flows to dilute pyroclastic surges. Dense pyroclastic flows tend to travel at a few tens of meters per second while the dilute surges can travel much faster (200-300 m/s). The main differences between the two end-member currents are their densities and the modes by which entrained pyroclasts and lithic clasts are transported and deposited.

Pyroclastic Surges

Pyroclastic surges are low-concentration, turbulent, density currents that can be produced by either the partial collapse of a rising eruption column, base surge, dome collapse, or through a directed lateral blast (Rose et al., 1977; Fisher, 1990; Houghton et al., 2004; Fig. 2.5). In pyroclastic surges, particle mass and momentum are evenly distributed

throughout the current with the lowest particle velocities concentrated at the base where sedimentation occurs. Particle transport occurs in a high-velocity turbulent zone above the lower zone of sedimentation (Wilson and Houghton, 2000.)

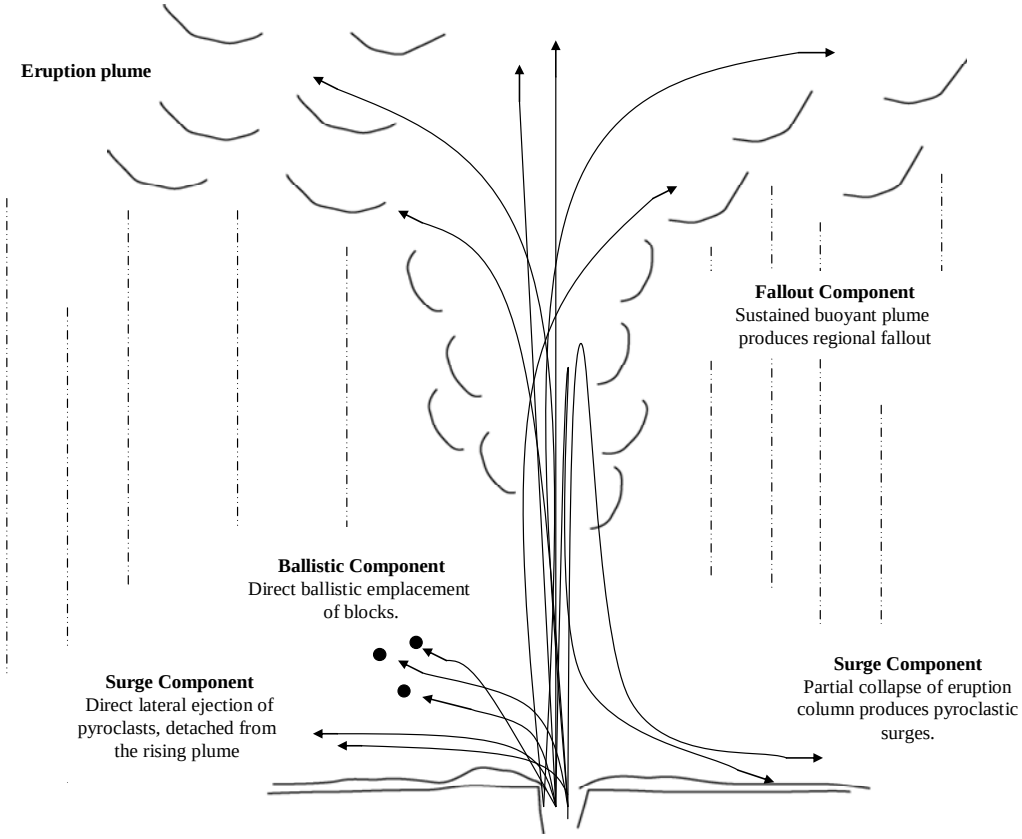

Figure 2.5. Multiple depositional regimes that combine to produce the hybrid surge/fallout deposits common to Cerro Pinto. (Adapted from Houghton et al., 2004)

Depositional processes and flow regimes for pyroclastic surges have been inferred from sedimentary processes that produce similar bedding structures (Chough and Sohn, 1990; Bull and Cas, 2000) and from theoretical modeling (Wohletz and Sheridan, 1979). Surge deposits are commonly stratified and composed of well to moderately sorted planar and cross beds (e.g. Cas and Wright, 1987). This internal stratification of surge beds is

primarily due to the sedimentary processes of suspension-load fallout, rolling, and saltation (Burgisser and Gardner, 2006).

As summarized by Valentine and Fisher (2000), surges can be either “wet” or “dry” depending on their emplacement temperature (Fig. 2.6 A & B). Wet surges are those surges that are emplaced when water is in liquid form (< 100^{o} C), producing a three-phase system involving water droplets, solid particles, and gas. Wet surge deposits tend to have higher concentrations of accretionary lapilli and soft-sediment deformation. Dry surges are produced when water is in vapor form (>100^{o} C) at the time of emplacement. It is possible for surges to shift between wet and dry depositional environments depending on the temperature of the flow and the relative homogeneity of the flow. For example, a pyroclastic surge can be very hot when first erupted, but heterogeneous. If the heat has not been well circulated, certain parts of the flow may still produce wet deposits. As the surge travels and mixes, the heat is more evenly distributed and the flow becomes dry. Then finally as the surge cools distally from the vent, it can shift back to a wet surge conditions.

The amount of material deposited by a pyroclastic surge is dependent upon the energy of the surge and the thickness of the zone of deposition. Surges are density stratified, with a depositional zone overlain by a turbulent zone of flow (Valentine, 1987). High-energy surges keep more material entrained in the turbulent flow zone, producing thinner deposits. However, as the surge loses energy, the turbulent zone shrinks and more

material is provided to the zone of deposition, resulting in thicker deposits (Schroeder, 1996).

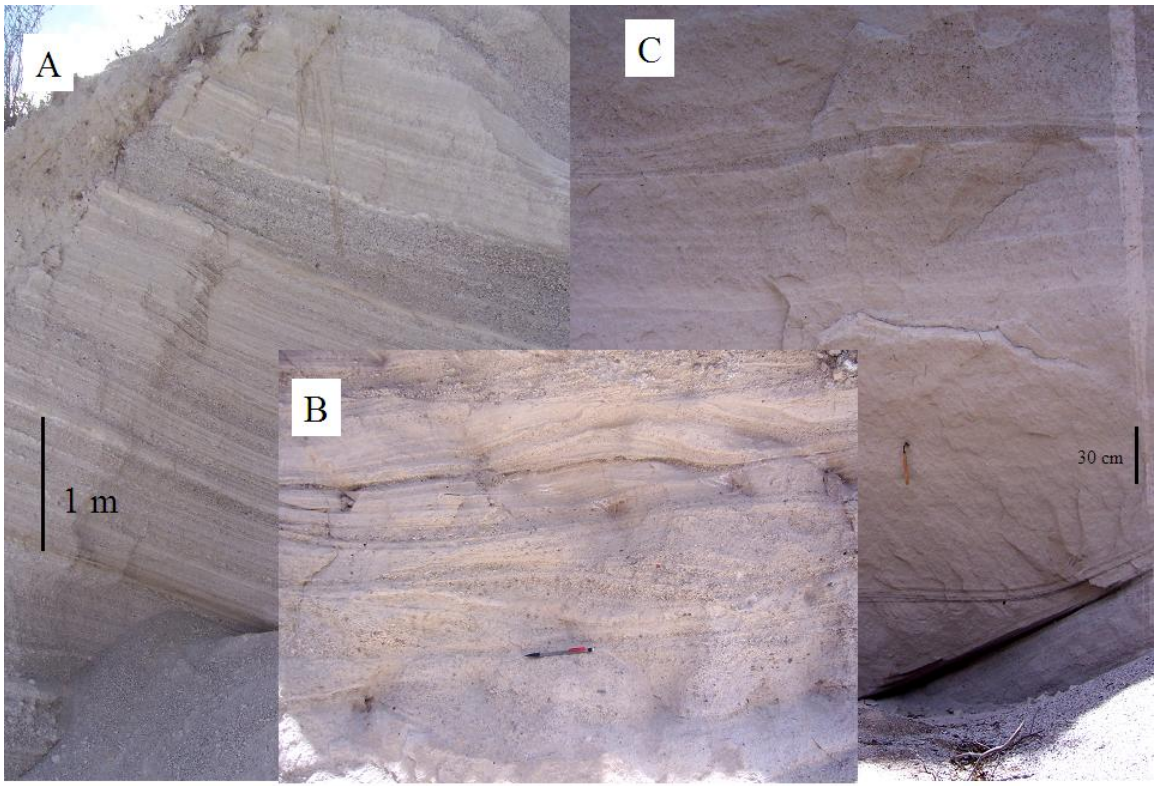

Figure 2.6. A) "Dry" pyroclastic fall and surge deposits. Deposits are dominated by moderately sorted planar beds. B) "Wet" pyroclastic surge deposit is cross-bedded and contains accretionary lapilli. C) Massive pyroclastic flow deposit. Note weak bedding.

Pyroclastic Flows

The dense end-member of the pyroclastic density current spectrum is the pyroclastic flow. In pyroclastic flows, mass and lateral momentum are concentrated at the base of the current where particle velocities are the highest. Often a co-ignimbrite fine-ash cloud is produced, but these clouds are not significant to the dynamics of overall flow deposition and often produce only small, accessory fallout deposits (Wilson and Houghton, 2000).

Two models have been created to explain the depositional mechanism of pyroclastic flows. Wilson and Walker (1982) suggest that pyroclastic flows deposit en masse where the total thickness of the deposit is a minimum thickness of the flow itself. Because of their high particle concentrations, pyroclastic flows act more like particle flows, preferentially traveling down valleys and into topographic lows. If pyroclastic flows encounter areas of high topographic relief, turbidity increases and pyroclastic flows can decouple, producing both near-ground, high-density currents and airborne, low-density surges that are capable of crossing topographic highs (Fisher, 1995).

Alternatively, Branney and Kokelaar (1992) suggest that pyroclastic flows are density stratified like pyroclastic surges with a high-density depositional zone overlain by a turbulent transport zone. However, pyroclastic flows have much higher overall particle concentration than pyroclastic surges and tend to produce much thicker, more massive deposits (Fisher et al., 1993; Fig 2.6 C). Branney and Kokelaar (1992) further suggest that the deposition of massive pyroclastic flows is aggradational where the boundary from one pulse to the next is not evident in the rock record.

Hybrid Deposits

Because pyroclastic surges and pyroclastic flows are merely the end members of the spectrum of pyroclastic density currents, there is ongoing debate over the boundary between the two, especially with regard to laterally directed density currents (Wilson and Houghton, 2000). Hybridization of depositional mechanisms also occurs with respect to fallout deposits. Pyroclastic surge and flow deposits can become hybridized with fallout

when they are deposited beneath a stable, fallout-producing plume (Fig. 2.5). Pyroclastic surge beds at Cerro Pinto commonly contain numerous very angular clasts of stony rhyolite and pumice that are larger than the average clast size. The angular clasts are too numerous and well sorted to be co-surge ballistic blocks. The preferred interpretation is that erupted clasts were deposited by surge and fallout mechanisms simultaneously. When clast sizes of the two mechanisms are similar, or if surges entrain larger clasts, it is very difficult to distinguish pure surge beds from hybrid surge-fallout beds (Wilson and Hildreth, 1998). Pure fallout deposits are easily identified in the field because they are well sorted, mantle topography evenly, have bedding consistency over large areas, and are dominated by angular clasts. The interplay between fallout and surge mechanisms was significant in the production of the pyroclastic deposits at Cerro Pinto. It should be noted that because of the ambient difficulties in discerning one from the other, no distinction was made between pure surge and hybrid surge-fallout deposits in the mapping of Cerro Pinto, nor in the facies descriptions.

CHAPTER III

FACIES OF CERRO PINTO

Geologic maps of Cerro Pinto are presented in figure 3.1 and plate 1. Dome characteristics are presented in Table 3.1 and the descriptions and interpretations of volcaniclastic lithofacies are presented in Table 3.2. For the facies descriptions and interpretations, proximal deposits are those deposits located inside of the rim of the tuff ring produced by that particular eruption and distal deposits are those deposits found on the outer flanks of the rings and out onto the country rock. In most cases, proximal deposits are found within 1 km of their source vents.

Dome Facies Overview

The Cerro Pinto dome complex includes four domes, three of which are in the southern tuff ring, rising up to 750 m above the valley floor (Fig. 1.4). The remaining dome is much smaller and is located within the northern tuff ring and may have been mostly destroyed during its growth phase. The four domes at Cerro Pinto are chemically similar, but compositionally distinct from one another in mineralogy and in the abundance and size of phenocrysts. Internal petrologic heterogeneities within individual domes are very small to non-existent. The four domes have a combined volume of ~ 0.5 km^3 (Table 3.1).

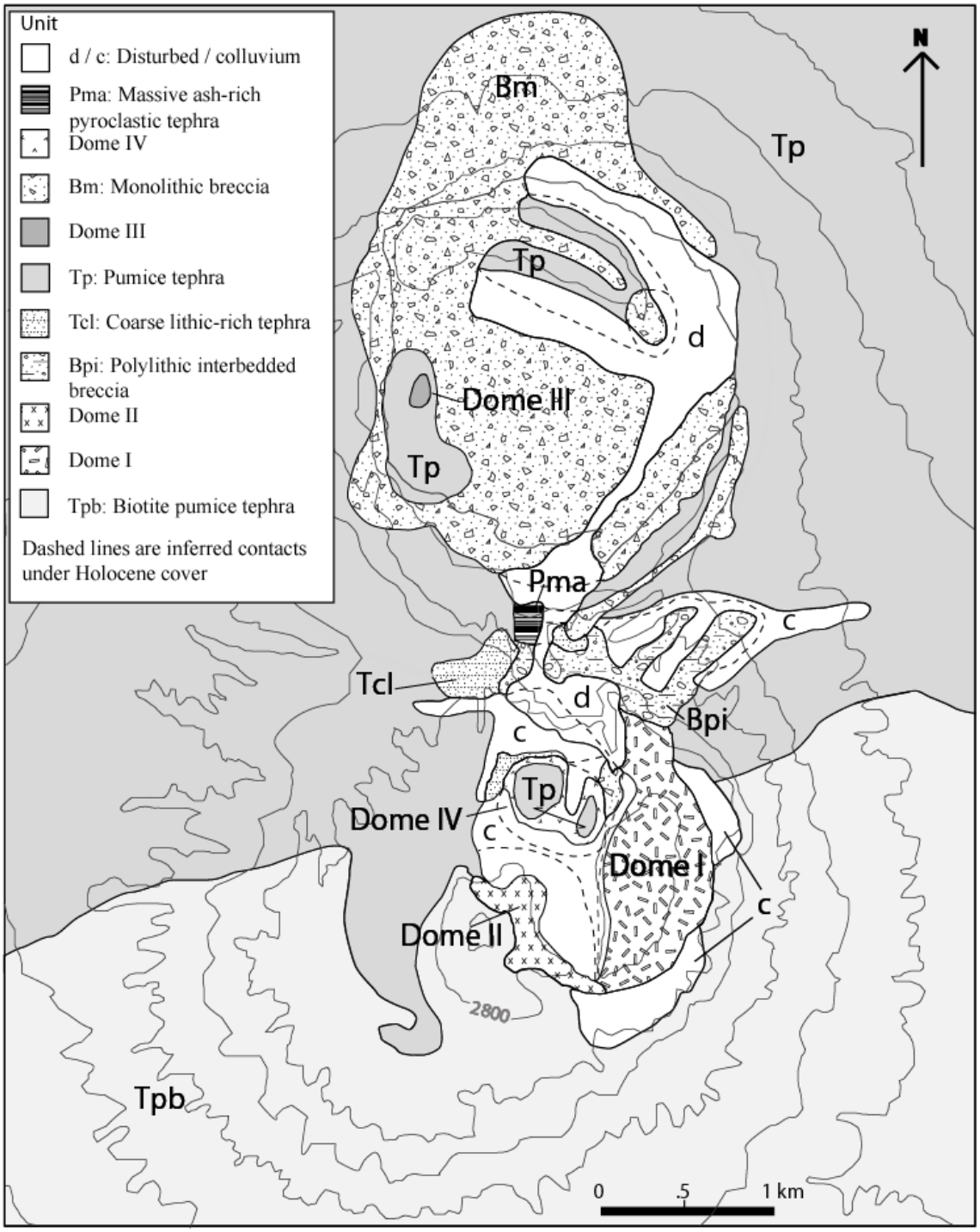

Figure 3.1. Simplified Geologic map of Cerro Pinto. For detailed map, see Plate 1.
Contour interval 50 m.

Table 3.1. Distinguishing characteristics of the four domes.

Dome	Sample description	Volume	Location	Associated mass-flow deposits
Dome I	Massive, pink-grey to white rhyolite with < 5 mm subhedral phenocrysts of biotite (< 1%), sanidine (< 1%), and plagioclase (2%) in glassy groundmass. Autobreccia clasts have a glassy shell and a pumiceous cryptocrystalline interior. Biotite and plagioclase phenocrysts are commonly intergrown. Clasts of microlitic groundmass are entrained in the glassy matrix.	0.26 km^3	Eastern half of the southern tuff ring	Grain-flow deposits down two major paleo-drainages as well as multiple debris-flow deposits.
Dome II	Stony blue and orange flow-banded rhyolite. The bands are 5-20 mm thick. Euhedral phenocrysts (< 1.5 mm) of plagioclase (3%), quartz (1%), sanidine (< 1%), and biotite (1%). Trachytic groundmass is dominated by plagioclase microlites with rare zircon microphenocrysts.	0.21 km^3	Western half of the southern tuff ring	Few debris-flow deposits to the south and west of the dome.
Dome III	Sugary grey stony rhyolite with subhedral phenocrysts (< 2.5 mm) of biotite (< 1%), quartz (< 1%), plagioclase (2%), and sanidine (< 1%). Dome lava is punky and altered. Groundmass is trachytic with microlitic plagioclase and microphenocrysts of zircon. Phenocrysts are commonly intergrown.	0.025 km^3	Central part of the northern tuff ring	May be source of the maelstrom deposit
Dome IV	Massive sugary white rhyolite with plagioclase and biotite phenocrysts up to 2.2 mm in diameter. Microphenocrysts of plagioclase, zircon, and biotite are found sporadically in the groundmass.	0.04 km^3	Northern edge of the southern tuff ring	One grain-flow and a few small pyroclastic-flow and debris-flow deposits.

Textural variations among the domes are evident in thin section. Sample DI-2 was taken from the autobreccia surrounding dome I. The groundmass is glassy and the phenocrysts

are dominantly euhedral plagioclase (Fig. 3.2A). Sample UO-10b (Fig. 3.2B) is lava from the a collapse scar on the west face of dome I. The carapace breccia and modern talus were removed during the collapse, leaving only coherent dome lava. The coherent dome material also is dominated by euhedral plagioclase, but this sample has a microlitic groundmass and intergrowth of quartz and orthoclase, indicating that more crystal nucleation and growth occurred within the dome's interior (Manley and Fink, 1987). Porphyritic texture, like that of sample UO-10b, is indicative of a two-stage crystallization process (Swanson et al., 1989). Shear stresses produced both flow banding (Fig. 3.2C) and shadow zones surrounding phenocrysts. The banding also appears to be a result of textural heterogeneities between dense and pumiceous bands of rhyolite (Fig. 3.2D). These variations could all be a result of post-extrusion cooling rates and do not necessarily indicate differences in source material.

Autobreccia

The domes at Cerro Pinto are partially covered in autobreccia shells that are up to 50 m thick. The autobreccia is well cemented and has been subjected to varying degrees of alteration. The matrix within the autobreccia shells is composed of cemented coarse ash and fine lapilli of stony rhyolite and minor crystals. Alteration has turned the matrix red-orange and obscured clast edges. The alteration is thought to be hydrothermal due to degradation of the volcanic glass and hydrous-phase minerals and the oxidation rims surrounding many clasts.

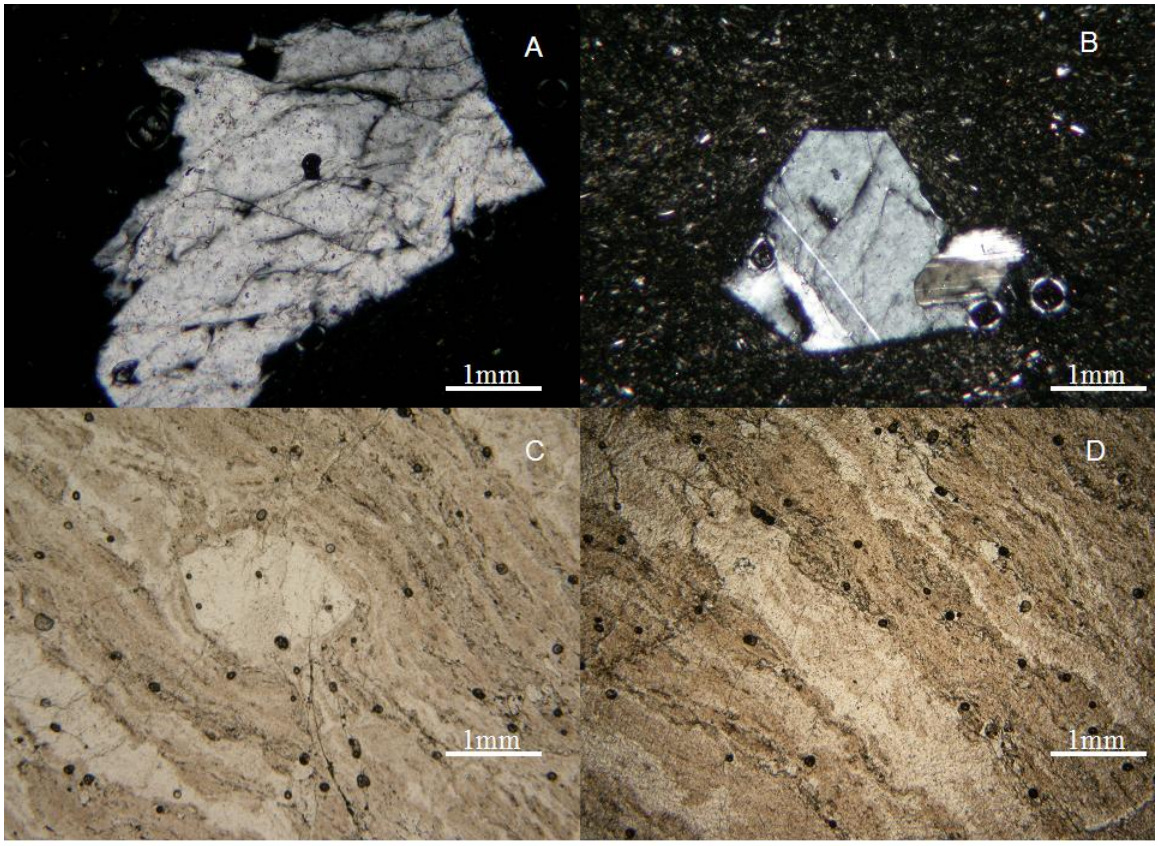

Figure 3.2. A) Plagioclase phenocryst in glassy groundmass. Sample DI-2. B) Plagioclase phenocrysts in a microlitic groundmass. Sample UO-10b. C) Phenocryst entrainment in flow banding as seen in plane light thin section. Sample DII-2. D) Pumiceous flow banding textures as seen in plane light. Sample DII-2.

Identifiable clasts within the autobreccia are angular to sub-angular and are 1 – 25 cm in diameter. Autobreccia clasts are generally glassier in thin-section than coherent dome lava (Table 3.1). Weathering has reduced parts of the autobreccia shells into loose talus piles around the two largest domes. Because internal dome material is rarely exposed, no distinction was made between autobreccia and coherent dome material during the mapping of Cerro Pinto. The autobreccia is visible only on top and at the edges of the domes.

Volcaniclastic Overview

Volcaniclastic deposits comprise pyroclastic rocks and sediments and mass-flow deposits. These form the bulk of the volcano and nearly the entirety of the north ring. Pyroclastic deposits cover approximately 220 km^2 (Garcia-Banda, 1984) and are 150-200 m thick in some localities. The primary volcaniclastic lithofacies at Cerro Pinto are biotite-rich pumice tephra, pumice tephra, massive ash-rich pyroclastic tephra, monolithic breccia, mono- and polylithic breccia with interbedded tephra, and cross-bedded lithic-rich tephra (Table 3.2; fig 3.3). Tephras produced during different eruptive stages are distinguished from one another by phenocryst types, sizes, and abundances. Based on the primary lithology of larger clasts, the mass-flow deposits can be correlated with the dome from which they originated. The colluvium deposits are generally younger, more heterogeneous, and substantially less voluminous than the primary volcaniclastic deposits.

Table 3.2. Table of tephras and mass flow deposits.

Map Units	Characteristics	Interpretation
Pumiceous tephra and biotite-rich pumiceous tephra (Tp / Tpb)	Clast-supported, well-bedded deposits with plane-parallel laminations of ash to lapilli. Bedding thickness 0.1-40 cm. Cross-bedding common in some areas. Rare normal grading. Well sorted. Accretionary lapilli common. Beds of small-amplitude starved ripples common in distal deposits. Composed of moderately vesiculated white rhyolite (~60%) and minor amounts of stony banded rhyolite (~25%) and perlite (~10%). Outsized clasts are rare. Phenocryst assemblages include subhedral crystals of quartz, plagioclase, sanidine, and biotite up to 1.75 mm in diameter. Small zircons (<0.05 mm) make up ~1% of the groundmass. Phenocryst intergrowth is common between quartz and biotite and quartz and sanidine. The Tpb facies is distinguished from Tp by the abundance of biotite phenocrysts in hand specimen.	Fallout-dominated tephra with some surge deposits originating from the north ring (Tp) and from the south ring (Tpb).
Crossbedded lithic-rich tephra (Tcl)	Clasts are medium-grained sand to lapilli. Bedding structures include tangential cross-bedding, tabular forsets, anti-dunes, and bomb sags. Beds are poorly to moderately sorted with reverse or no grading. Beds are 1.5-70 cm thick. Tcl deposits commonly scour into underlying deposits and truncate other Tcl beds. Some massive ash beds have accretionary lapilli. Clasts are white stony rhyolite (~45%), pumiceous white rhyolite (~25%), lithic clasts (~25%) and banded stony rhyolite (~5%). Lithic clasts include granite, andesite, green schist, and minor limestone. Oxide rings are common surrounding lithic clasts. Outsized clasts are common (<25 cm). The rhyolite clasts contain occasional phenocrysts of biotite and plagioclase.	"Wet" pyroclastic surge-dominated tephra with few fallout beds.

Table 3.2 (Con't). Table of tephras and mass flow deposits.

Facies	Clast Description	Interpretation
Monolithic / Polylithic interbedded breccia (Bmi / Pmi)	Massive, clast-supported, reversely graded, and poorly sorted beds of blocks and lapilli with a fine sand to ash matrix. Beds are 0.25-1.5 m thick. Coarse clasts define weak cross bedding. Interbedded ash deposits cover ~10% of the outcrop and mantle undulating underlying beds. Breccia is composed of almost exclusively angular to sub-angular sugary white phenocryst-poor clasts of dome lava (98%) with minor white pumice (2%). Phenocrysts < 3 mm of plagioclase (2%) and biotite (2%) present.	Grain-flow
Monolithic breccia and monolithic ash-rich breccia (Bm / Bma)	Two-part monolithic breccia with clast-supported beds of sand to blocks with minor laminations of coarse material. Beds are moderately sorted and have repetitious reverse or no grading. Beds are 0.1-0.45 m thick. Rare bomb sags. Tabular forsets and ripple marks common in the upper meter of the deposit. Deposit is composed of angular clasts of stony blue-gray banded rhyolite (70%), white rhyolite (5%), and perlite / obsidian (25%). Clasts are <20 cm. Hydrothermal alteration of small clasts common. Clasts contain plagioclase and quartz phenocrysts (<4 mm). The lower bed (Bma) is white due to a high concentration of light-colored ash in the matrix. The upper bed (Bm) has little ash in the matrix and is a dark blue-gray.	Maelstrom. Interplay of ballistic clasts, fallout, pyroclastic surges, and high winds during dome destruction.
Massive ash-rich pyroclastic tephra (Pma)	Massive, matrix-supported, moderately sorted, channel-confined beds ranging from 1-15 m thick. Laminations present in upper portion of the deposit. ~5% clasts of stony white rhyolite, white pumice, banded rhyolite, perlite, and lithic clasts (andesite and granite). Fe oxidation rims common around lithic clasts. Matrix is composed of fine to medium grained ash particles. Clasts are 0.2-2 cm in diameter with outsized clasts as large as 25 cm.	Pyroclastic flow

Table 3.2 (Con't). Table of tephras and mass flow deposits.

Facies	Clast Description	Interpretation
Colluvium (C)	Two types of colluvium; 1) Matrix-supported, poorly sorted and reversely graded beds, 0.3-2 m thick with weak laminations of coarse material. Occasional organic material (i.e. branches and soils). Beds contain sub-angular to sub-rounded clasts of stony white rhyolite, banded rhyolite, perlite, and lithic clasts (andesite, granite, green schist). The matrix is medium-coarse-grained sand. Clasts are 2-40 cm in diameter. Large lithic clasts (<40 cm) are common. 2) Clast-supported massive beds 0.5-6 m in thickness with poor sorting, reverse grading, and minor coarse laminations. Contains sub-angular clasts of lava with some minor lithic clasts and juvenile clasts of white stony rhyolite and banded rhyolite. Matrix is medium- to coarse-grained sand and clasts are 1-30 cm in diameter.	1) Debris flow, 2) Talus

Pumice Tephra & Biotite-rich Pumice Tephra (Tpb/Tp)

Tp and Tpb deposits at Cerro Pinto mantle topography and are well bedded with angular clasts. These deposits dominate the distal deposits of the northern and southern tuff rings (Fig. 3.1) with thin (<3 cm), laterally extensive beds (Fig. 3.3A & B). Some beds can be easily traced over a hundred meters of exposure with only slight decreases in overall bed thickness moving away from source. Some fine beds contain stranded ripples (Fig. 3.3 C). Cross-bedded beds make up a minor constituent (< 15%) of the Tp and Tpb deposits and include few outsized clasts and no lithic clasts. Some barrancas contain <10 m thick beds of cross-bedded Tpb tephra (Fig. 3.3D). These deposits are concentrated on the

southern flank of the southern tuff ring and are composed of medium- to fine-grained sand-sized ash and lapilli.

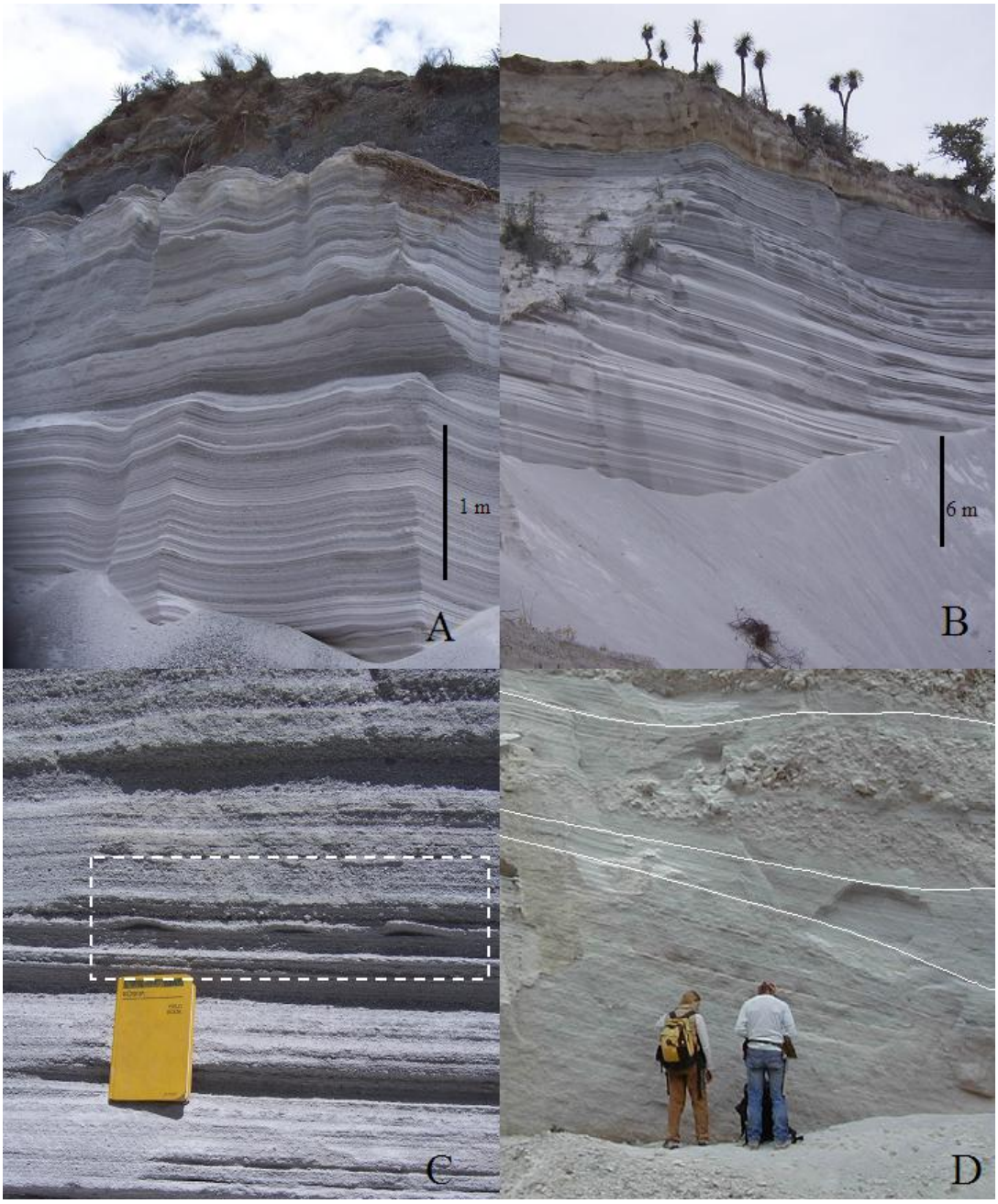

Figure 3.3. A) Finely laminated fallout deposit of stony rhyolite and pumice. B) ~30 m exposure of dry pyroclastic fallout and surge deposits. C) Stranded ripples in distal fallout deposits. D) Cross-bedded surge deposits located in drainages on the southern flank of the southern tuff ring (photo courtesy of Gerardo Carrasco-Nuñez).

The Tp and Tpb tephras are interpreted to be primarily emplaced by fallout, but the thick cross-bedded beds in the south and the sparse cross-bedded interbeds located within the proximal deposits suggest that pyroclastic surges also played an important role in the emplacement of these two tephras. The stranded ripples in the distal deposits likely indicate brief periods of eolian reworking.

Cross-bedded lithic-rich tephra (Tcl)

In areas proximal to the vent (<1 km) and in areas of severe changes in relief, cross-bedded deposits dominate. Compared to the Tp and Tpb deposits, Tcl deposits are generally more poorly sorted but can contain fine laminations of moderately well-sorted clasts (Fig. 3.4). Bed forms such as tabular forsets, anti-dunes, and parallel laminations are common and clasts are usually sub-angular to sub-rounded. Lithic clast concentrations are highest in the Tcl deposits (< 25%). Tcl deposits are interpreted to be surge deposits because of their bedding structures (tabular forsets, anti-dunes, etc.), sorting, and their morphology. Tcl deposits are also interpreted as surges because they tend to thicken in topographic lows and thin over topographic highs. Where these deposits were emplaced over areas of steep topography, such as where currents encountered tuff rings or domes, cross-bedding structures and scouring surfaces increase substantially.

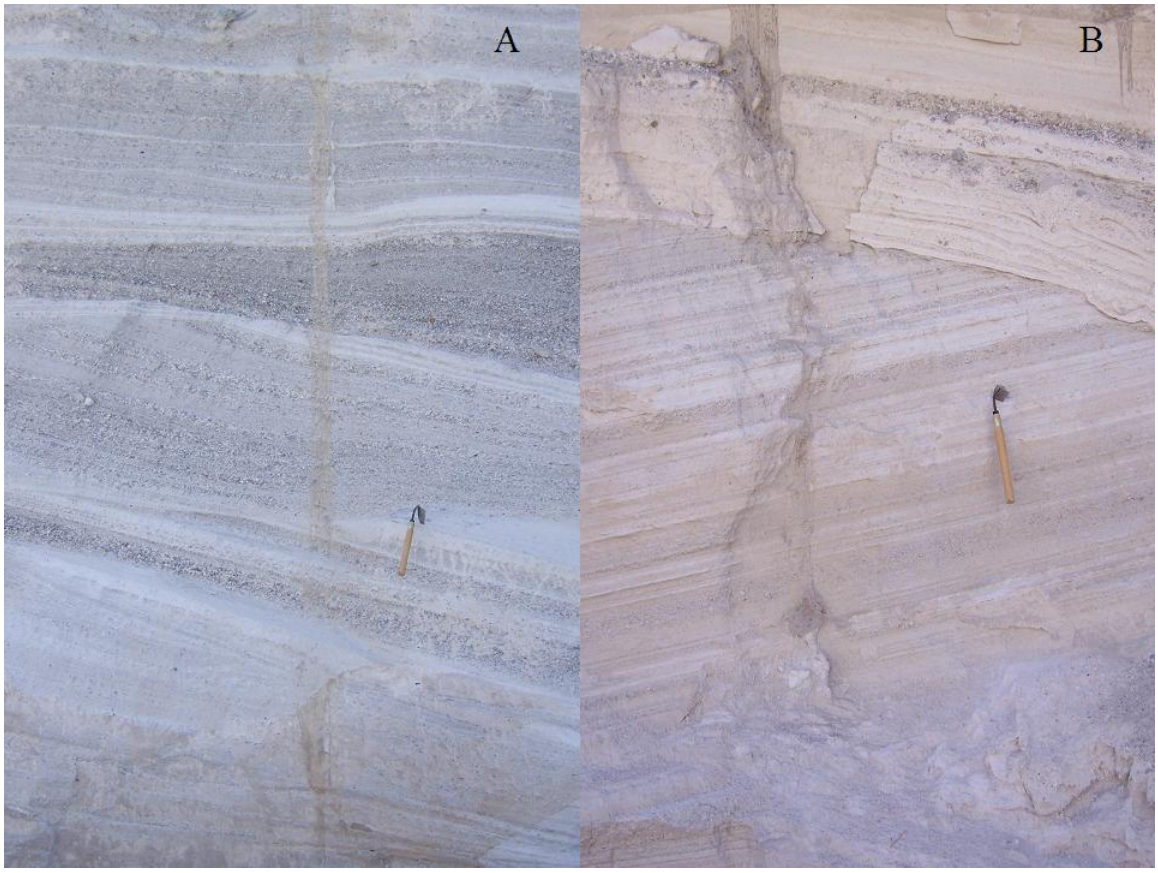

Figure 3.4. A) Cross-bedded lithic-rich tephra (Tcl). B) Biotite-rich tephra (Tpb) from the south ring overlain by Tcl tephra from the north ring. Scraper is 25 cm long.

A distinction was made between "wet" pyroclastic surge deposits and "dry" surge deposits while differentiating the facies at Cerro Pinto. The Tcl deposits are generally considered wet surge deposits based on the abundance of lithic clasts and bedding structures, such as anti-dunes and ripple bundles that are commonly associated with pyroclastic deposits in which water is in the liquid form at time of deposition (Chough and Sohn, 1990; Table 3.2; facies Tcl; Fig. 2.6B). The wet surge deposits also have a ballistic or fallout component evident by the presence of block sags and small accretionary lapilli beds interspersed within the deposits (Fig. 3.5). Most of the surge deposits that are part of Tp and Tpb deposits are dry surge deposits.

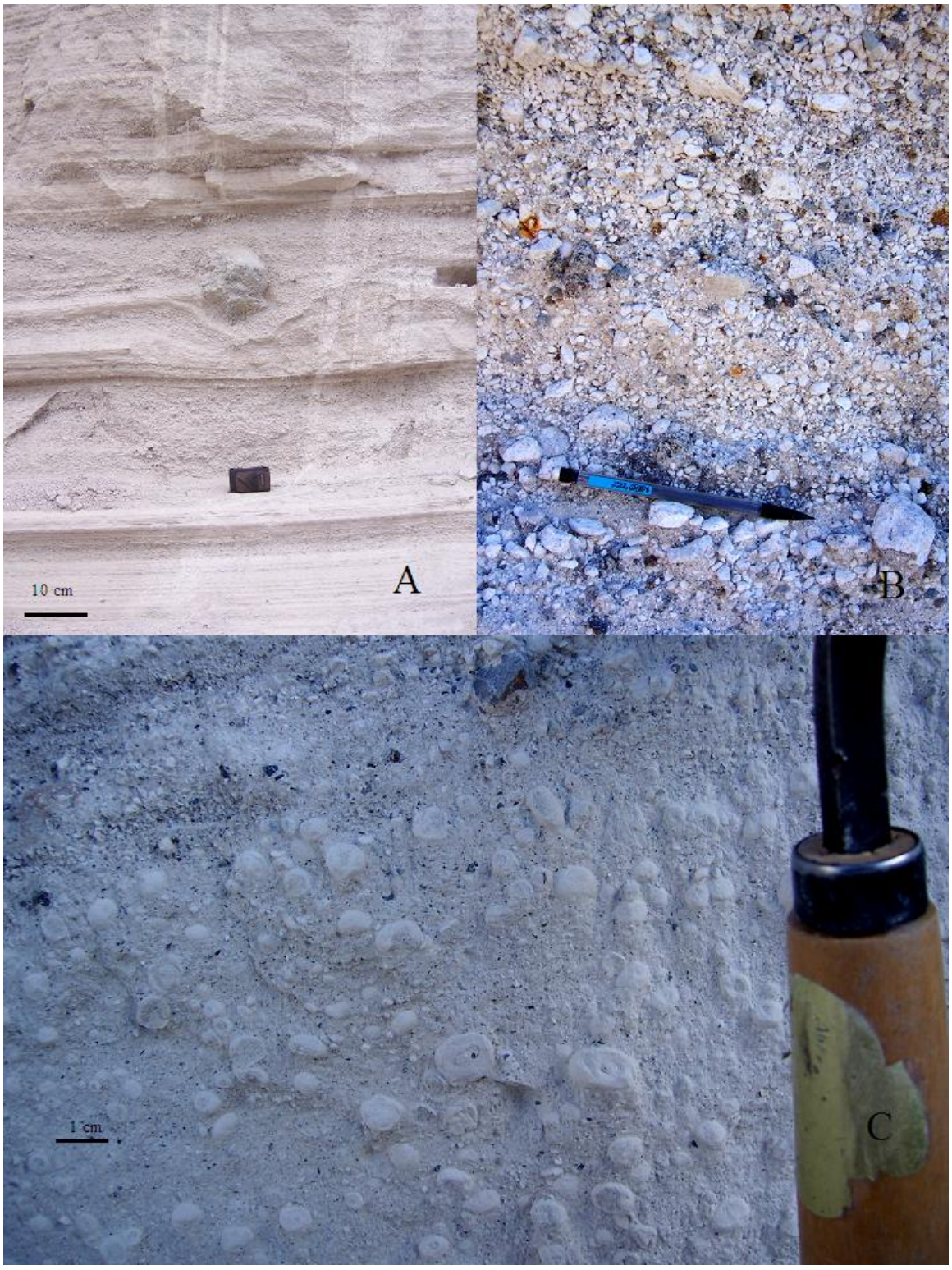

Figure 3.5. Characteristics of "wet" pyroclastic deposits; A) ballistic block sags in fallout, B) high lithic clast concentration in fallout deposit, C) accretionary lapilli in fallout.

Massive ash-rich pyroclastic tephra (Pma)

Pma deposits at Cerro Pinto are massive ash beds that are poorly sorted and matrix supported. Clasts of pumice, dome lava, and occasional lithic clasts are common. The deposits are channel confined and are commonly coarsely laminated in the upper section of the deposit. These deposits are interpreted to have been emplaced by pyroclastic flows based on their clast compositions (juvenile pumice, explosively fragmented or entrained dome material and lithic clasts), poor sorting, ash matrices, and deposit morphologies. The Pma deposits are lenticular, appearing to fill paleodrainages. Large pumice blocks are concentrated in the upper portion of the deposits, consistent with rafting of the blocks during transport.

Polylithic Interbedded Breccia & Monolithic Interbedded Breccia (Bpi & Bmi)

The interbedded breccia deposits are characterized by angular, monolithic or polylithic, clast-supported beds within a coarse- to fine-grained sand-sized matrix. The monolithic breccia clasts are solely sugary white rhyolite lava and the polylithic clasts are a mixture of banded blue and gray lava, stony white lava, and white pumice. Deposits are very poorly sorted with weak repetitious reverse grading. These deposits are found only within 400 m of the domes in inferred paleodrainages. The interbedded breccia deposits contain numerous discrete beds <1 m thick that are composed of coarse ash and individual crystals of plagioclase and occasional quartz, similar to Tp tephras (Fig. 3.6). These tephra interbeds extend to the edges of the outcrops and are thinly bedded with parallel

laminations. The tephra interbeds are not parallel with one another but rather mimic the weak tangential internal bedding structures of the breccia deposits.

Figure 3.6. Grain-flow deposit (Bpi). Note the thin lenses of finer white rhyolite tephra (<50 cm).

The Bpi and Bmi deposits are inferred to have been emplaced by gravity-driven grain-flows originating from growing domes that traveled down slope into drainages and filled in the topographic lows surrounding the domes in the south ring. The interbedded tephra deposits within the coarse beds were deposited as fallout and pyroclastic surges from explosive eruptions occurring in the north ring between grain-flow events. Because the grain flows were dense and coarse, they did not settle to a flat, uniform surface, but instead settled as undulating lobes extending out from the base of dome I and filling in localized topographic lows. The fall and surge deposits that were subsequently deposited on top of the grain flows retained the undulose shape of the underlying grain flows.

The grain-flow deposits extend up to 300 m laterally from their source domes and preferentially filled paleo-drainages. The apparent dips of the grain-flow beds also vary from nearly horizontal to greater than 30 degrees. The height to runout ratios for these deposits are as high as 0.24. This value is right at the boundary between volcanic debris avalanches and non-volcanic landslides (Siebert, 1984). Based on the preferential distribution of the grain-flow deposits in drainages and the presence of an ash matrix, it is believed that there was a dry-flow component to the depositional mechanism. If the flow was wet, like a debris flow, then the ash component would have been preferentially removed. The flow was probably a result of the steep gradient of the source dome, the large mass of the flows themselves, and the presence of a fine-grained matrix to act as a lubricant for the flow. While the grain flows were more mobile than rock falls or talus slopes, they were not sufficiently fluid to make them synonymous with debris flows.

The grain-flow deposit originating from dome I (Bpi), as identified by phenocryst assemblages, contains interbedded fallout deposits originating from the northern tuff ring (Tp) (Fig. 3.6). This places a temporal constraint on the deposition of these grain-flow deposits, indicating that they were emplaced while explosive activity was occurring in the north ring. The most likely scenario is that explosive activity migrated from the south ring to the north ring while dome I was still unstable and shedding large volumes of dome material in mass movements. These grain-flow mass movements spent only a few seconds in transit from the domes to the lower reaches of the paleo-drainages.

Across the entire dome complex, there is no evidence of a hiatus in the eruption lasting for more than a few hours to days. It is likely that all of the grain-flow deposits were deposited in fairly quick succession, allowing time for 10-50 cm of tephra to accumulate between collapse events (Fig. 3.6). The interbedded tephras are dominantly fine-grained fallout, but some fine-grained surge deposits may also have been preserved as the two mechanisms were depositing simultaneously.

An alternate mechanism for the formation of these interbedded breccia and ash deposits would be to consider them the products of very coarse Peléean-type pyroclastic flow produced during dome collapse. During the collapse, fine fallout was produced by pulverization of dome material and was convected for a short period of time before settling out on top of the coarse flow deposit. Peléean-type flows were triggered by

explosive disruption of a growing lava dome as at Mount Lamington, Papua New Guinea, in 1951 (Taylor, 1958) and at Soufriere Hills Volcano (Boudon et al., 1984).

This decoupling phenomena has also been observed in high-density pyroclastic currents (Fisher, 1995). A decoupled pyroclastic flow is capable of producing both the coarse deposits in the near-ground, high-density current and the finer deposits in the low-density, co-ignimbrite surge clouds. Whether a flow decouples or not is contingent on variations in water content, topography, and grain densities (Fisher, 1990). The topography surrounding dome I during the emplacement of the grain-flow deposits (Bpi) was likely steep and undulating due to the rim of the southern crater and the proximity of dome II. Any flows shed off of dome I would have encountered steep terrain within a few hundred meters of its origin. The increased turbidity produced by the collision between a flow originating at dome I and steep topography of the surrounding tuff ring may have caused the flow to decouple. The grain-flow deposits have much higher clast percentages than the pyroclastic flows that Fisher (1995) discussed and the sizes of the flows described by Fisher (1995) were also much larger than Cerro Pinto would have produced. However, because ash is still a primary constituent of breccia deposits and since density stratification is an important aspect of decoupling flows, it is possible for pyroclastic flows to produce small co-ignimbrite surge clouds (Fisher and Schmincke, 1984).

Valentine and Fisher (2000) postulate that co-ignimbrite pyroclastic surges can also be produced when a dome fails and blocks of dome lava break explosively, generating dust and dilute pyroclastic density currents ahead of the block-and-ash flows. Surges and

block-and-ash flows produced in this manner would be distributed in only a single direction and would be preferentially deposited in topographic lows. The grain-flow deposits at Cerro Pinto have the elongate, sinuous distribution of channel-influenced flow deposits, but are simply too coarse and matrix poor to be considered analogs for pyroclastic density currents (Fig. 3.1). Additional work, including fractal analysis of clasts and componentry analysis and granulametric studies of the interbedded ash deposits could help identify the source location and depositional mechanism of the ash beds and the grain-flow deposits.

Monolithic Breccia & Monolithic Ash-rich Breccia (Bm/Bma)

The monolithic breccia comprises a lower member, Bma, and an upper member, Bm that are differentiated by the presence of white ash within the matrix (Table 3.2; Fig. 3.7). Clasts within the Bm are sub-angular blocks of banded, stony rhyolite (<20 cm) within a gravel matrix. The Bma has the same clasts in an ash to gravel matrix. The monolithic breccia is characterized by multiple weakly graded and moderately sorted beds within a single massive unit. The bedding structures are weak and only locally identifiable in the outcrop. Obvious cross-bedding structures and rare block sags and accretionary lapilli are found in the upper beds of the Bm deposits.

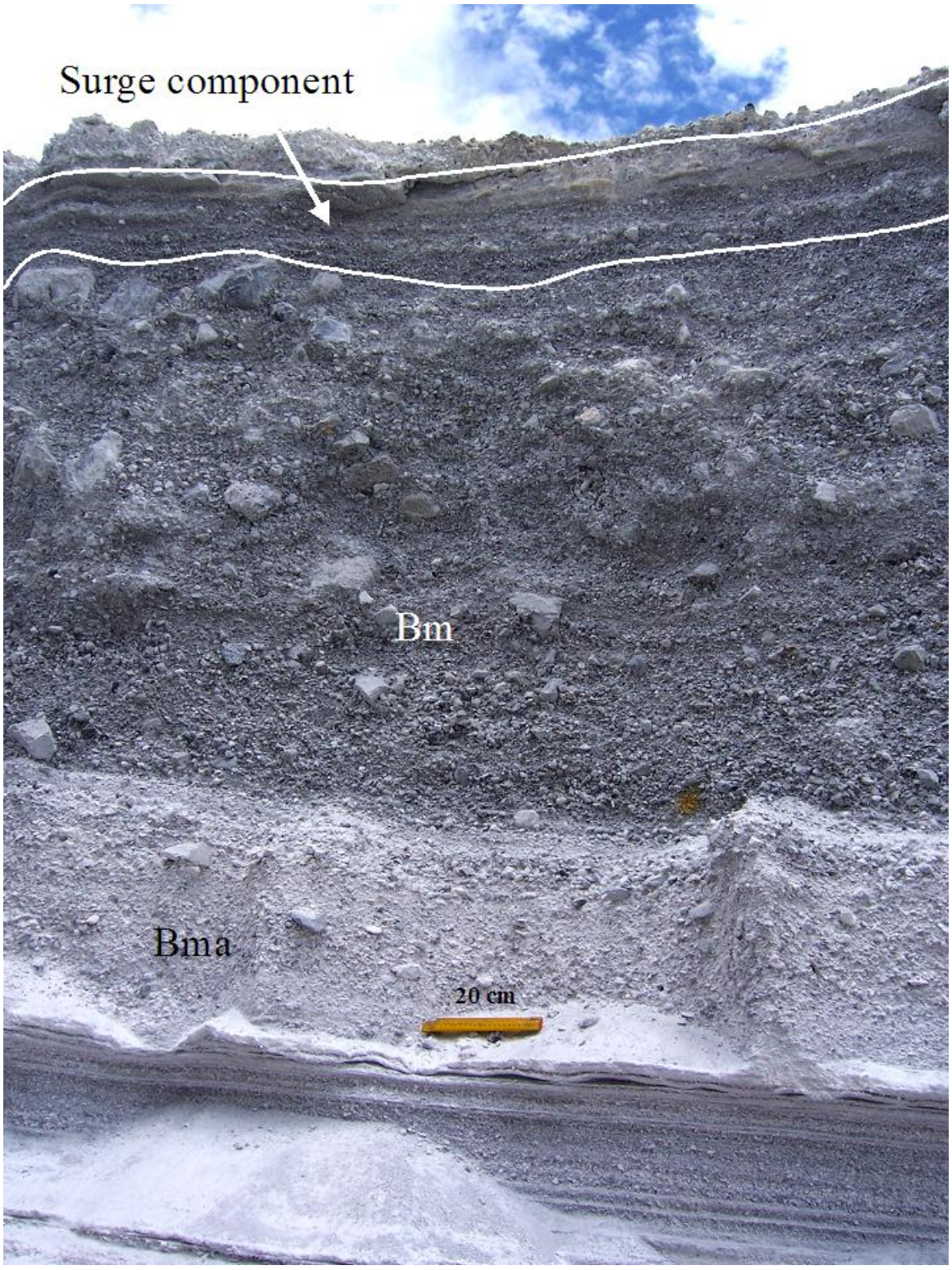

Figure 3.7. The maelstrom deposit. Note the sharp contact between the Bma and Bm deposits. Cross-bedded component of the Bm deposit is ~20 cm thick at this location.

In a plot showing grain-size distributions, two major population peaks (-6.33, -2.56 phi) and numerous minor population peaks (-1, 1, 2) were identified (Fig. 3.8). The –6.33 phi spike represents a ballistic block component of the deposit. These blocks are angular and glassy and composed of stony white rhyolite or blue-gray banded rhyolite. The –6.33 phi population accounts for nearly 28% of the total weight percentage despite having very few clasts. The second major peak occurs around –2.56 phi and is composed primarily of angular glass shards (50%), finely vesiculated pumice (28%), and stony rhyolite (22%). The rhyolite and pumice fragments commonly display minor alteration and tend to be blockier than the glass shards. All clasts are covered in a fine ash residue, suggesting that the eruption may have been phreatomagmatic, or at least water-rich.

The minor population peaks are more subdued than the peaks at –6.33 and –2.56 (Fig. 3.8). At -1 phi, blocky, banded rhyolite (55%) that is sub-angular to sub-rounded dominates. Pumice clasts decrease in concentration as the average grain size decreases. At -1 phi, pumice accounts for 10% of the clasts and the clasts are well rounded, suggesting some aspect of flow transport. Glass shards account for 35% of the population and are blocky. A fine ash veneer covers the entire sample. This sample displays the best evidence for mechanical weathering of clasts during transport.

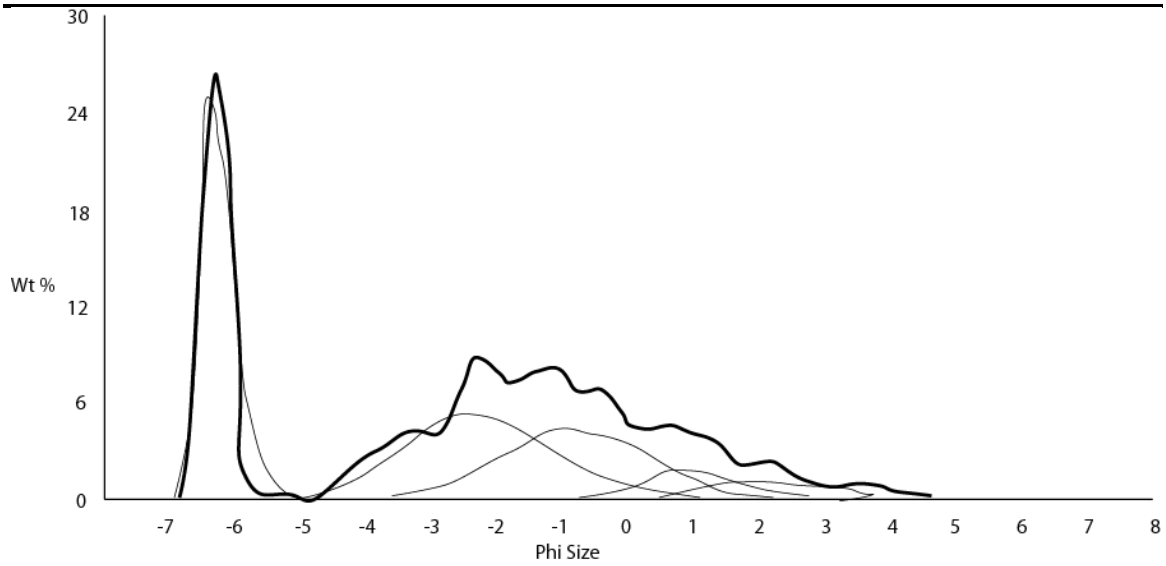

Figure 3.8. Particle distribution curves for the maelstrom deposit. Light gray curves represent localized population spikes at –6.33, -2.56, -1.07, 0.90, 2.12, and 3.97ϕ.

At 1 phi, pumice is even more rare (4%) while volcanogenic crystals (20%) and lithic clasts (1%) are present. Glass shards are both angular bubble-wall shards and heavily fractured blocky clasts, making up ~65% of the population. A number of eruptive characteristics are identifiable at this phi size. The shattered glass fragments and the high abundance of surficial pitting suggest that phreatomagmatism was a prevalent eruptive mechanism. The first appearance of lithic clasts at this phi size suggests that most of the incorporated country rock was pulverized to a very small median grain size. At 2 phi, the evidence of phreatomagmatism seen at 1 phi still remains; however, clean bubble-wall shards are more numerous. Glass shards, both angular and blocky account for 85% of the population.

The Bm and Bma deposits are interpreted to have been emplaced by a combination of ballistics represented by the coarse blocks, fallout represented by the lapilli-sized lava clasts that support the bed, and surge processes that are evident by the presence of cross-bedded sections of the upper bed (Fig. 3.7). All of these processes combined in the near-vent area during dome destruction. High winds may have been influential in the preferential removal of fines as well. The term “maelstrom” has been given to this depositional facies and the resulting deposit is called the “maelstrom deposit”.

Colluvium (C)

Debris-flow deposits are characterized by matrix-supported, channel-confined beds that are rich in sub-rounded lithic clasts up to 40 cm in diameter. These deposits are interpreted to represent more recent erosion of the dome complex based on their distribution solely within the lower portions of modern drainages. Deposits characterized by reversely graded and angular clast-supported beds of stony rhyolite with a coarse sand-sized matrix of lithic clasts are considered recent talus deposits. These deposits are poorly consolidated, and tend to form slopes at the angle of repose and are not overlain by any pyroclastic materials originating from Cerro Pinto. Consequently, it is inferred that the deposits were emplaced well after volcanic activity at Cerro Pinto had ceased.

CHAPTER IV

HISTORY OF CERRO PINTO

Cerro Pinto's evolution occurred in three major eruptive stages; Stage I - southern tuff ring activity; Stage II - northern tuff ring activity; and Stage III - final dome emplacement. Each eruptive stage began with an explosive event in which tuff rings or explosion craters were formed and was followed by effusive dome growth. New eruptive stages were designated by shifts back to explosive volcanism following passive dome emplacement. Vent migration accompanied each new eruptive stage, but also occurred within single eruptive stages. For example, during Stage II, three tuff rings were produced by eruptions at three different vents.

$^{40}Ar/^{39}Ar$ dating of sanidine in juvenile pumice from the northern tuff ring have given Cerro Pinto an age of 62 +/- 8 ka. It should be noted that this date is not very reliable as the step-heating process returned highly variable data (Lisa Peters, Personal Communication, 2006; Appendix B). Because field evidence suggests that there was no significant hiatus in activity during the emplacement of Cerro Pinto, the date from the north ring is inferred to approximate the age for the structure as a whole.

Stage I - Southern Tuff Ring Activity

Stage I – Pyroclastic Phase

Volcanic activity began with the explosive emplacement of the southern tuff ring (Fig. 4.1A; ~ 0.35 km^3) that emplaced tephras onto a landscape of middle-Tertiary plutons and Cretaceous limestone that currently dips ~7 degrees to the north (Plate 1). The southern tuff ring is composed of Tpb tephras (Table 3.2; Fig. 4.2). The presence of poorly sorted hybrid surge-fallout deposits, especially on the southern rim of the ring, suggests that both fallout and pyroclastic surges were being produced simultaneously. The eruption columns that produced these deposits did not entrain enough air to attain positive buoyancy and consequently, density currents containing both coarse and fine pumiceous and stony rhyolites were consistently produced from the failing eruption column along with a small quantity of fallout (e.g. Houghton et al., 2004). Most of the fallout lapilli from the eruption column were entrained into these surges and deposited in surge-fallout hybrid deposits. Surge deposits, both wet and dry, are common in areas proximal to the source vent and in areas of high topography and are rare on the outer flanks of the tuff rings, with the exception of the southern end of the southern tuff ring where surge deposits are up to 10 m thick.

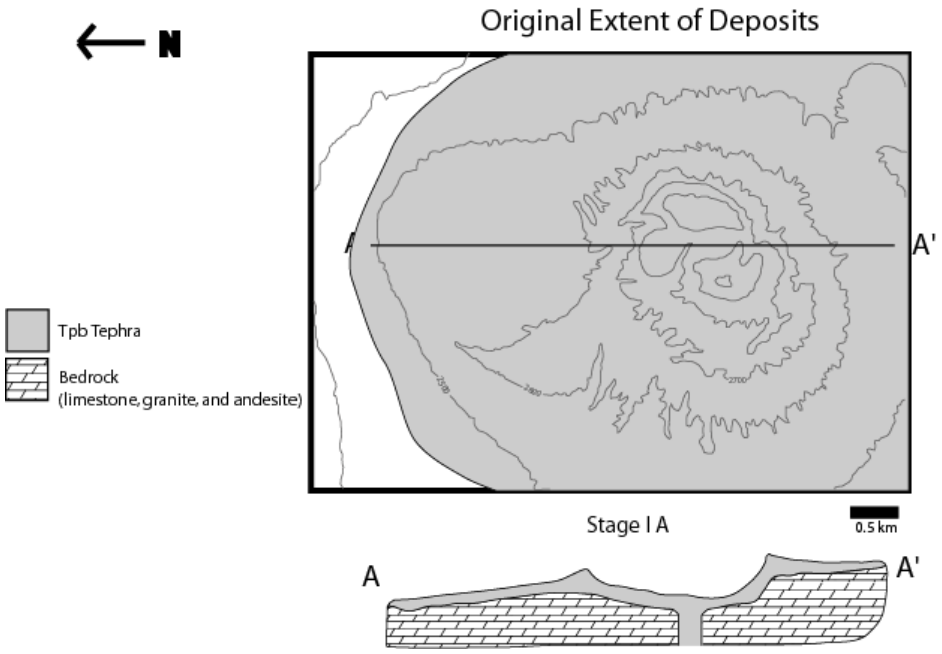

Figure 4.1a. Evacuation of bedrock in an explosive event produced a crater covered with tuff. The tuff is rich in biotite and plagioclase phenocrysts. Vertical exaggeration of cross sections are ~2x.

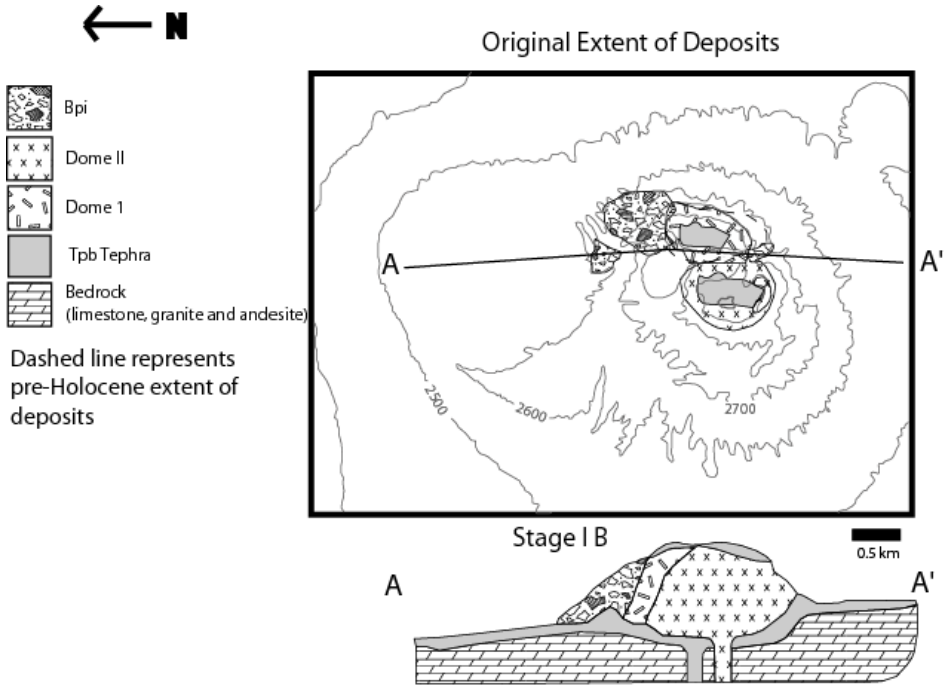

Figure 4.1b. Dome I was emplaced followed by dome II. Dome I produced two large talus deposits. Dome II produced no major volcanogenic mass-flow deposits. Tpb tephra was uplifted by both these domes and remains atop them today.

Key for stratigraphic sections

Fine, thinly laminated ash beds. Well sorted. Beds 1-5 cm.
Fallout

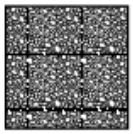

Clast-supported bed of angular coarse lapilli. Well sorted. Beds 10-40 cm.
Fallout

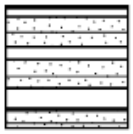

Medium-grained lapilli with ash interbeds. Well sorted. Beds 2-6 cm.
Fallout

Lapilli in parallel-laminated beds with outsized clasts and lithic clasts. Beds 5-10 cm.
Fallout

Cross-bedded deposits of med-grained lapilli with outsized clasts. Beds 5-15 cm.
Surge

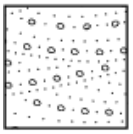

Cross-bedded deposits of lithic-rich lapilli. Beds 5-20 cm.
Surge

Clast supported massive bed of coarse banded rhyolite. Very poorly sorted. Beds .2-1 m
Maelstrom

Coarse angular clasts in ash matrix. Interbedded ash beds. Poorly sorted. Beds 1-5 m.
Grain-flow

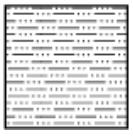

Parallel laminated, poorly consolidated deposit of very well-sorted sand. Beds 1-2 cm
Fluvial

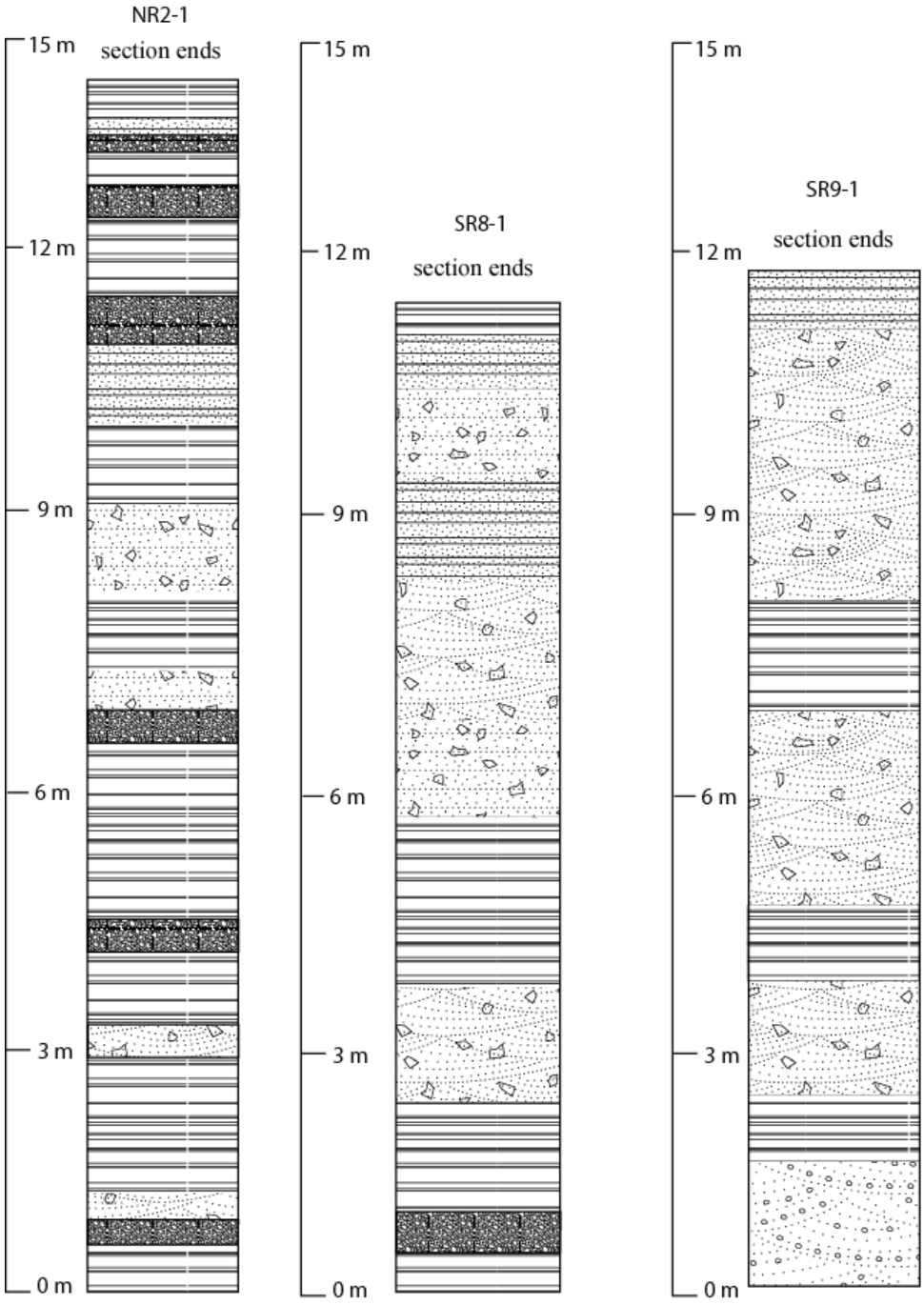

Figure 4.2. Three stratigraphic columns from the Tp and Tpb facies emplaced during Stage I and early Stage II. NR2-1 is representative of fallout-dominated tephras. SR8-1 is the result of a combination of fallout and surge processes. SR9-1 is representative of surge-dominated tephras. All stratigraphic section locations are shown on Plate 1 and explanation of patterns is located on pg. #59.

Early Dome Emplacement

As the energy of the initial eruption waned, dome I was emplaced within the southern tuff ring (Fig. 4.1B). A shell of autobreccia surrounded the dome upon emplacement. During its growth phase, dome I produced at least two grain-flow deposits (Bpi) that filled in much of the valley between the northern flank of dome I and the edge of the tuff ring (~200 m to the north). Numerous discrete lenses of ash originating from the north ring (Tp) are interbedded within the grain-flow deposit (Fig. 4.3).

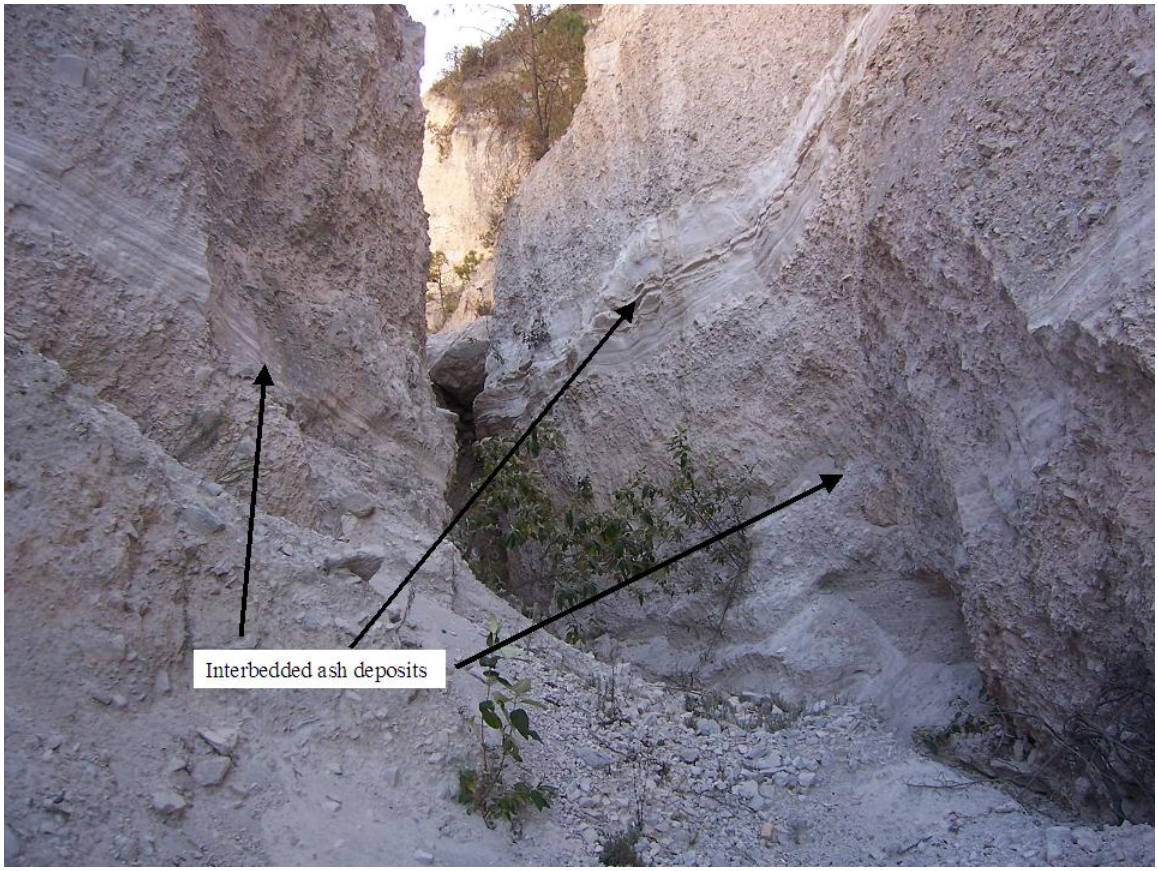

Figure 4.3. Bpi with interbedded ash deposits originating from the north ring. Ash interbeds are 35-50 cm thick at this location.

Dome II was emplaced to the west of dome I (Fig 3.1). There is no evidence of erosion between volcanogenic deposits originating at dome I and dome II, suggesting that the change in vent location was quick, possibly with no appreciable break in activity. Significant differences in hand sample between dome I and dome II lava (e.g. phenocryst assemblages, banding, and groundmass characteristics) indicate that the two domes are likely separate volcanic features, however it is possible that these differences reflect variations in the post-emplacement cooling processes of the domes (e.g. devitrification, strain rates, etc.) (Table 3.1). Endogenous growth of dome I and later dome II uplifted the Tpb tephra that was on the floor of the southern tuff ring prior to dome emplacement. Today, undisturbed beds of Tpb tephra are exposed near the summits of domes I and II (Fig. 4.4). Along the flanks of each dome, uplifted south ring (Tpb) tephras are deformed and bedding structures are weak to absent despite excellent exposure. Dome II is similar in elevation (~ 3000 m) and volume to dome I (0.21 vs. 0.26 km^3), but is distinct in hand sample and produced no grain flows during its emplacement.

Because of the lack of continuous exposure, internal structures, such as flow banding patterns, were very difficult to discern on the large scale. However, in hand sample, linear flow structures that indicate shearing stresses, such as asymmetrical folds, are ubiquitous. According to Christiansen and Lipman (1966), the quantity and sinuosity of flow structures tends to increase in near-vent areas of domes, where the lava was hottest and most mobile. Flow banding severity could not be used to locate vents due to insufficient exposure, but it was used to help correlate mass-flow deposits (such as those from debris

flows, pyroclastic flows, and talus) with their origins. Dome I has significantly more flow banding than any of the other domes and is easily recognizable in hand sample.

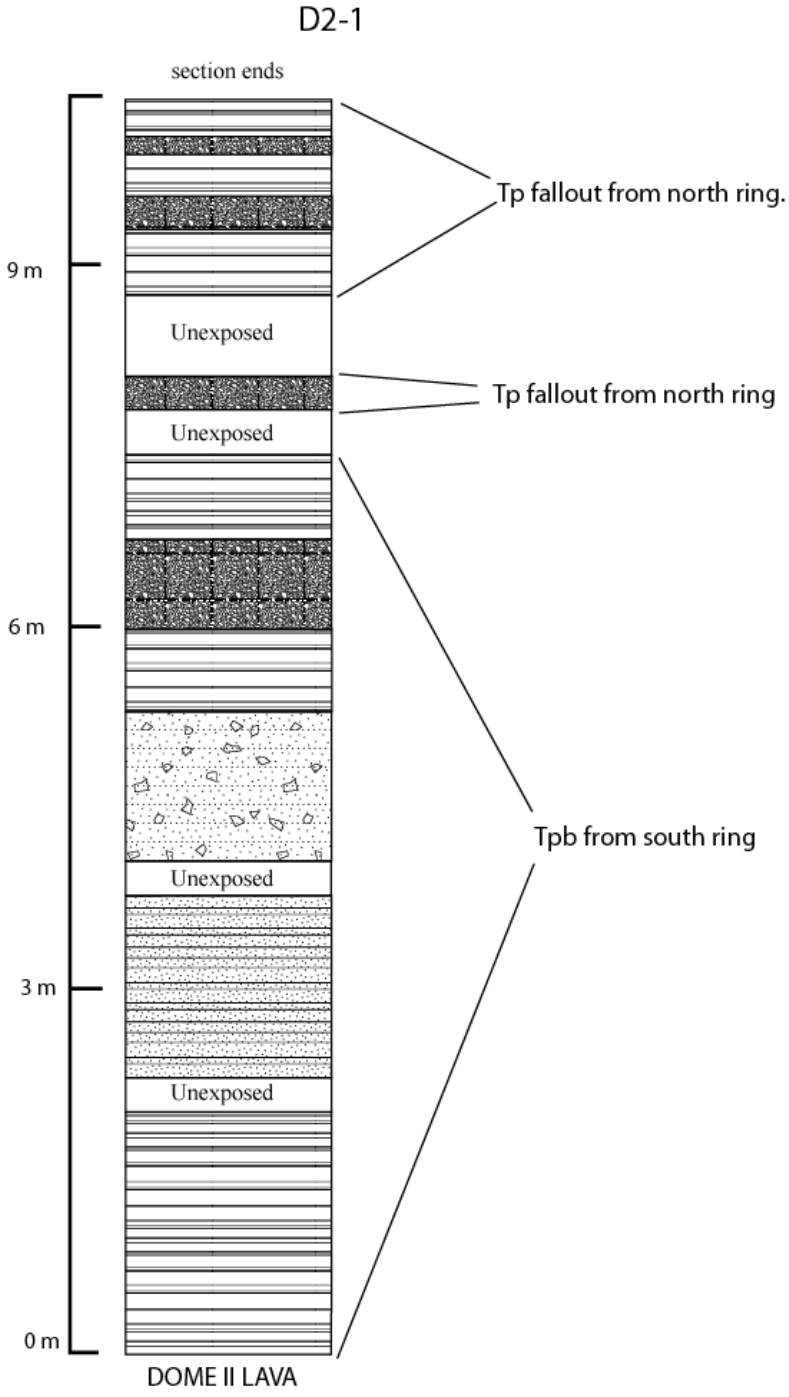

Figure 4.4. Stratigraphic section showing fallout deposits topping dome II. Composite section over 50 m. See pg. 59 for explanation of patterns.

Vent locations were inferred using modern dome topography and tuff ring morphology (Fig. 4.5). The idea is that the domes were thickest directly above the vent and vents should be under the areas of highest modern topography assuming a uniform erosion rate. The vent locations for the tuff rings were inferred through identifying the curvature of the rings based on their residual structures and extrapolating their total extents, placing the inferred vent in the middle. No evidence was found of any of the vents in the field and both of the aforementioned methods are considered approximate. The vents appear to align in correlation with the regional north/south tectonic trends described by Campos-Enríquez and Garduno-Monroy (1987) suggesting that pre-existing fractures in the bedrock may have influenced the magmatic pathways. Grain-flow deposits from Stage I are interbedded with tephra from Stage II, suggesting that little time elapsed between the two stages and that dome I was still unstable even as activity migrated to the north ring (Fig. 4.6).

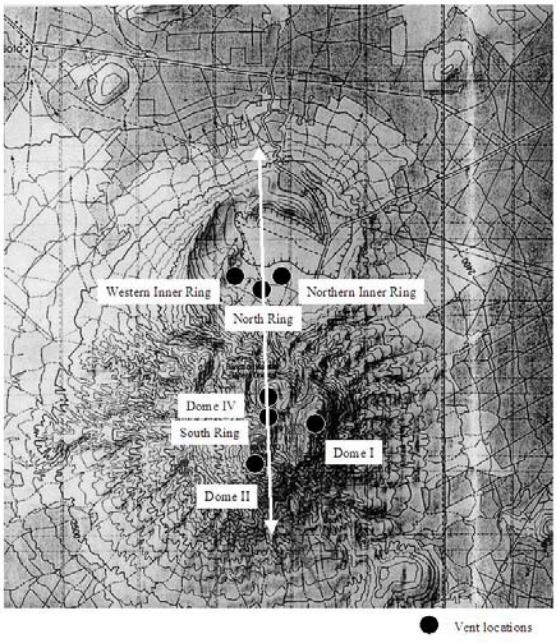

Figure 4.5. Stratigraphic section locations and inferred vent locations. Note the north/south alignment of the vents.

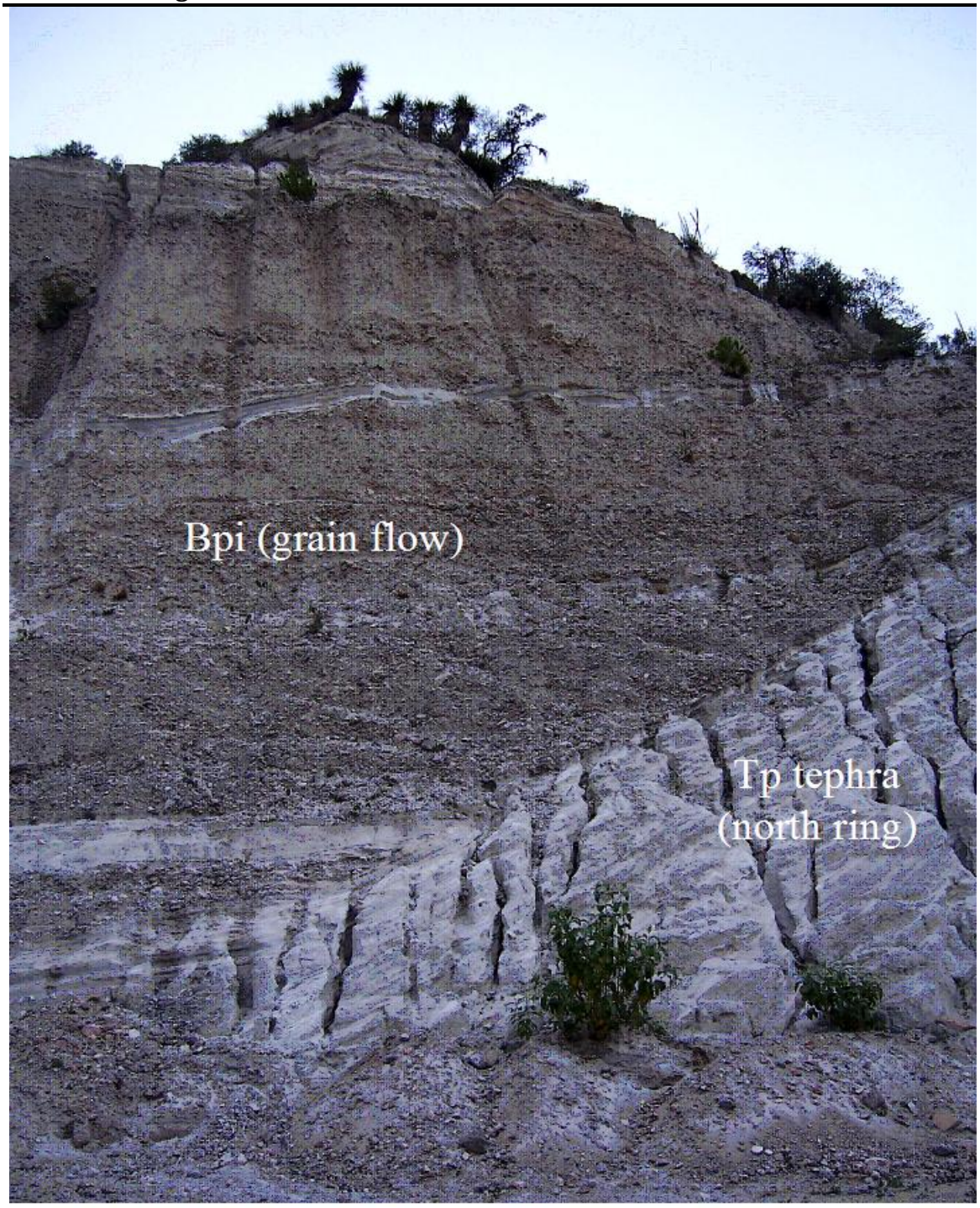

Figure 4.6. This exposure shows that the grain-flow deposit was channeled to the north by pre-existent north ring tephra. The interfingering of the two deposits suggests that they were deposited concurrently.

Stage II - Northern Tuff Ring Activity

Pyroclastic Phase

With no significant hiatus in the eruption, explosivity activity recurred, excavating a second tuff ring to the north (Fig. 4.7A; ~0.38 km^3). The basal 5-10 m of the northern ring is composed of cross-bedded, lithic-rich tephra (Tcl) and the remainder is composed of pumice tephra (Tp) (Fig 4.8). A thin, well-sorted bed, interpreted as a fluvial deposit based on its erosional lower contact and sorting, marks the boundary between late Tpb deposits of Stage I and the earliest Tcl deposits (Fig. 4.9). This thin fluvial deposit is the only evidence for any break in activity between Stage I and Stage II in the complex and probably represents a few hours to days at most. Block sags, cross-bedding, lithic clasts, and accretionary lapilli are more numerous within the Tcl facies than the Tp facies. These clasts and bed forms are commonly associated with phreatomagmatic activity. Because the Tcl deposit is a maximum of 10 m thick and is typically much thinner than that, it is inferred that the water source was the limiting reagent of the phreatomagmatic eruption. Once the water source was exhausted, the eruption continued as strictly magma-driven, producing dominantly dry surge and fallout deposits (Tp). The block sags and bed forms also aided in distinguishing source vents from one another in areas where northern and southern ring tephras were present.

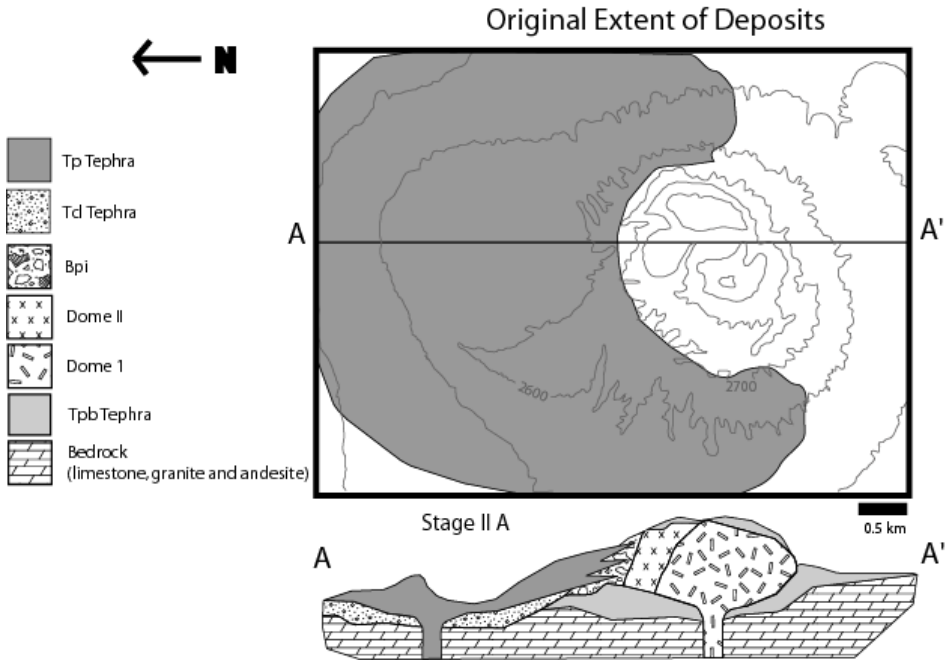

Figure 4.7a. Eruptions formed the north tuff ring that includes a thin (<10 m) layer of Tcl tephra overlain by Tp tephra. A later eruption formed the northern inner ring that is entirely Tp tephra.

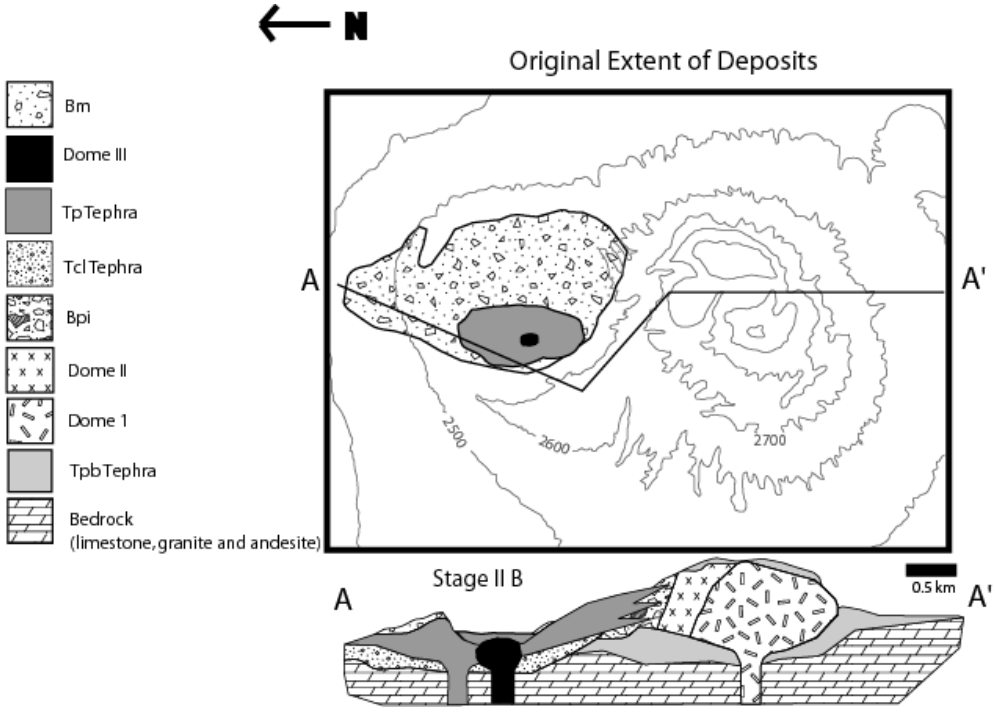

Figure 4.7b. The western inner ring was emplaced along with dome III. Destruction of a dome within the northern ring produced the maelstrom deposit. Dome III is a possible source.

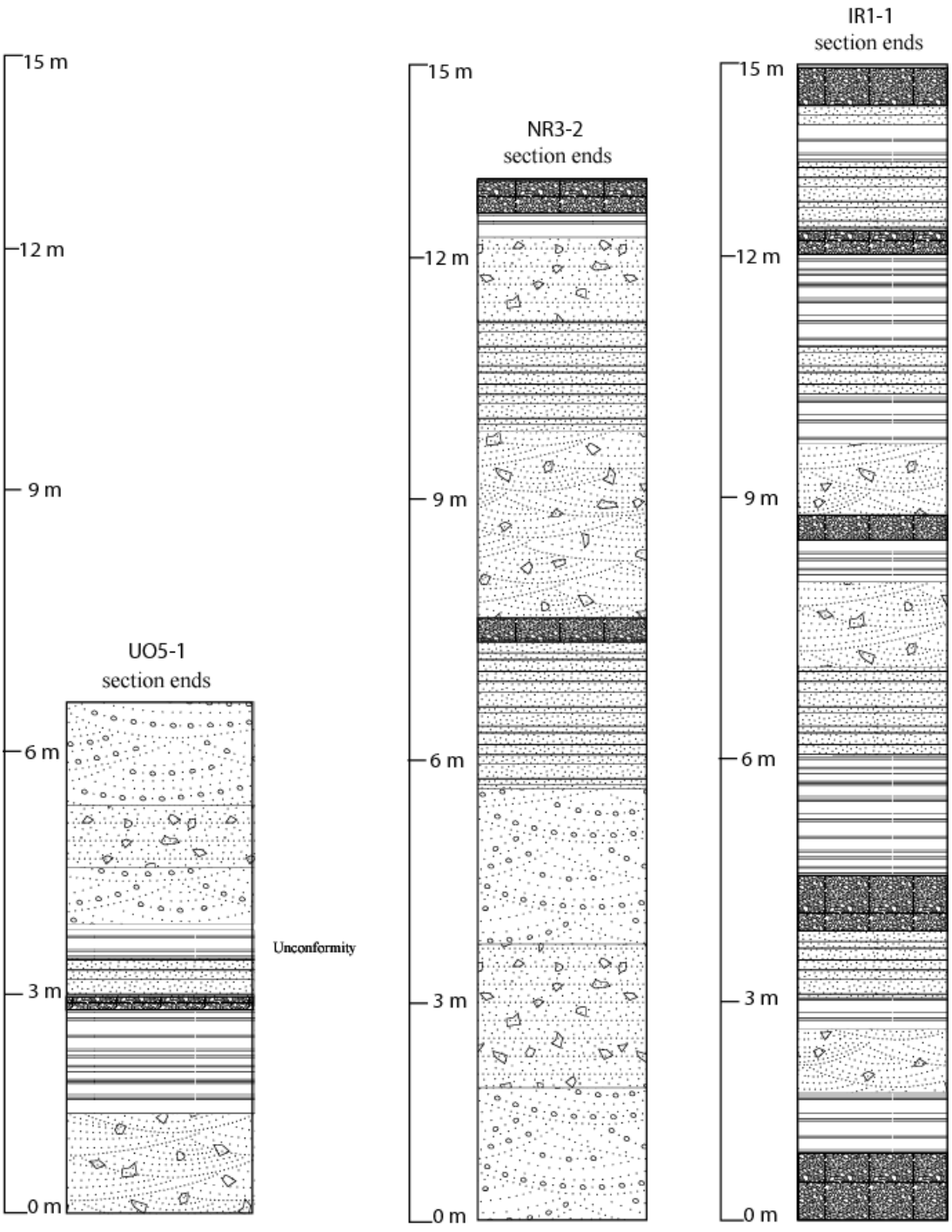

Figure 4.8. Stratigraphic sections from Stage II. UO5-1 shows the transition from south ring Tpb tephra to north ring Tcl tephra. NR3-2 shows the gradual shift from wet, lithic-rich Tcl tephra in the basal 6m to dry Tp tephra. IR1-1 is representative of the dry-fallout-dominated tephras of the inner northern rings. See pg. 59 for pattern explanations.

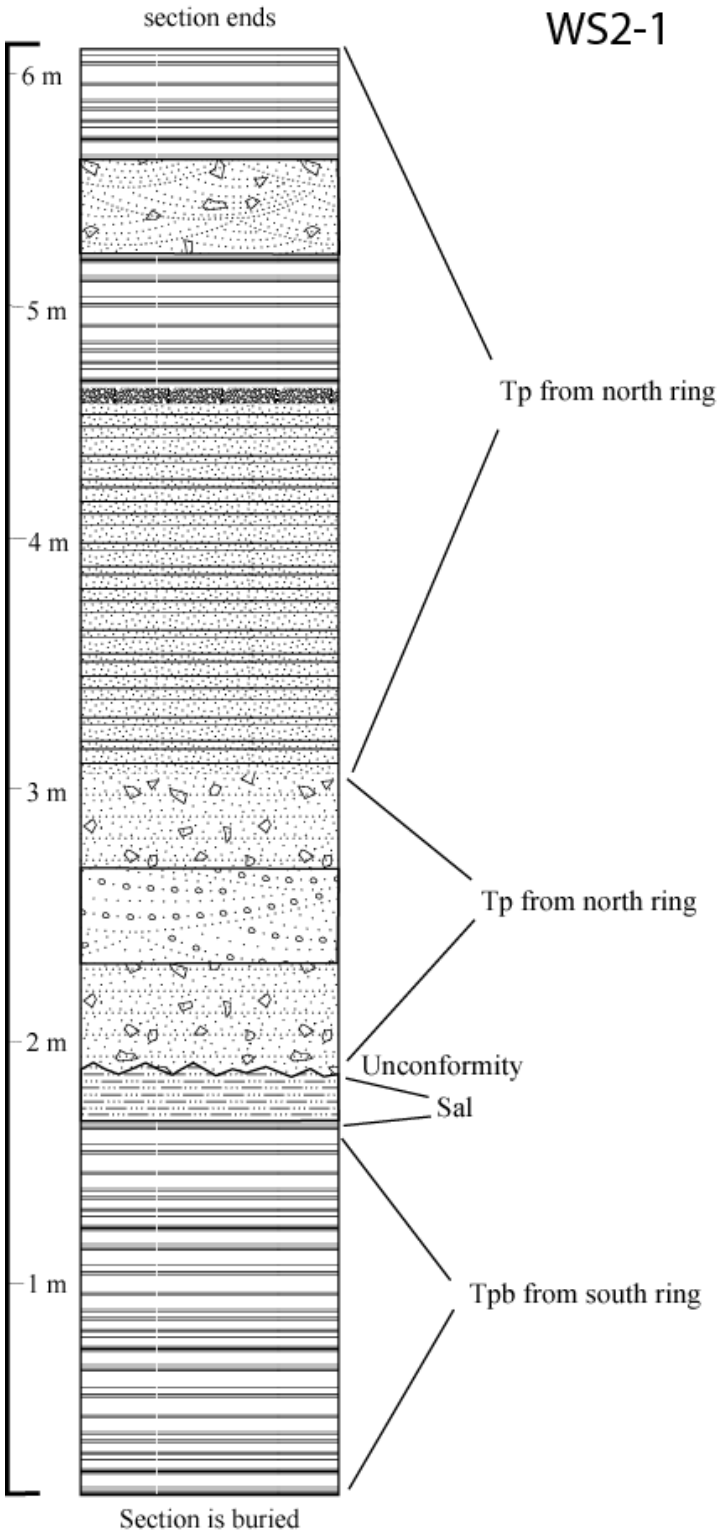

Figure 4.9A. Stratigraphic section showing the small fluvial deposit that marks the contact between south and north ring tephras. See pg. 59 for pattern explanations.

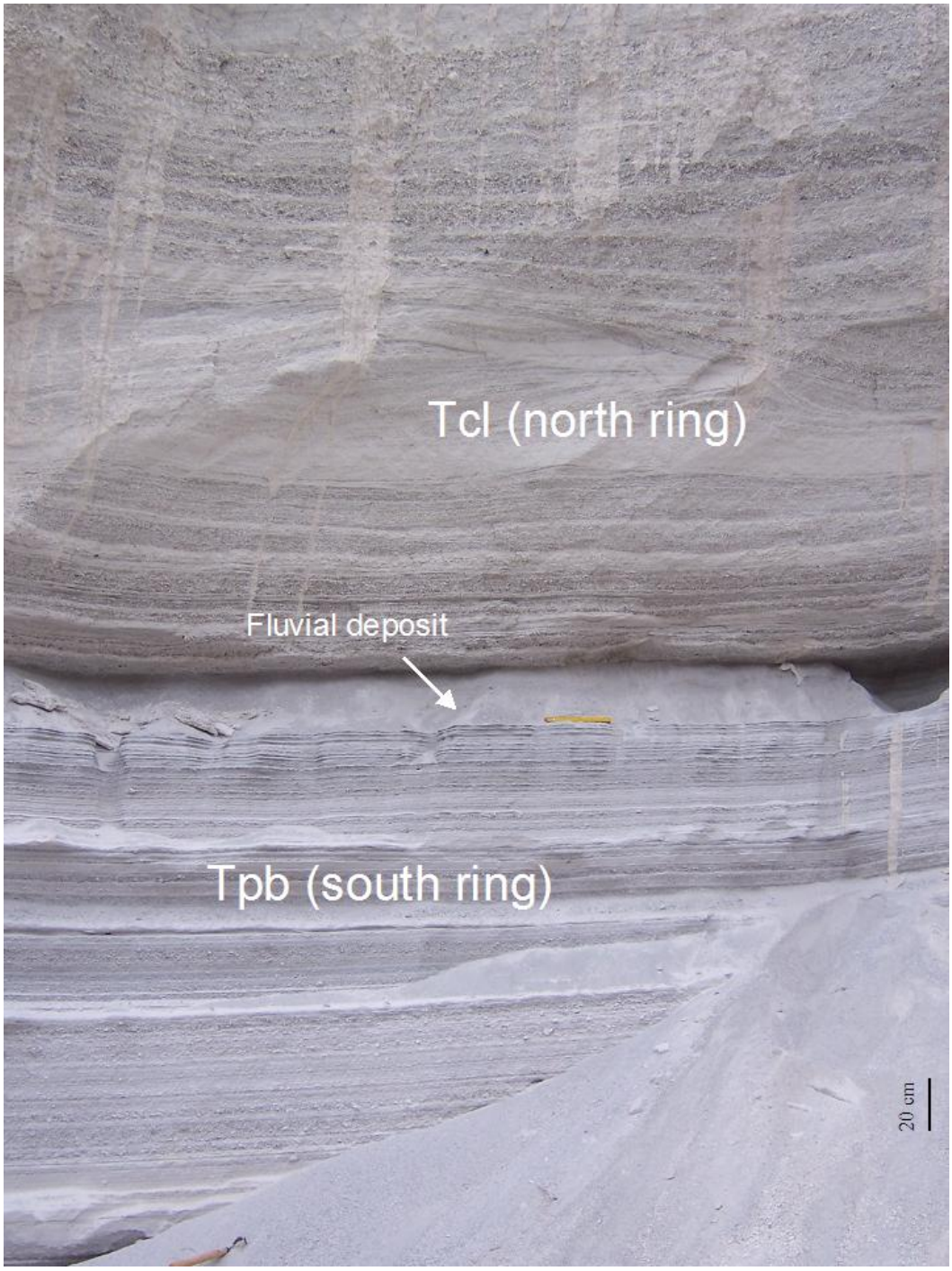

Figure 4.9B. Unconformity marked by a fluvial deposit between biotite-rich tephra (Tpb) from the south ring and cross-bedded lithic-rich tephra (Tcl) from the north ring.

Pyroclastic surges experience flow transformation through time and space as they travel away from the vent due to decreases in particle concentration and increases in traction and sorting (Chough and Sohn, 1990). Generally, this means that facies change from planar bedded to cross-bedded with dune forms possible. Pyroclastic currents are also known to increase in turbidity and change flow regimes when encountering significant changes in topography (e.g. Mt. Unzen, Japan; Fisher, 1995). At the junction between the north and south ring, north ring surge deposits (Tp and Tcl) show evidence of increased turbidity. Surge beds are thicker with undulating contacts, truncation of underlying beds is more common and anti-dunes are more common than on the other three-quarters of the northern tuff ring. During deposition, the surges that collided with dome I and dome II and those that climbed the southern tuff ring were much more turbulent than the surges that deposited over flat or gently sloping terrain.

On the outer flanks of the northern tuff ring, surge deposits are thin with parallel contacts and are difficult to distinguish from pure fallout deposits. Dune forms are not common. Thin beds (<1 cm) that are traceable over long distances are fallout beds while beds that pinch out are considered surges. Where exposures are small and poorly exposed, differentiation is impossible.

Eruptions that produce tuff rings begin with water/magma explosions occurring at shallow depths and this locus deepens through time as the vent clears and widens (Chough and Sohn, 1990). Based on the small volume of the crossbedded lithic-rich tephra (Tcl) deposits, it can be inferred that the Stage II eruption ejected lithic clasts only

during the initial phreatomagmatic vent-opening eruptions. The pumice tephra (Tp) deposits include occasional biotite-rich pumice tephra (Tpb) clasts that can be attributed to entrainment of previously deposited Tpb tephras by the north ring eruptions.

Vent migration during this eruption produced a third tuff ring located within the northern tuff ring. This ring is referred to as the northern inner (Fig. 3.1). Tp fallout and surge deposits from the northern inner ring are not as widely distributed as north ring tephras, but the northern inner ring deposits are generally thicker, indicating that this eruption was less powerful, but more voluminous (~0.40 km^3) than that which produced the northern ring. The basal deposits of the northern inner ring contain very few lithic clasts (Fig. 4.10; Fig 4.8), suggesting that the eruption was very shallow, perhaps mixing previously erupted biotite-rich pumice (Tpb) with juvenile pumice tephra (Tp).

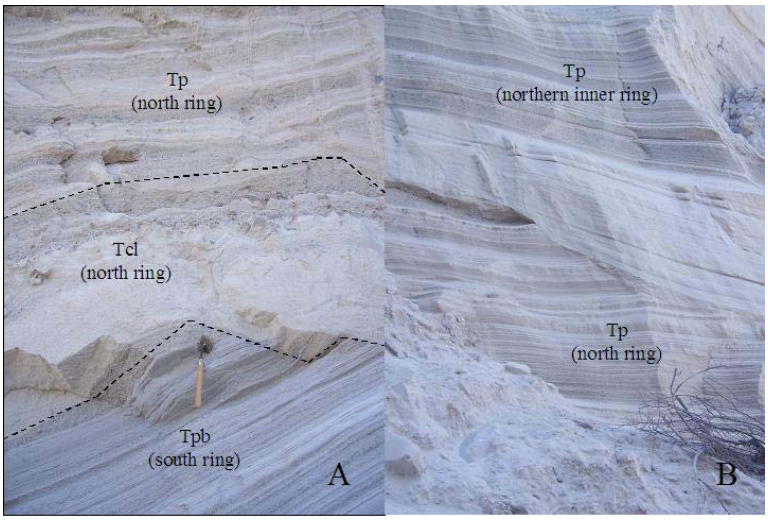

Figure 4.10. A) A contact between biotite-rich pumice tephra (Tpb) and a relatively thin coarse lithic-rich tephra (Tcl) bed that represents the phreatomagmatic stage of the north ring's emplacement. Tpb tephras are distinguished from pumice tephra (Tp) deposits by the presence of large biotite phenocrysts in the Tpb. B) Inferred contact between Tp tephras of the north ring and Tp of the northern inner ring tephras. The tephras are indistinguishable in hand sample and contacts are primarily identified by angular unconformities.

The western inner tuff ring, an oblate ring elongated north/south, was then emplaced within the northern tuff ring (Fig. 4.7B; ~0.015 km^3). This ring is dominated by Tp fallout and surge deposits that were deformed by the intrusion of a small dome (dome III). Bedding structures of the western inner ring are very difficult to distinguish and outcrops are small and localized. The overall topography of the western inner ring is much more subdued than any of the other tuff rings at Cerro Pinto. Because of the lack of good exposures and the petrologic similarities of all Tp tephras, the extent of the western inner ring tephras is not well constrained. The nesting of the northern rings suggests a gradual decrease in the overall energy of the eruption as time progressed with the western inner ring representing the last and least powerful tuff ring eruption of Stage II.

Dome Emplacement and Maelstrom

Stage II continued with the effusive emplacement of a small dome (dome III) within the western inner ring. The dome is exposed at only a single, 3-meter-high exposure and it is possible that dome III was a cryptodome that did not emerge from beneath the uplifted tephra blanket during its emplacement (Fig. 4.11). The dome lava is punky and internal structures are masked by alteration. A few small outcrops of heavily altered tephra are located 100 m south of the dome III exposure. The tephra is red-orange and cemented, making the identification of individual clasts difficult. The alteration is likely due to partial saturation by ground and meteoric water while the intruding dome was still hot. XRD analyses on the altered dome cement could prove or disprove this hypothesis.

The final event of Stage II was the explosive destruction of a dome that produced a maelstrom deposit that covers much of the northern tuff ring and extends up to 1 km northeast of the north ring's rim (Fig. 3.1). The maelstrom deposit resulted from interplay of flow, fallout, and ballistic processes in the near-vent area. High winds associated with the explosive eruption may also have played a significant role in the distribution of the fallout deposits as well as reworking finer deposits. The maelstrom deposit is a two-part monolithic breccia with clast-supported beds characterized by minor laminations of coarse material. The deposit comprises a lower, ash-rich breccia (Bma) and an upper, ash-poor breccia (Bm), capped by a cross-bedded, thin, moderately sorted undulating bed that contains block sags and accretionary lapilli (Fig. 3.7). The change in ash content between the two breccias represents either a change in the efficiency of the eruption or a change in the pulverized dome material. Due to the similarity of the monolithic clasts, it does not appear to be a change of dome material.

In outcrop, the maelstrom deposit appeared to be a coarse fallout deposit or a clast-rich pyroclastic flow. Clean, angular bubble-wall shards in the ash fraction and rare block sags show a fallout component. The rounding of the pumice and some of the rhyolite clasts at the 1 phi grain size suggest transport by a flow mechanism. Evidence is also strong for efficient phreatomagmatic fragmentation during the eruption that affected the smaller grain-size populations the most. This is evident in the ash veneer that covers most of the fine-grained clasts and the pitting of ash-size glass shards.

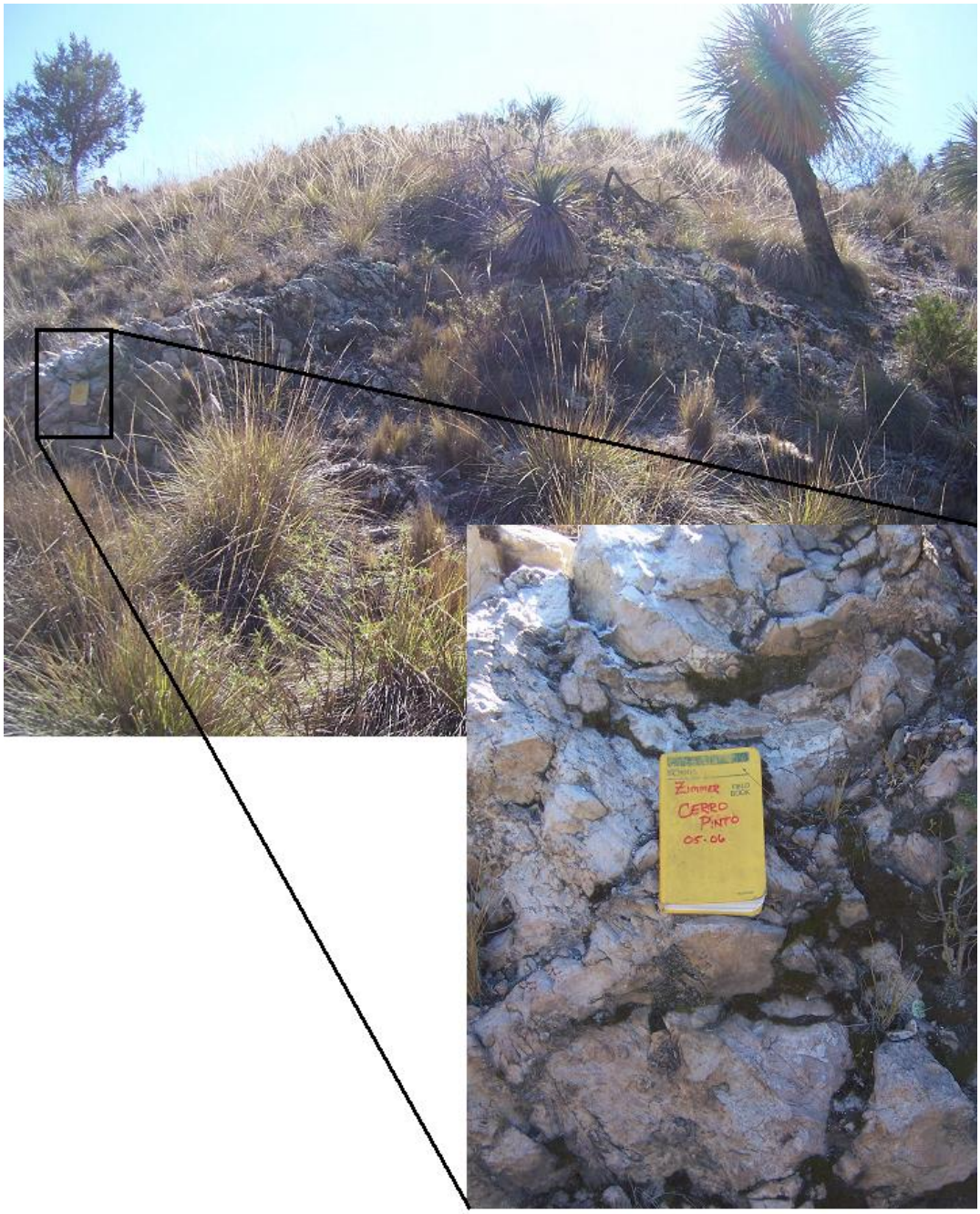

Figure 4.11. Remaining exposure of unaltered Dome III lava. Hydrothermally altered dome material is also present in the area.

The maelstrom deposit has a granulometric histogram that resembles a pyroclastic surge or a poorly sorted fallout. It has multiple grain-size population spikes and a broad bell curve indicating moderate sorting. The grain-size curve also has the relatively broad fine-skewed tail indicative of pure fallout deposits (Fig 3.8). If the maelstrom deposit was produced by only fallout, then the clasts must not have remained buoyant in a stable eruption column long enough to sort efficiently. The clasts would have to have been deposited more quickly in pulsulatory manner from the failing column, resulting in the poorly sorted deposit.

Field evidence, however, suggests that fallout could not have been the lone depositional mechanism. The heavily cross-bedded upper 0.5 m of the Bm suggests that that portion of the deposits was either emplaced or reworked by pyroclastic surges (Fig 3.7). Despite the fact that many ballistic blocks are over 20 cm in diameter, block sags or other evidence of impact are notably rare. The maelstrom deposit is primarily concentrated within the northern tuff ring but extends outside of the ring to the northeast. This deposit caps the remaining rim of the northern inner ring as well as parts of the north ring's rim and is not found anywhere in the south ring (Fig. 3.1). This distribution is uncharacteristic of most fallout.

The maelstrom deposit is comparatively thin (<30 cm) and fine grained on the outer flanks of most of the north ring as well as within the north ring. The deposit notably thins even more (<10 cm) over areas of high relief, like the rims of the north rim and the northern inner ring. It should be noted that these thicknesses are all minimum values due

to the undetermined amount of erosion that has occurred since emplacement. The maelstrom deposit's thickest exposure (<2.5 m) is located in a major drainage north of the northern tuff ring and it is not found thicker than 1 m anywhere else in the complex ,suggesting preferred deposition in a narrow band to the northeast. The greatest unit thickness correlates with the largest preserved clasts and is found just outside the northern rim of the north ring, and gradually fines farther to the north.

Topographic highs, such as the rims of the tuff rings, may have received greater amounts of weathering, but the average clast sizes of the remaining deposits in these areas are still significantly smaller than deposits preserved in topographic lows or on flat land. Erosion may have played a role in the modern-day distribution of the deposit, but the primary constraint on the spatial distribution is inferred to be the depositional mechanism. The maelstrom deposit is inferred to have been a result of a combination of ballistics, fallout, and surge processes associated with dome destruction. The preferential accumulation of the thick, coarse deposit in the major drainage north of the northern tuff ring could have been produced in two ways; 1) a northeasterly directed vulcanian blast with a large ballistic component (e.g. Shtyubel Volcano, Kamchatka, 1907; Macias and Sheridan, 1995) or 2) a laterally-directed blast and an associated clast-rich density current that preferentially flowed to the northeast (e.g. Cerro Quemado, Guatemala; Conway, et al., 1992). These two mechanisms are discussed in greater detail in Chapter VI.

The location of the source of the maelstrom deposit is uncertain. The volume of the maelstrom deposit (<0.025 km^3; Table 3.2) suggests that the initial volume of the source

dome was very small. Based solely on the spatial distribution of the maelstrom deposit and the apparent lack of any other probable sources, dome III is inferred to be the source dome for the deposit. Trace-element geochemistry (discussed in Chapter V) suggests that the maelstrom deposit is similar in composition to other structures formed during Stage II (e.g. north ring, northern inner ring, western inner ring, and dome III). However, the composition of the entire complex is so similar that it is impossible to quantifiably and definitively demonstrate that the maelstrom deposit originated from any one of these vents.

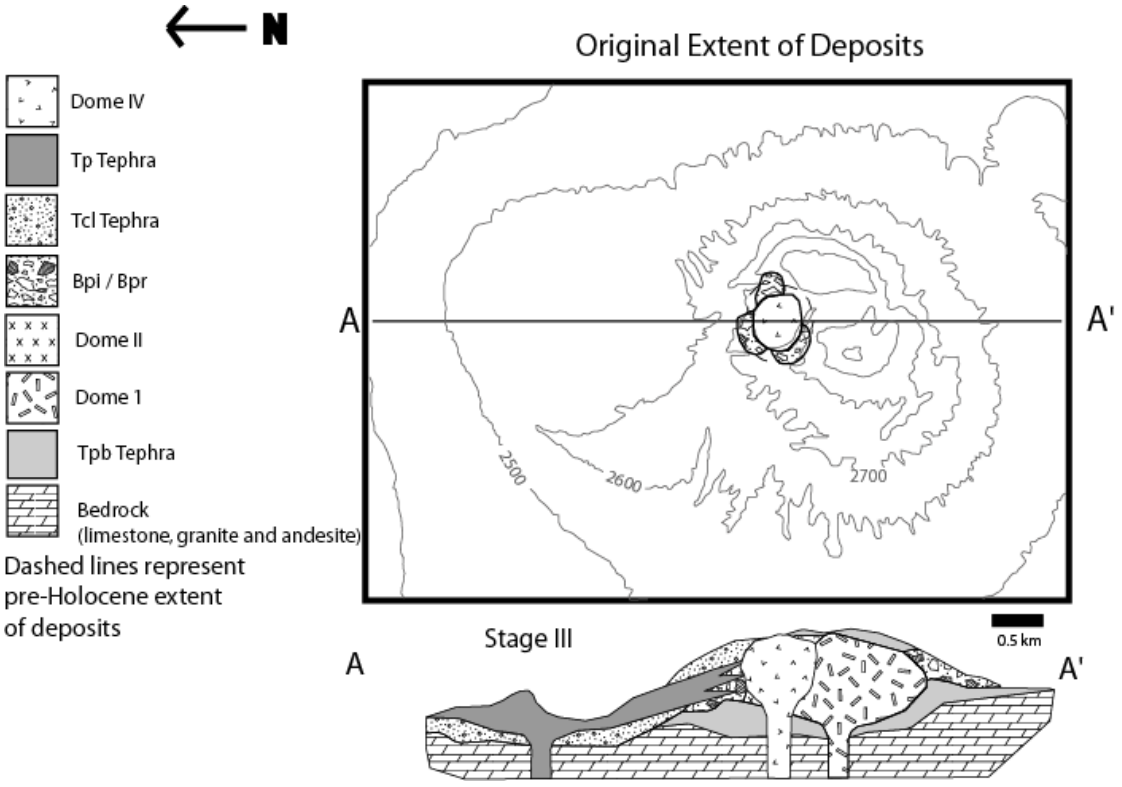

Figure 4.12. Dome IV was emplaced at the northern edge of the southern tuff ring. Dome IV produced a small grain flow to the north as well as debris flows to the southwest.

Stage III - Final dome emplacement

During the final eruptive stage, activity migrated back to the southern tuff ring where vent clearing produced an ejecta ring within volcaniclastic deposits at the northern edge of the southern tuff ring (Fig. 4.12; Fig 4.13). Moderate amounts of Tcl and Tp surge and fallout tephras are correlated with this pyroclastic phase, but the deposits are small and localized around Dome IV and in a quarry located at the contact of the north and south rings.

The tephras produced during the pyroclastic phase of dome IV do not extend out to dome III in the north ring. This makes absolute correlations between the two events impossible. It is possible that dome III was still growing as dome IV was being emplaced. The tephras from dome IV directly overlie the maelstrom deposit and so it is known that dome IV initiated after the maelstrom explosion. If dome III was the source of the maelstrom deposit, then an absolute timeline could be produced, but because dome III is not the only possible source, the timing of dome III and dome IV is not absolute.

The Tcl deposits produced during dome IV's emplacement have block sags and accretionary lapilli, suggesting that the Tcl surges and fallout tephras were emplaced in a wet environment. Dome IV grew endogenously within the crater and produced one small grain-flow deposit (~30,000 m^3) to the northeast (Facies Bmi; Fig. 4.14). The dome IV eruption also included a pyroclastic flow (~ 25,000 m^3) that filled a paleodrainage to the north of the crater and fanned out into the north ring (Fig 4.15). The pyroclastic flow has coarse laminations of pumice clasts (<5 cm) at the top of the deposit, possibly a result of pumice rafting during transport.

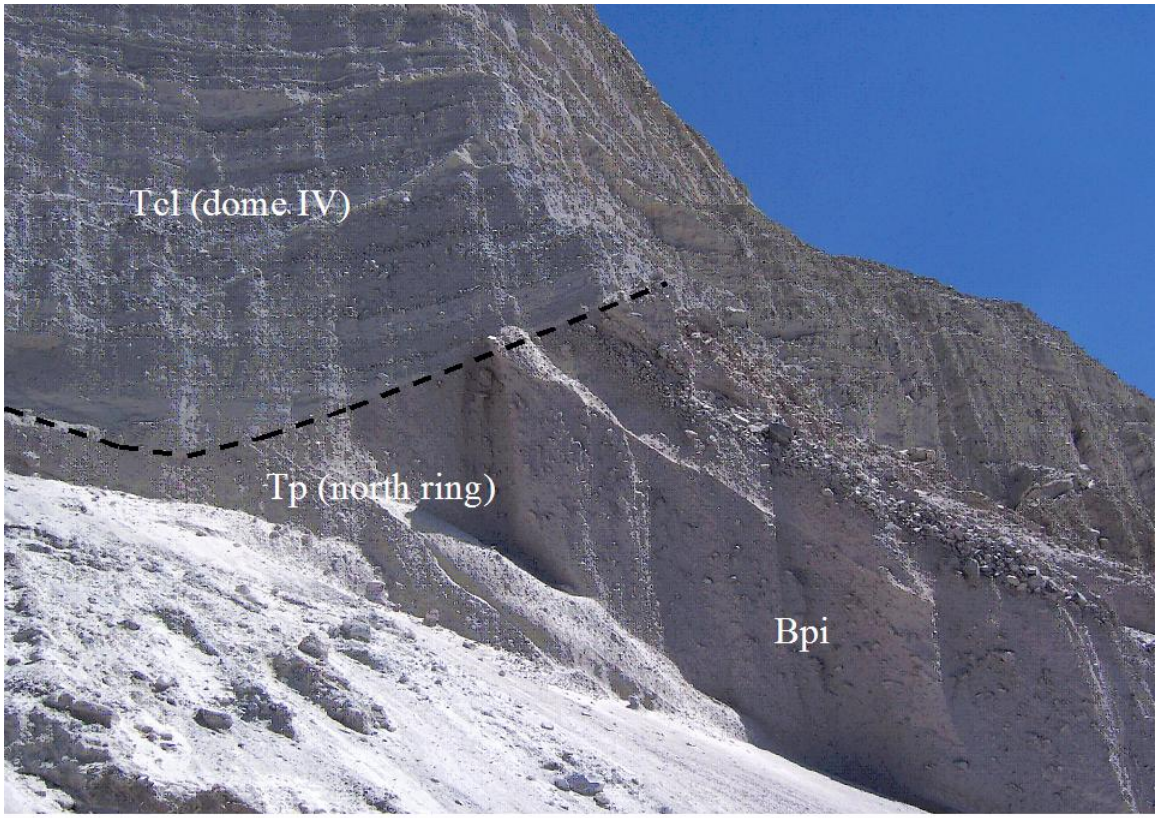

Figure 4.13. Unconformity where a crater was blasted out of the grain-flow and tephra deposits in the northern part of the South Ring.

Tephras from both north and south ring eruptions were uplifted as dome IV grew, and remain undisturbed atop the dome. The emplacement of dome IV marked the end of volcanic activity at Cerro Pinto. Since the cessation of volcanic activity, weathering of the domes has produced additional debris-flow and talus deposits along the flanks of the domes and in the surrounding drainages (Facies C, Table 3.2). An abandoned quarry located at the contact between the northern and southern tuff rings provides excellent exposure of nearly the entire eruptive sequence (Fig. 4.16 & 4.17).

Figure 4.14. Picture of grain-flow deposits (Bmi) originating from dome IV. This deposit has structures similar to those found in Bpi deposits (i.e. interbedded ash beds, poorly sorted massive beds with many outsized clasts, etc.), but Bmi deposits are monolithic, composed of sugary white rhyolite. These clasts are very different from the banded blue rhyolites common to Bpi deposits.

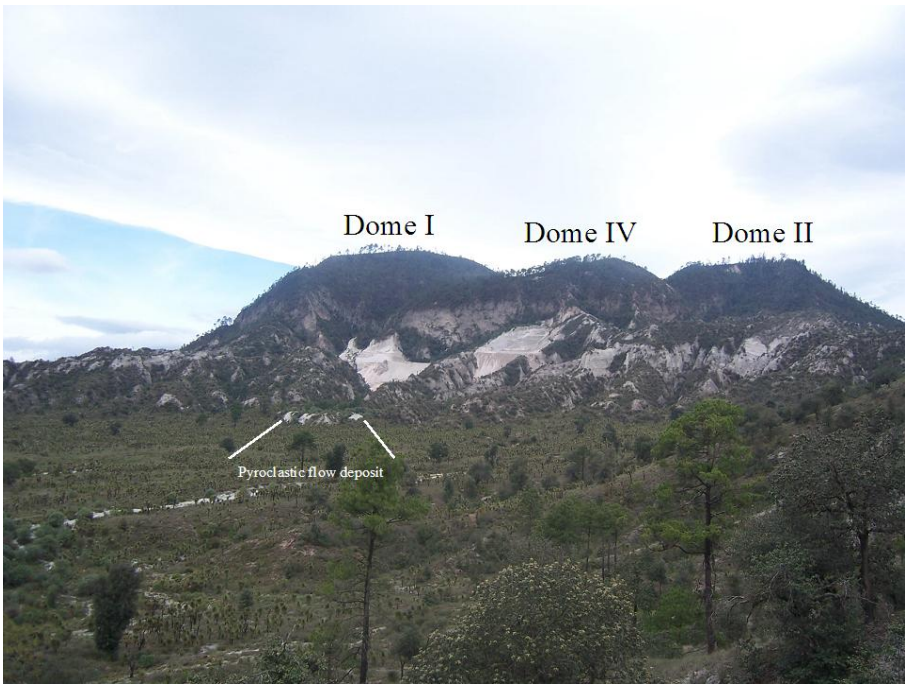

Figure 4.15. Overview of the south ring domes as seen from the western inner ring, looking southeast.

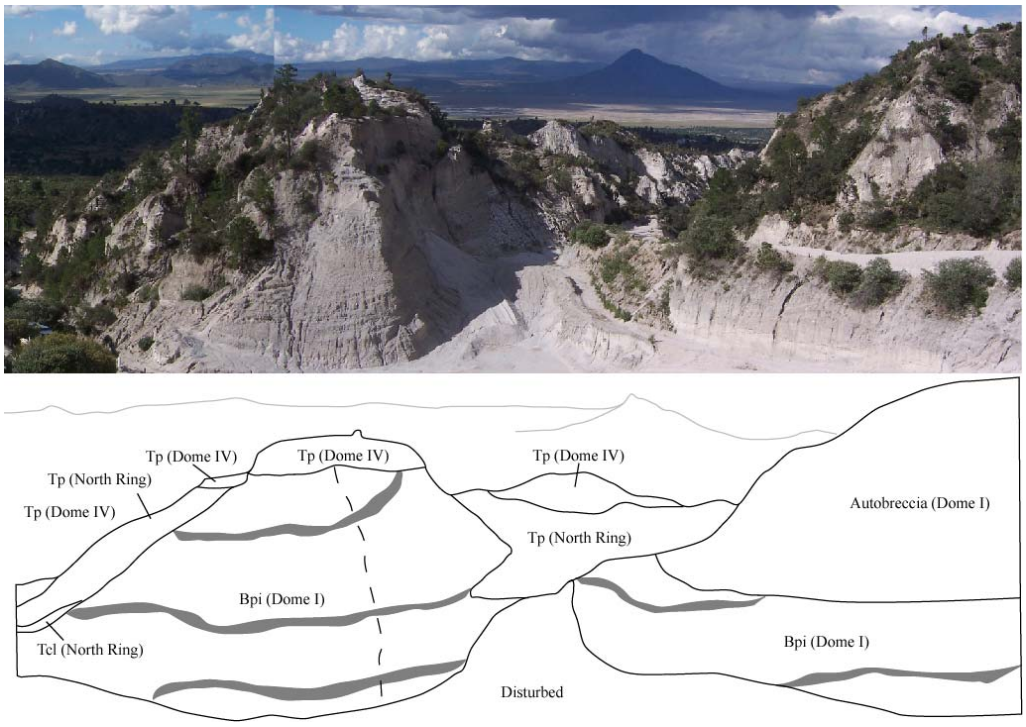

Figure 4.16. Distribution of deposits within the abandoned rock quarry. Origin of each deposit type is in parenthesis. Shaded bands represent interbedded Tp (north ring) tephra.

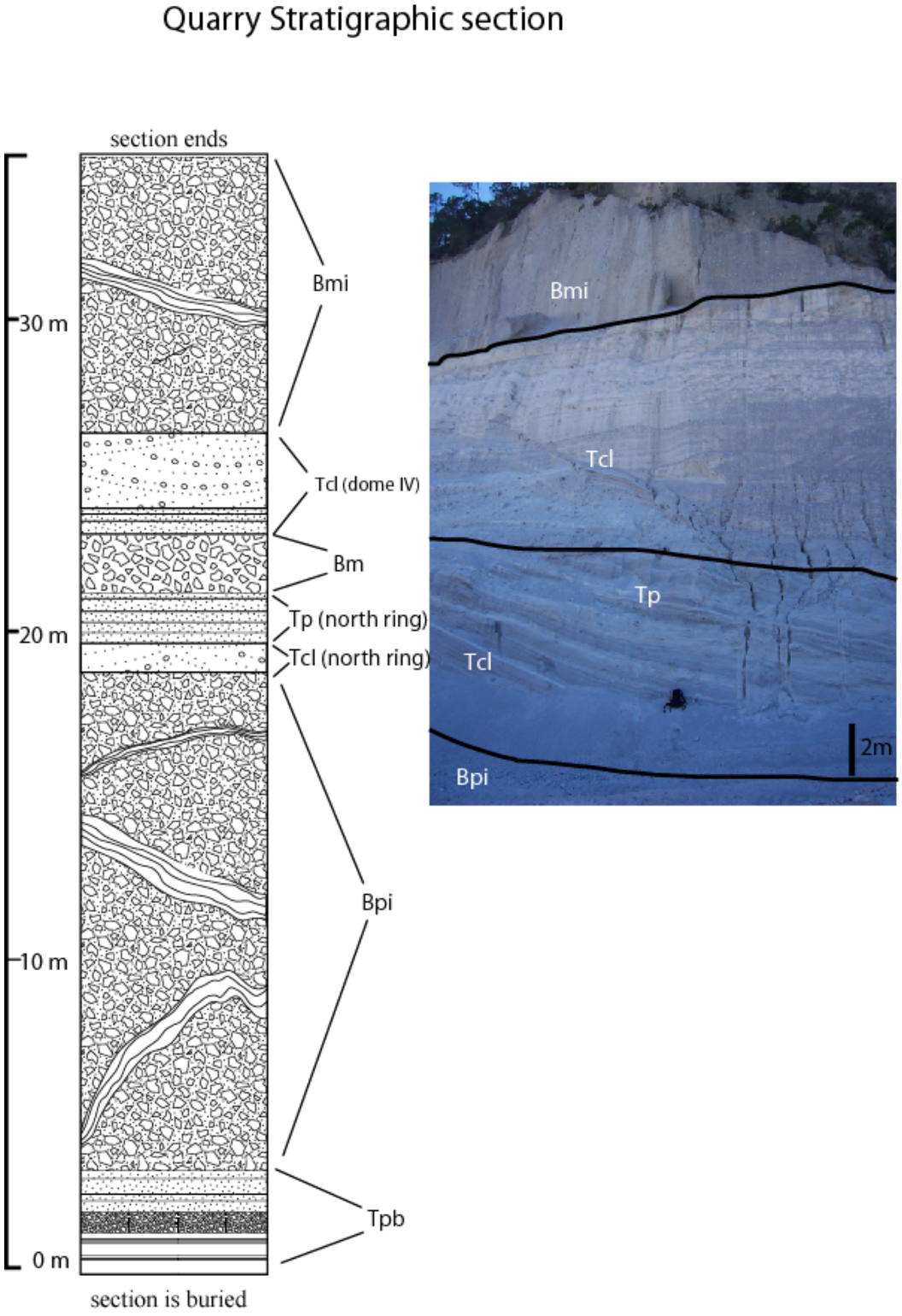

Figure 4.17. Stratigraphic section showing relations between the fallout, maelstrom, and grain-flow deposits. Note that the maelstrom deposit (Bm) is not shown in the photo, but is located between Tp and Tcl tephras elsewhere. See pg. #59 for explanation of patterns.

CHAPTER V

PETROLOGY AND CHEMISTRY

Geochemistry

Major Element Chemistry

Major-element concentrations derived from whole-rock geochemistry of juvenile clasts vary little throughout the dome complex (Table 5.1). This homogeneity suggests that Cerro Pinto evolved from a single magma batch that was not significantly altered during the course of the eruption. Analyzed samples were either juvenile pumice from the tuff rings, or, in the absence of sufficient pumice clasts, stony rhyolite. Pieces of breccia containing any lithic clasts are considered non-juvenile and were not analyzed. All samples that were collected from Cerro Pinto are high-silica rhyolite and are chemically and compositionally distinct from the andesitic and dacitic products of the larger volcanoes that mark the outer boundary of the Serdán-Oriental Basin (Riggs and Carrasco-Nuñez, 2004).

Within the basin, other volcanoes are at least in part high-silica rhyolite (e.g. Las Derrumbadas, Siebe and Verma, 1988; Cerro Pizarro, Riggs and Carrasco-Nuñez, 2004; Tepexitl Maar, Austin, unpublished data, 2006). When major elements for the each of these volcanoes are compared with reference to SiO_2, the volcanoes are generally similar for Al_2O_3, P_2O_5, and CaO, but are significantly scattered for the other major elements (Fig. 5.1; Appendix C). The volcano most similar to Cerro Pinto is Tepexitl maar, a small

rhyolitic maar located to the southeast of Cerro Pinto and directly to the east of Las Derrumbadas (Fig. 1.1). Cerro Pinto and Tepexitl are still significantly different in FeO, CaO, and MgO, but both volcanoes may have drawn from the same original deep magma source before separating and fractionating in the upper crust. This differentiation occurred prior to the emplacement of each volcano, accounting for the variability in chemistry between the two volcanoes. Based on the narrow range of Cerro Pinto's data, it is inferred that Cerro Pinto was produced by an eruption from a small magma batch separate from any of the other volcano in the basin.

Table 5.1 Major element concentrations for the different eruptive stages.

	Stage I			**Stage II**				**Stage III**
Element	South Ring	Dome I	Dome II	North Ring	Northern Inner Ring	Western Inner Ring	Dome III	Dome IV
SiO_2	75.46	75.51	75.30	75.60	75.58	75.57	75.35	75.49
TiO_2	0.03	0.03	0.03	0.02	0.03	0.03	0.03	0.03
Al_2O_3	14.20	14.11	14.28	14.10	13.97	13.97	14.12	14.08
Fe_2O_3	0.79	0.74	0.82	0.75	0.80	0.79	0.78	0.80
MnO	0.11	0.11	0.08	0.11	0.11	0.11	0.11	0.11
MgO	0.16	0.18	0.16	0.15	0.16	0.17	0.22	0.17
CaO	0.50	0.52	0.57	0.52	0.53	0.52	0.53	0.52
Na_2O	4.54	4.52	4.52	4.48	4.51	4.56	4.55	4.50
K_2O	4.15	4.23	4.20	4.21	4.26	4.24	4.25	4.25
P_2O_5	0.05	0.05	0.05	0.06	0.05	0.05	0.06	0.05
LOI	**2.42**	**1.35**	**0.83**	**2.20**	**0.52**	**0.39**	**0.29**	**2.97**

One area of interest is the cyclic pattern of LOI concentrations associated with each stage of the eruption (Table 5.1). Each eruptive stage begins with relatively high LOI concentrations that decrease significantly throughout each stage before spiking at the start of the next stage. LOI is not a direct measurement of magmatic H_2O vapor, but rather a measurement of magmatic volatiles that are driven off by ignition at 1000^{o} C. Meteoric

water in the sample was first driven off at 200^{o} C before LOI was measured, so the LOI is strictly magmatic volatiles. In addition to magmatic H_2O vapor, CO_2, CL, F, and Na_2O_3 can also be volatilized by ignition at 1000^{o} C. Even with these variables taken into account, a significant cyclic pattern still remains in the whole-rock LOI values (Table 5.1).

Large dome complexes have been produced by single, homogeneous magma reservoirs (e.g. Taylor Creek Rhyolite, NM, Duffield et al., 1995) and by magma mixing (e.g. Inyo Domes, CA, Vogel et al., 1987). At Cerro Pinto, the dome system was apparently very short lived and was produced by a small, isolated magma chamber. Therefore, magmatic variables, such as variations in the concentrations of volatiles (e.g. dissolved H_2O or CO_2) in the magma reservoir, or external variables, like groundwater or meteoric water fluxes, must have been paramount in the periodic explosivity of Cerro Pinto.

The dissolved water content of erupting magmas is a major control on the explosivity of silicic melts (Newhall and Melson, 1982). Silicic magma bodies have been inferred to be zoned or stratified with respect to volatiles as observations of deposits from silicic volcanoes show a general decrease in explosivity through time associated with a concurrent decrease in water content (Fink and Manley, 1987). Dissolved H_2O is a catalyst for the vesiculation and fragmentation of magmas as well as a critical constituent during the acceleration of pyroclasts out of the vent (Sigurdsson, 2000). The solubility of water decreases substantially with decreased pressure. Because high-silica lava is extremely viscous, gases exsolved during depressurization have a difficult time escaping.

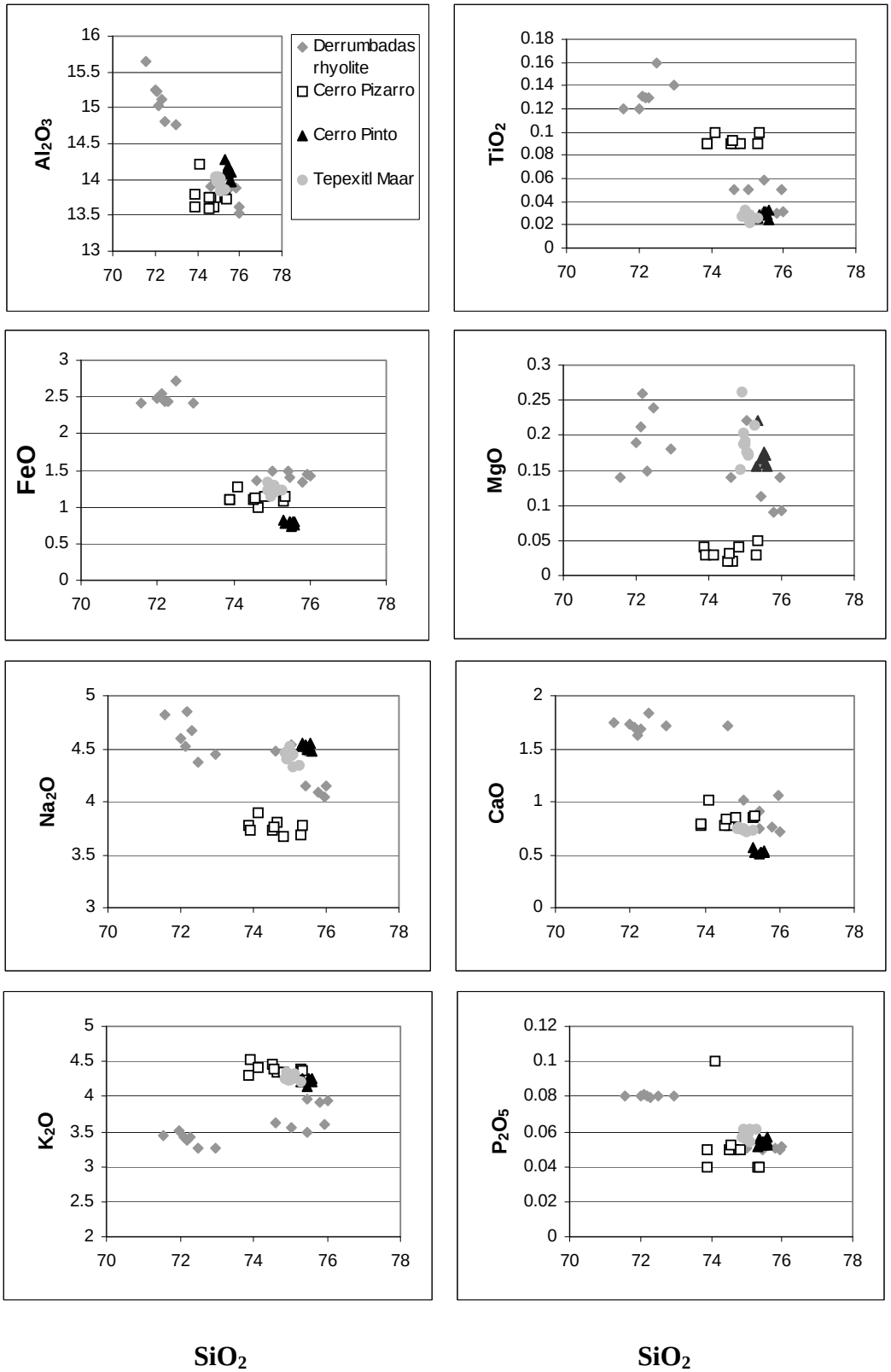

Figure 5.1 Element variation diagrams for rhyolitic volcanoes within the Serdan-Oriental Basin.

This can lead to overpressure and eventually explosive eruptions. In the samples taken from Cerro Pinto, the highest LOI concentrations are found in the volcanic features produced immediately after vent migration and at the start of new eruptive stages. This suggests that the enrichment of volatiles (observed as LOI) was influential in the initiation of a new, explosive eruptive stage (Table 5.1). Subsequent volcanic features of each eruptive stage had gradually less LOI and were gradually less explosive. The gradual decrease of dissolved volatiles throughout an eruption has been documented at Medicine Lake Highland Volcano, Newberry caldera, Long Valley caldera, and Lassen Peak (Fink and Manley, 1987).

Trace Element Geochemistry

Trace-element geochemistry of structures at Cerro Pinto varies little throughout the eruptive sequence. A trend of increasing rare-earth-element concentrations through time is present (Table 5.2) with volcanic features produced during Stage I (southern tuff ring, dome I and dome II) containing some of the lowest REE concentrations and dome IV, emplaced during Stage III, containing the highest. This trend is strongest in the heavy rare earth elements, but the greatest variation in elemental concentrations is found in the lightest REEs, La and Ce (Fig. 5.2). It is unlikely that this progressive enrichment of REEs over time is due to crystal fractionation between eruptive events as the lack of erosional features between deposits in the field suggests that only short hiatuses (at most a few hours to a few days) occurred between eruptive stages and did not allow sufficient time for appreciable fractionation to occur. The variation is most likely the result of a

compositionally stratified magma chamber, as described by Fink and Manley (1987). The clear negative Eu anomaly in most of the samples suggests that the source melt was shallow (< 30 km) and was in equilibrium with plagioclase during crystal fractionation prior to eruption (Winter, 2001) (Fig. 5.2). Because the REE patterns are parallel with one another, it appears that the magma body was consistently fractionating the same mineral phases, but the Stage I volcanic features were produced by a part of the reservoir that had fractionated less.

Table 5.2. Whole-rock trace element values for the rare earth elements.

Structure	La	Ce	Pr	Nd	Pm	Sm	Eu	Gd	Tb	Dy	Ho	Er	Tm	Yb	Lu
Southern Ring	25	23	16	13	15	16	1	3	9	10	7	9	8	10	9
Dome I	30	27	19	16	17	18	1	4	7	9	6	8	7	9	8
Dome II	27	24	17	14	15	16	1	2	8	10	7	8	8	9	9
Northern Ring	43	34	23	19	20	21	1	10	10	13	9	11	11	12	11
Northern Inner Ring	36	31	21	17	18	19	1	1	10	12	8	10	10	11	10
Western Inner Ring	33	30	21	18	19	20	1	7	11	14	10	12	11	13	12
Dome III	25	23	17	15	17	18	1	4	10	13	9	11	11	12	11
Maelstrom Deposit	28	26	15	15	17	19	1	3	11	12	10	11	11	12	11
Dome IV	46	38	25	21	22	22	2	16	10	14	10	12	11	13	12

The relatively low light-rare-earth-element concentrations suggest that the evolution to rhyolite was done through high degrees of partial melting of a depleted mantle source as opposed to crustal assimilation (Sampson and Cameron, 1987). Crustal assimilation of the local granitic plutons would result in a magma chamber with localized strong LREE

enrichments. Because all structures emplaced at Cerro Pinto are similar to one another in relative REE abundance, it can be inferred that partial melting and crystal fractionation were the driving forces behind the evolution of this magma batch and not crustal assimilation (Gill, 1981). It should be noted that high-silica rhyolites requires around 90% crystal fractionation of a basaltic melts suggesting that the Cerro Pinto reservoir was a highly evolved (Winter, 2001).

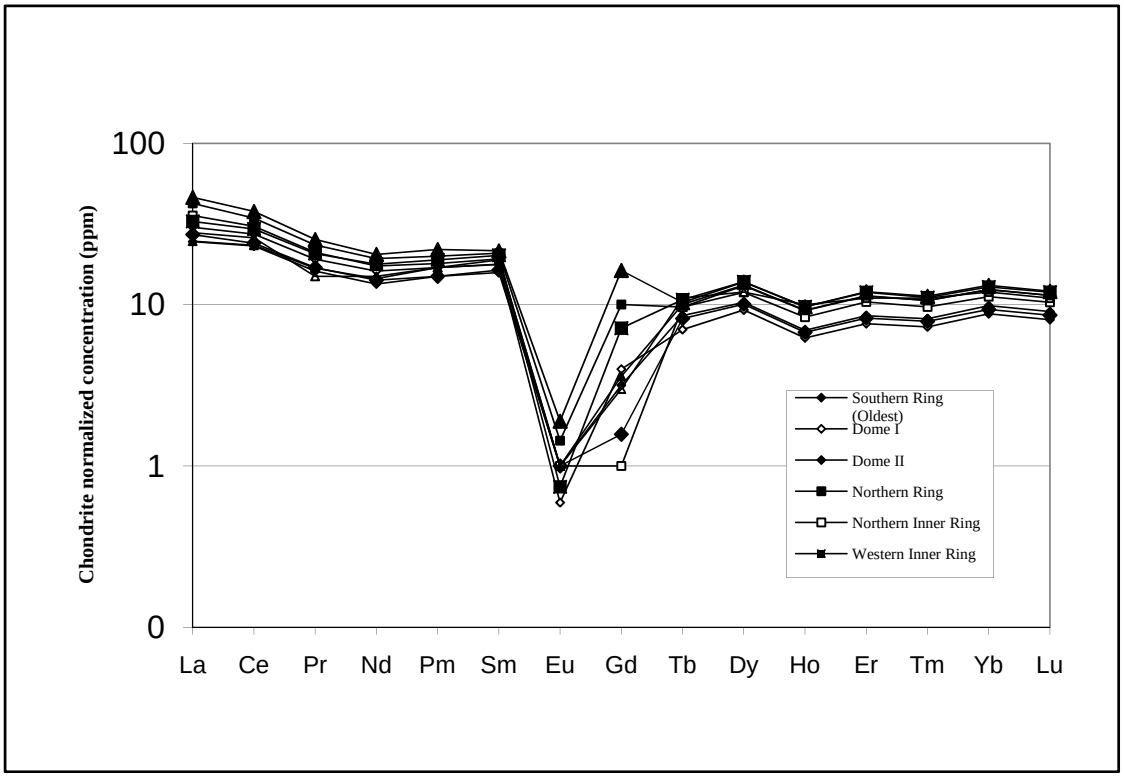

Figure 5.2. Logarithmic scaled graph of rare earth element concentrations. Chondrite values from Sun and MacDonough (1989).

CHAPTER VI

DISCUSSION

In the literature, rhyolite domes have been perceived as simple, monogenetic structures (Christiansen and Lipman, 1966; Swanson et al., 1989; Duffield et al., 1995) with localized hazard potential. In these cases, explosive activity is limited to the tuff ring production stage of the dome emplacement sequence. Only recently have isolated rhyolite domes been identified as having the potential to explosively reactivate (Riggs and Carrasco-Nuñez, 2004), an event of considerable implication when making hazard assessments. The arresting feature of Cerro Pinto that separates it from other documented cases of rhyolitic dome growth is that Cerro Pinto oscillated multiple times between explosive and effusive behavior over a relatively short time interval while sourced by a single, small, chemically distinctive, magma chamber. This eruptive history is primarily a result of phreatomagmatic activity and volatile stratification within the magma chamber. Bedrock morphology may have played a small role in the distribution of the mass-flow deposits.

Variables Affecting Eruption Style

Magma Chamber Variations

Fink and Manley (1987) report that silicic magma bodies are commonly compositionally stratified and that these localized chemical heterogeneities can account for variations in the vesicularity, crystallinity, mineralogy, color, and flow banding of silicic lavas with

similar chemistries. This can explain the differences in hand sample between the domes at Cerro Pinto despite the domes having very similar chemical compositions (Table 3.1). When the magma chamber is stratified with respect to volatiles such as dissolved H_2O, the explosivity mimics the relative level of dissolved volatiles; increasing when the magma has high levels of dissolved H_2O and decreasing as the concentration wanes (Fink and Manley, 1987). The oscillations in explosivity that occurred at Cerro Pinto correspond well with the variations in LOI, a proxy for dissolved volatiles shown in Table 5.1. This, of course assumes that there is no appreciable change in magma viscosity between the eruptive stages.

The cyclic changes seen in the LOI data could also represent differences in the mode of degassing. During explosive phases, magma rises quickly and is not able to effectively degas, resulting in higher LOI values in the pyroclasts produced. During dome emplacement, the magma rises more slowly allowing for exsolution of gas through the conduit walls resulting in lower LOI values.

According to Newhall and Melson (1983), water content is the dominant control on explosions from water-rich magmas. During isothermal decompression volatiles are lost due to the decreasing solubility that accompanies pressure loss. Westrich et al. (1988) state that the complete dewatering of an extruding magma strongly undercools the system, suppresses crystallization, and produces glassy, volatile-rich rhyolite. Partial degassing of shallow magmas, on the other hand, does not undercool the system as effectively and permits extensive crystallization even when the cooling rate is high.

How magma facilitates the growth of phenocrysts and microlites is important because phenocryst growth can lead to the development of large excess pressure gradients in the upper conduit and dome interior (Sparks, 2003). This can be a function of increase magmatic degassing that accompanies phenocryst crystallization or increased amounts of fluid pressure due to shallow microlite crystallization, especially in closed-system degassing (Sparks, 1997).

Cerro Pinto does vary significantly in groundmass crystallinity. Microlite crystallization occurring in a closed system is theoretically capable of increasing gas pressure by 10 Mpa and is most influential when it occurs at shallow depths (Sparks, 2003). The type of groundmass, whether glassy or microlitic, is not consistent within any single volcanic feature, though some features, such as dome IV and the northern inner ring, appear to be more consistently glassy. Localized areas of vitric dome lava are more susceptible to post-depositional hydration from volcanic glass to perlite. Consequently, the domes at Cerro Pinto contain unevenly distributed areas of weakness that may lead to large-scale gravitational collapses in the future. Both dome I and dome IV have produced large talus aprons since the end of volcanic activity. Dome II has also produced recent talus deposits, but they are smaller than the aprons around dome I and dome IV.

Phreatomagmatism

Meteoric water and groundwater also appear to have played significant roles in giving Cerro Pinto its unique character. New stages of eruptive activity commonly began with a

wet, lithic-rich, surge-dominated phase (Tcl), but changed to a dry, fallout-dominated environment after a short time interval (Tp & Tpb). The thickest wet-surge deposits are only 10 m thick, whereas the Tp tephra is commonly over 50 m thick. The relatively small volume of wet pyroclastic material and the lack of any cementation or ubiquitous hydrothermal alteration suggests that the water in this interaction was either groundwater or saturated pre-existing tephras and not a lake. A lake would have held enough water to make a substantially larger volume of phreatomagmatic deposits and would also have significantly influenced the sorting, distribution, and subsequent alteration of the pyroclastic tephras. Phreatomagmatic eruptions also often lead to highly heterogeneous erupted material including high concentrations of lithic clasts and hydrothermally altered clasts (White and Houghton, 2000). These clasts are found only in the <10 m thick cross-bedded lithic-rich (Tcl) tephras located between the biotite-rich pumice tephra (Tpb) of the south ring and the pumice tephra (Tp) of the north ring.

Tuff rings are commonly produced by violent phreatomagmatic eruptions with water:magma mass ratios around 1 (Morrissey et al., 2000). Higher water:magma mass ratios result in less explosive Surtseyan eruptions. Violent phreatomagmatic eruptions produced the south ring and the north ring, but the northern inner ring and western inner rings formed without any apparent phreatomagmatic activity (Fig 4.10B). It must therefore be allowed that even dry magmatic eruptions can produce tuff rings and that tuff ring morphology is predominately a surficial expression of the underlying explosion crater.

During dome emplacement, meteoric water may have been responsible for initiating some of the dome failures that resulted in the grain-flow deposits. At Mt. Unzen, Japan, and at Soufriere Hills Volcano, Montserrat, heavy rainfall has been directly correlated with an increase in the frequency of dome collapse and associated pyroclastic flows during dome growth (Yamasato et al., 1998; Carn et al., 2004). The grain-flow deposits appear to have been emplaced en masse. They are reversely graded and poorly sorted, attributes common to debris-flow deposits. Phreatic or phreatomagmatic dome explosions could have acted as the triggering mechanism for these flows.

Even after effusion has ceased, dome surfaces can remain well over 100^{o} C for days to weeks, with the interior remaining hot much longer depending on emplacement temperature, dome morphology, and atmospheric conditions (Matthews and Barclay, 2004). As long as the interior of a dome remains hot and under pressure, it has the potential to explode and spawn pyroclastic density currents, especially if meteoric water or groundwater is introduced into the system. For this reason, it is possible that eruptive activity had migrated completely to the northern tuff ring while dome I continued to shed grain flows that were either gravity driven, or possibly initiated by small phreatic explosions as the hot dome interacted with meteoric water or groundwater.

The strong influence that phreatomagmatism can have on simple dome growth is well documented at Puketarata tuff ring in the Taupo Volcanic Zone, New Zealand. Brooker et al. (1993) studied the effects of shallow groundwater and surface water on the emplacement of this small, high-silica rhyolite dome complex. The Puketarata complex

contains one tuff ring, two domes and three phreatic explosion craters and was emplaced at ~14 ka as part of the Maroa caldera complex. During emplacement, a highly viscous feeder dike encountered groundwater, an event that resulted in shallow-seated explosions. Without the groundwater interaction, these authors believe that the lava would have effused passively. Instead, moderate water:magma ratios resulted in multiple, highly-explosive, shallow explosions. When the localized water sources were depleted, dome effusion commenced, but the extrusion rate was high and led to multiple collapse events and secondary explosions.

From the findings of Brooker et al. (1993), it is clear that Cerro Pinto is similar to Puketarata in three major aspects: 1) magmatic composition, 2) influence of phreatomagmatism, and 3) eruptive products. Both Puketarata and Cerro Pinto were high-silica rhyolites that were compositionally homogeneous throughout the entire eruption. Both were, on the whole, volatile-poor, but contained localized areas of volatile accumulation. If these magmas were emplaced into dry environments, they likely would have behaved in accordance with the simple-dome growth model. However, both magma bodies encountered shallow groundwater during emplacement thus complicating their eruptive sequence.

The tephras at Cerro Pinto and Puketarata are both dominated by dense juvenile clasts and are poor in lithic clasts, suggesting that all the eruptions were shallow with little bedrock interaction. In both instances, the eruptions began as phreatomagmatic and dried out as the immediate groundwater sources were exhausted. The eruptions reactivated

explosively again when either groundwater recharge or volcano morphology allowed for the accumulation of water in the near-vent area. The extrusion rate of magma at both locations was high enough to produce unstable frontal lobes and collapse-generated flows.

Puketarata differs from Cerro Pinto in a few key aspects. Puketarata was emplaced within Maroa caldera and can be correlated with nearly 70 other domes (Brooker et al., 1993). Although Puketarata was part of a larger volcanic system, its total erupted volume is less than 25% of that of Cerro Pinto and its magma contained a significantly higher percentage of phenocrysts (16-20% vs. 1-4%). Despite these differences, the variations in eruptive character identified at Puketarata are similar to the variations that occurred at Cerro Pinto. A single, small pulse of magma also sourced Puketarata and variations in its eruptive nature were not due to additional pulses of magma, but were due to interactions with groundwater. These attributes make the Puketarata tuff ring eruption a good analog for the Cerro Pinto eruption.

Dome III and the Maelstrom Deposit

The small, highly altered lava of dome III is the only relict dome material found anywhere within the northern tuff ring. Other domes may have been produced during Stage II, but any evidence of their existence has been buried by alluvium or destroyed by farming within the northern tuff ring. The remaining dome III lava is punky and brittle and was likely subjected to extensive hydrothermal alteration during emplacement. Based on the hydrothermal alteration and the lack of juvenile pumice in the maelstrom deposit,

it is inferred that a phreatic or phreatomagmatic explosion was the trigger for the blast(s) that destroyed dome III and may have produced the maelstrom deposit. The phreatic or phreatomagmatic eruptions were a result from either groundwater infiltration or the percolation of meteoric water through the fractured outer shell of the dome. If dome III was the source of the maelstrom deposit, then the spatial distribution of the deposit would suggest that the blast that destroyed most of the dome must have been directed to the northeast with the vast majority of its material concentrated in a 75^{o} sector north of northeast (Fig. 3.1).

The term “maelstrom” has been adopted to describe this deposit because there is strong evidence of multiple depositional mechanisms occurring simultaneously in the near-vent area during the eruptions that destroyed a dome, whether it is dome III or another, unidentified dome. A maelstrom is envisaged as an environment dominated by coarse-grained fallout that never attained positive buoyancy in an eruption column and rained down in a pulsulatory manner over the course of a few minutes to hours. The maelstrom deposit at Cerro Pinto is well sorted and clast-supported like many fallout deposits. But it also has the granulometry, cross-bedding structures, and interactions with topography commonly associated with pyroclastic density currents and the distribution of a laterally directed blast. As discussed earlier, two depositional mechanisms have been postulated to explain how the maelstrom deposit was emplaced; 1) a vulcanian blast to the northeast and 2) a coarse-grained lateral blast.

Vulcanian Blast

This scenario suggests that the maelstrom deposit was produced by a vulcanian blast originating at dome III within the western inner tuff ring. An inefficient phreatomagmatic eruption pulverized dome III and vent morphology directed a coarse-grained fallout to the northeast. The initial, coarse eruption column did not attain buoyancy and most of the clasts traveled on a ballistic path. After the initial explosion, finer material was entrained in a short-lived eruption column that distributed finer material over a wider area and may have collapsed to produce a few pyroclastic surges that were deposited on top of the maelstrom deposit.

Macias and Sheridan (1995) documented a similar sequence of events identified in the deposits of the 1907 eruption of Shtyubel' Volcano in Kamchatka, Russia. In the 1907 eruption, a rhyolite dome inside the Ksudach Caldera complex was destroyed in what Macias and Sheridan called a breccia blast. This blast breccia at Shtyubel' Volcano is similar to Cerro Pinto's maelstrom deposit in three respects, 1) the distribution of the deposits, 2) the granulometry, and 3) the structure of the resulting deposits and their associations with subsequent surge deposits.

Both the maelstrom deposit and the blast-breccia were directed to the northeast, leaving horseshoe-shaped explosion craters at their vents. At Shtyubel', this crater formed a partial tuff cone and, at Cerro Pinto, the eruption destroyed half of the western inner ring, removing the north and eastern flanks (Fig. 3.1). Both the maelstrom deposit and the blast breccia acted as capstone rocks and have undergone an undetermined amount of erosion

since deposition. It can be inferred that less erosion has occurred at Shtyubel' than at Cerro Pinto based on the large discrepancy in age (~62 ka vs. 100 y). It should be noted that the blast breccia was produced by a much larger explosion and extends over 7 km from source as opposed to 1 km from source at Cerro Pinto.

Despite the significant differences in volume, both eruptions produced deposits that are massive, coarse, angular, and clast-supported. The componentry is similar in that both deposits are largely composed of dome lava with minor juvenile components. Even the average (~8 cm) and maximum (10-20 cm) clast sizes are similar. The granulometric histograms of the two deposits are remarkably similar, both having wide bell-curve distributions and primary modes of around –3 phi with broad, fine-skewed tails. Both deposits appeared to have been influenced by phreatomagmatism as identified by the presence of ash coatings on fine-grained material, pitting of glass shards, and hydrothermal alteration of clasts. In both cases, thinner surge beds with similar componentry immediately overlie the breccias. Macias and Sheridan (1995) suggest that this is evidence of a laterally directed blast-surge that was produced during or immediately following the breccia blast.

Problems still remain when trying to explain the maelstrom deposit by using a directed vulcanian blast like that documented at Shtyubel' Volcano. While the directed blasts can account for the distribution of the maelstrom deposit to the northeast, the mechanism does not adequately explain the accumulation of the deposit in topographic lows and the apparent decrease in abundance on topographic highs. The maelstrom is thickest (~2.5 m)

in a drainage on the north flank of the northern tuff ring, about 700 m from the inferred source. The maelstrom deposit is a maximum of 30 cm thick between the northern drainage and the vent. The energy of the eruption, the ballistic paths, and uneven erosion since deposition may play a factor in this apparent preferential distribution in the topographic low, but the problem still necessitates some additional explanation.

Coarse-Grained Lateral Blast

The lateral blast scenario suggests that the maelstrom deposit was produced by a coarse-grained lateral blast that initiated from dome III within the western inner tuff ring. Either through overpressure or flank collapse, catastrophic failure on the northeastern flank of the dome released a lateral blast that destroyed part of the western inner ring and climbed the 60-m-tall northern inner ring before slowing down and depositing the majority of its material on the outer flank of the northern tuff ring. A coarse-grained lateral blast deposit would account for the lack of uniformity in the thickness of the maelstrom deposit and for its preferential distribution on topographic lows.

Because of the popularity of the Mount St. Helens eruption of 1980, the term lateral blast deposit has connotations that intimately correlate it to the fine-grained, thin deposit described by Miller and Hoblitt (1980) and Fisher (1990). Lateral blasts can also be coarse-grained, fines-poor, thick deposits. Lateral blast deposits of this variety have been described at Novarupta, Alaska, 1912 (Houghton et al., 2004), and at Cerro Quemado, Guatemala, 842 A.D. (Conway et al., 1992). The deposit at Cerro Quemado is similar to the maelstrom deposit in a few respects. Both deposits have sharp upper and lower

contacts, are coarse-grained, clast-supported, and fines-poor. Both deposits are about 2 m thick at their thickest locations, and both deposits are composed dominantly of angular dense lava. The lateral blast deposit at Cerro Quemado also tends to thicken in paleodrainages while thinning substantially over ridges (Conway et al., 1992). A fines-poor pyroclastic flow overlies the lateral blast breccia at Cerro Quemado instead of the pyroclastic surge seen at Cerro Pinto. If the breccia at Cerro Pinto did come from a laterally directed blast, it was a much less efficient and obviously less powerful and voluminous blast than those at Cerro Quemado and Mount St. Helens.

Boudon et al. (1984) suggest that coarse, poorly sorted breccias can be one component of a two-part lateral-blast deposit. The second component includes surge and fallout deposits produced during the blast that are initially deposited on top of the blast breccia deposit. Eventually, the surges overrun the advancing blast-density current farther away from the vent. At some distance from the vent, the two mechanisms deposit simultaneously. At Cerro Pinto, the uppermost 0.3 m of the maelstrom deposit is composed of fine-grained surge deposits that may represent the time when the surge had not yet outstripped the coarse-grained lateral blast.

Conclusions

The evolution of Cerro Pinto included three distinct stages of development, stages that in part adhered to current simple dome models, but also diverged significantly in other aspects including the oscillations between explosive and effusive activity. Stage I began with the emplacement of the southern tuff ring and domes I and II (Fig. 4.1). During

Stage II, activity moved north, creating the northern tuff ring, the northern inner ring, the western inner ring and dome III (Fig. 4.7). In the final stage, Stage III, dome IV was emplaced along the northern margin of the southern tuff ring, lifting up and deforming previously emplaced tephra deposits (Fig. 4.12).

Dome growth throughout the eruptive sequence at Cerro Pinto was more intricate than envisaged by the commonly accepted rhyolite dome models. Variations on the models include explosive reactivation with the production of multiple tuff rings, vent migration, and dome collapses. The emplacement sequence was complicated by phreatomagmatic interactions with meteoric and ground water, as well as the presence of a magma chamber zoned in volatiles. This magma chamber was likely small and isolated from surrounding volcanic structures. No field evidence exists to suggest a significant hiatus of activity at any point during the eruptive sequence and it can therefore be inferred that the entire emplacement of the dome complex could not have taken more than a few months to years.

The deviations in eruptive style displayed at Cerro Pinto were not produced by exotic compositions or extenuating geomorphology but rather by the influence of water combined with other normal volcanic processes. Because of this, we should consider the variations in eruptive character displayed by Cerro Pinto as distinct possibilities when assessing hazards of newly emerging rhyolite domes, whether they are emplaced in fields, in isolation, or near calderas and stratovolcanoes.

References

Abrams, M.J. and Siebe, C., 1994. Cerro Xalapaxco: an unusual tuff cone with multiple explosion craters, in central Mexico (Puebla). Journal of Volcanology and Geothermal Research. 63, 183-199.

Adams, N.K., Houghton, B.F., Fagents, S.A., and Hildreth, W., 2006. The transition from explosive to effusive eruptive regime: the example of the 1912 Novarupta eruption, Alaska. Geological Society of America Bulletin. 118, 620-634.

Anderson, S.W., Fink, J.H. and Rose, W.I., 1995. Mount St. Helens and Santiaguito lava domes: the effect of short-term eruption rate on surface texture and degassing processes. Journal of Volcanology and Geothermal Research. 69, 105-116.

Barmin, A., Melnik, O., and Sparks, R.S.J., 2002. Periodic behavior in lava dome eruptions. Earth and Planetary Science Letters. 199, 173-184.

Boudon, G., Semet, M.P., and Vincent, P.M., 1984. Flank failure-directed blast eruption at Soufriere, Guadeloupe, French West Indies: A 3,000-yr-old Mt. St. Helens? Geology. 12, 350-353.

Branney, M.J., and Kokelaar, P., 1992. A reappraisal of ignimbrite emplacement: progressive aggredation and changes from particulate to non-particulate flow during emplacement of high-grade ignimbrite. Bulletin of Volcanology. 54, 504-520.

Brooker, M.R., Houghton, B.F., Wilson, C.J.N., and Gamble, J.A., 1993. Pyroclastic phases of a rhyolitic dome-building eruption: Puketarata tuff ring, Taupo Volcanic Zone, New Zealand. Bulletin of Volcanology. 55, 395-406.

Bull, S.W., and Cas, R.A.F., 2000. Distinguishing base-surge deposits and volcaniclastic fluviatile sediments: an ancient example from the Lower Devonian Snowy River volcanics, south-eastern Australia. Sedimentology. 47, 87-98.

Burgisser, A. and Gardner, J.E., 2006. Using hydraulic equivalences to discriminate transport processes of volcanic flows. Geology (Boulder). 34, 157-160.

Campos-Enrìquez, J.O., and Garduno-Monroy, V.H., 1987. The shallow structure of Los Humeros and Las Derrumbadas geothermal fields, Mexico. Geothermics. 16, 539-554.

Carn, S.A., Watts, R.B., Thompson, G., and Norton, G.E., 2004. Anatomy of a lava dome collapse; the 20 March 2000 event at Soufriere Hills Volcano, Montserrat. Journal of Volcanology and Geothermal Research. 131, 241-264.

Carrasco-Nuñez, G., Gomez Tuena, A., and Rose, W.I., 1997. Volcanogenic sedimentation around Citlaltepetl (Pico de Orizaba) Volcano and surroundings. IAVCEI, International (III). Excursion 16.

Cas, R.A.F., and Wright, 1987. Volcanic Successions, Modern and Ancient: A geological approach to processes, products and successions. Allen & Unwin, London, 528.

Cashman, K.V., Sturtevant, B., Papale., and Navon, O., 2000. Magmatic fragmentation. In: Encyclopedia of Volcanoes, Sigurdsson, H., Houghton, B.F., McNutt, S.R., Rymer, H., and Stix, J. (Eds.). Academic Press, San Diego, CA, 421-430.

Chough, S.K., and Sohn, Y.K., 1990. Depositional mechanics and sequences of base surges, Songaksan tuff ring, Cheju Island, Korea. Sedimentology. 37, 1115-1135.

Christiansen, R.L., and Lipman, P.W., 1966. Emplacement and thermal history of a rhyolite lava flow near Fortymile Canyon, southern Nevada. Geological Society of America Bulletin. 77, 671-684.

Conway, M.F., Vallance, J.W., Rose, W.I., Johns, G.W., and Paniagua, S, 1992. Cerro Quemado, Guatemala: the volcanic history and hazards of an exogenous volcanic dome complex. Journal of Volcanology and Geothermal Research. 52, 303-323.

Duffield, W.A., and Dalrymple, G.B., 1990. The Taylor Creek Rhyolite of New Mexico; a rapidly emplaced field of lava domes and flows. Bulletin of Volcanology. 52, 475-487.

Duffield, W.A., Richter, D.H., and Priest, S.S., 1995. Physical volcanology of silicic lava domes as exemplified by the Taylor Creek Rhyolite, Catron and Sierra Counties, New Mexico. USGS Map I-2399. 1:50,000, 16.

Ferriz, H. and Mahood, G., 1984. Eruption rate and compositional trends at Los Humeros volcanic center, Puebla, Mexico. Journal of Geothermal Research. 88, 8551-8524.

Fink, J.H., and Griffiths, R.W., 1998. Morphology, eruption rates, and rheology of lava domes; insights from laboratory models. Journal of Geophysical Research. 103, 527-545.

Fink, J.H., and Manley, C.R., 1987. Origin of pumiceous and glassy textures in rhyolite flows and domes. In: The emplacement of silicic domes and lava flows. Geological Society of America Special Paper. 212, 77-88.

Fink, J.H., and Anderson, S.W., 2000. Lava domes and coulees. In: Encyclopedia of Volcanoes, Sigurdsson, H., Houghton, B.F., McNutt, S.R., Rymer, H., and Stix, J. (Eds.). Academic Press, San Diego, CA, 307-320.

Fisher, R.V., 1990. Transport and deposition of a pyroclastic surge across an area of high relief; the 18 May 1980 eruption of Mount St. Helens, Washington. Geological Society of America Bulletin. 102, 1038-1054.

Fisher, R.V., 1995. Decoupling of pyroclastic currents: hazard assessments. Journal of Volcanology and Geothermal Research. 66, 257-263.

Fisher, R.V., Orsi, G., Ort, M., and Heiken, G., 1993. Mobility of a large-volume pyroclastic flow – emplacement of the Campanian ignimbrite, Italy. Journal of Volcanology and Geothermal Research. 56, 205-220.

Fisher, R.V., and Schmincke, H.U., 1984. Pyroclastic Rocks. Springer-Verlag, Berlin. 472.

Garcia-Banda, R.,1984. Geology, geochemistry, and petrology of the Pizarro and Pinto domes and the Tepeyahualco flows related to the Los Humeros caldera complex, Puebla, Mexico [MS. thesis]. McGill University, 67.

Gill, J., 1981. Orogenic Andesites and Plate Tectonics. Springer-Verlag, Berlin. 390.

Heiken, G.H., and Wohletz, K., 1987. Tephra deposits associated with silicic domes and lava flows. In: The emplacement of silicic domes and lava flows. Geological Society of America Special Paper. 212, 55-76.

Heiken, G. and Wohletz, K., 1985. Volcanic Ash: Berkeley, University of California Press, 246.

Houghton, B.F., Wilson, C.J.N., Fierstein, J., and Hildreth, W., 2004. Complex proximal deposition during the Plinian eruptions of 1912 at Novarupta, Alaska. Bulletin of Volcanology. 66, 95-133.

Houghton, B.F., Wilson, C.J.N., and Pyle, D.M., 2000. Pyroclastic fall deposits. In: Encyclopedia of Volcanoes, Sigurdsson, H., Houghton, B.F., McNutt, S.R., Rymer, H., and Stix, J. (Eds.). Academic Press, San Diego, CA, 555-570.

Lorenz, V., 1970. On the formation of maars. Bulletin of Volcanology. 37, 183-204.

Lorenz, V., 1986. On the growth of maars and diatremes and its relevance to the formation of tuff rings. Bulletin of Volcanology. 48, 265-274.

Luhr, J.F., 1997. Extensional tectonics and the diverse primitive volcanic rocks in the western Mexican volcanic belt. The Canadian Mineralogist. 35, 473-500.

Macias, J.L, and Sheridan, M.F., 1995. Products of the 1907 eruption of Shtyubel'

Volcano, Ksudach Caldera, Kamchatka, Russia. Geological Society of America Bulletin. 107, 969-985.

Maldonado-Sanchez, G and Schaaf, P., 2005. Geochemical and isotope data from the Acatlan Volcanic Field, western Trans-Mexican Volcanic Belt: Origin and Evolution. Lithos (in press).

Manea, V.C., Manea, M., Kostoglodov, V., and Sewell, G., 2005. Thermo-mechanical model of the mantle wedge in Central Mexican subduction zone and a blob tracing approach for the magma transport. Physics of the Earth and Planetary Interiors. 149, 165-186.

Mangan, M.T., Mastin, L., and Sisson., T, 2004. Gas evolution in eruptive conduits: combining insights from high temperature and pressure decompression experiments with steady-state flow modeling. Journal of Volcanology and Geothermal Research. 183, 441-455.

Manley, C.R. and Fink, J.H., 1987. Internal textures of rhyolite flows as revealed by research drilling. Geology. 15, 549-552.

Marquez, A., and DeIgnacio, C., 2002, Minerological and geochemical constraints for the origin and evolution of magmas in Sierra Chichinautzin, Central Mexican Volcanic Belt. Lithos. 62, 35-62.

Marquez, A., Verma, S., Francisco, A., Oyarzun, R., and Brandle, J., 1999. Tectonics and volcanism of Sierra Chichinautzin: extension and the front of the Central Trans-Mexican Volcanic Belt. Journal of Volcanology and Geothermal Research. 93, 125-150.

Marquez, A., Oyarzum, R., Doblas, M., and Verma, S.P., 1999. Alkalic (ocean-island basalt type) and calc-alkalic volcanism in the Mexican volcanic belt: A case for plume-relater magmatism and propagation rifting in an active margin? Reply: Geology. 27, 51-53.

Marquez, A., Oyarzun, R., de Ignacio, C., and Doblas, M., 2001. Southward migration of volcanic activity in the central Mexican Volcanic Belt: asymmetric extension within a two-layer crustal streching model. Journal of Volcanology and Geothermal Research. 112, 175-187.

Matthews, A., and Barclay, J., 2004. A thermodynamical model for rainfall-triggered volcanic collapses. Geophysical Research Letters. 31, 1-4.

Matthews , S.J., Gardeweg, M.C., and Sparks, R.S.L., 1997. The 1984 to 1996 cyclic activity of Lascar volcano, northern Chile: cycles of dome growth, dome subsidence, degassing and explosive eruptions. Bulletin of Volcanology. 59, 72-82.

McConnell, S., 2004. An analytical approach to the interpretation of complex dome Formation: Cerro Pizarro, Mexico [MS. Thesis]. Northern Arizona University, 226.

Miller, D.C., 1985. Holocene eruptions at the Inyo volcanic chain, California; implications for possible eruptions in Long Valley Caldera. Geology (Boulder). 13, 14-17.

Miller, D.C., and Hoblitt, R.P., 1980. Stratigraphy and deposits produced by the May 18th, 1980 , lateral blast at Mount St. Helens, Washington. EOS. 61, 1135.

Metz, J.M., and Bailey, R.A., 1993. Geologic map of Glass Mountain. USGS Miscellaneous Investigation series map I-1995. 1:24,000.

Morrissey, M.M., Zimanowski, B., Wholetz, K., and Buettner, R., 2000. Phreatomagmatic fragmentation. In: Encyclopedia of Volcanoes, Sigurdsson, H., Houghton, B.F., McNutt, S.R., Rymer, H., and Stix, J. (Eds.). Academic Press, San Diego, CA, 463-475.

Nakada, S., Miyake, Y., Sato, H., Oshima, O., and Fujinawa, A., 1995. Endogenous growth of dacite dome at Unzen Volcano (Japan), 1993-1994. Geology. 23, 157-160.

Newhall, C.G., and Melson, W.G., 1983. Explosive activity associated with the growth of volcanic domes; Explosive volcanism. Journal of Volcanology and Geothermal Research. 17, 111-131.

Riggs, N.R., and Carrasco-Nuñez, G., 2004. Evolution of a complex isolated dome, Cerro Pizarro, east Mexico. Bulletin of Volcanology. 66, 322-335.

Rose, W.I., Jr. Pearson, T., and Bonis, S., 1977. Nu'ee ardente eruption from the foot of a dacite lava flow, Santiaguito volcano, Guatemala. Bulletin of Volcanology. 40, 23-38.

Sampson, D.E., and Cameron, K.L., 1987. The geochemistry of the Inyo volcanic chain; Multiple magma systems in the Long Valley region, eastern California. Journal of Geophysical Research. 92, 403-410.

Schroeder, T., 1996. Physical volcanology of the Enebro Mountain Rhyolite. [MS. Thesis]. Northern Arizona University, 226.

Scott, W.E., 1987. Holocene rhyodacite eruptions on the flanks of South Sister Volcano, Oregon. In: The emplacement of silicic domes and lava flows. Geological Society of America Special Paper. 212, 35-53.

Sheridan, M.F., and Wohletz, K.H., 1983. Hydrovolcanic explosions: the systematics of water-pyroclast equilibration. Science. 212, 1387-1389.

Sigurdsson, H., 2000. Introduction. In: Encyclopedia of Volcanoes, Sigurdsson, H., Houghton, B.F., McNutt, S.R., Rymer, H., and Stix, J. (Eds.). Academic Press, San Diego, CA, 1-13.

Siebe, C., Macias, J.L., Abrams, M., Rodriguez, S., Castro, R., and Delgado, H., 1995. Quaternary explosive volcanism and pyroclastic deposits in east central Mexico: implications for future hazards. Geological Society of America Field Guide. 47.

Siebe, C., Rodriguez-Lara, V., Schaaf, P., and Abrams, M., 2004, Geochemistry, Sr-Nd isotope composition and tectonic setting of Holocene Pelado, Guespalapa and Chichinautzin scoria cones, south of Mexico City. Journal of Volcanology and Geothermal Research. 130, 197-226.

Siebe, C., and Verma, S.P., 1988. Major element geochemistry and tectonic setting of Las Derrumbadas rhyolitic dome, Puebla, Mexico. Chemie Der Erde. 48, 177-189.

Siebert, L., 1984. Large volcanic debris avalanches; characteristics of source areas, deposits, and associated eruptions. Journal of Volcanology and Geothermal Research. 22, 163-197.

Siebert, L. and Carrasco-Nunez, G, 2002. Late-Pleistocene to precolumbian behind-the-arc mafic volcanism in the eastern Mexican Volcanic Belt; implications for future hazards. Journal of Volcanology and Geothermal research. 115, 179-205.

Sparks, R.S.J., 1997. Causes and consequences of pressurization in lava dome eruptions. Earth and Planetary Science Letters. 150, 177-189.

Sparks, R.S.J., 2003. Dynamics of magma degassing. Geological Society Special Publications. 213, 5-22.

Sun, S., and McDonough, W.F., 1989. Chemical and isotopic systematics of ocean basalt: Implications for mantle composition and processes. In: Saunders, A.D., and Norry M.J., (Eds.). Magmatism in Ocean Basins. Geological Society of London Special Publication. 42, 313-345.

Swanson, S.E., Naney, M.T., Westrich, H.R., and Eichelberger, J.C., 1989. Crystallization history of Obsidian Dome, Inyo Domes, California. Bulletin of Volcanology. 51, 161-176.

Taylor, G.A.M., 1958. The 1951 eruption of Mount Lamington Papau. In: Geophysical Bulletin. Canberra, Australia. 117.

Valentine, G.A., 1987. Stratified flow in pyroclastic surges. Bulletin of Volcanology. 49, 616-630.

Valentine, G.A., and Fisher, R.V., 2000. Pyroclastic surges and blasts. In: Encyclopedia of Volcanoes, Sigurdsson, H., Houghton, B.F., McNutt, S.R., Rymer, H., and Stix, J. (Eds.). Academic Press, San Diego, CA, 571-580.

Verma, S.P., 1999. Geochemistry of evolved magmas and their relationship to subduction-unrelated mafic volcanism at the volcanic front of the central Mexican Volcanic Belt. Journal of Volcanology and Geothermal Research. 93, 151-171.

Vespermann, D. and Schmincke, H., 2000. Scoria cones and tuff rings. In: Encyclopedia Of Volcanoes, Sigurdsson, H., Houghton, B.F., McNutt, S.R., Rymer, H., and Stix, J. (Eds.). Academic Press, San Diego, CA, 683-694.

Vogel, T.A., Younker, L.W., Schuraytz, B.C., 1987. Constraints on magma ascent, emplacement, and eruption: geochemical and mineralogical data from drill-core samples at Obsidian dome, Inyo chain, California. Geology. 15, 405-408.

Wallace, P.J., and Anderson, A.T., 2000. Volatiles in magmas. In: Encyclopedia of Volcanoes, Sigurdsson, H., Houghton, B.F., McNutt, S.R., Rymer, H., and Stix, J. (Eds.). Academic Press, San Diego, CA, 149-170.

Wallace, P.J. and Carmichael, I.S.E., 1999. Quaternary volcanism near the Valley of Mexico: Implications for subduction zone magmatism and the effects of crustal thickness variations on primitive magma compositions. Contributions to Minerology and Petrology. 135, 291-314.

Westrich, H.R., Stockman, H.W., and Eichelberger, J.C., 1988. Degassing of rhyolitic magma during ascent and emplacement. Journal of Geophysical Research. 93, 6503-6511.

White, J.D.L. and Houghton, B.F., 2000. Surtseyan and related phreatomagmatic eruptions In: Encyclopedia of Volcanoes, Sigurdsson, H., Houghton, B.F., McNutt, S.R., Rymer, H., and Stix, J. (Eds.). Academic Press, San Diego, CA., 495-511.

Wilson, C.J.N., and Hildreth, W.H., 1998. Hybrid fall deposits in the Bishop Tuff, California; a novel pyroclastic depositional mechanism. Geology. 26, 7-10.

Wilson, C.J.N. and Houghton, B.F., 2000. Pyroclastic transport and deposition. In: Encyclopedia of Volcanoes, Sigurdsson, H., Houghton, B.F., McNutt, S.R., Rymer, H., and Stix, J. (Eds.). Academic Press, San Diego, CA, 545-554.

Wilson, C.J.N. and Walker, G.P.L., 1982. Ignimbrite depositional facies; the anatomy of a *pyroclastic* flow. Journal of the Geological Society of London. 136, 581-592.

Winter, J.D., 2001. An Introduction to Igneous and Metamorphic Petrology. Prentice Hall, Upper Saddle River, NJ. 697.

Wohletz, K.H. and Sheridan, M.F., 1979. A model of pyroclastic surge. Special Paper – Geological Society of America. 180, 177-194.

Yamasato, H., Kitagawa, S., and Komiya, M., 1998. Effect of rainfall on dacite lava dome collapse at Unzen volcano, Japan. Papers in Meteorology and Geophysics. 48, 73-78.

Yanez-Garcia, C., and Garcia D, S., 1982. Exploration methods and their results in the Humeros de Caldera and Derrumbadas areas of northern Puebla, Mexico. International conference on geothermal energy, Florence, Italy.

APPENDIX A

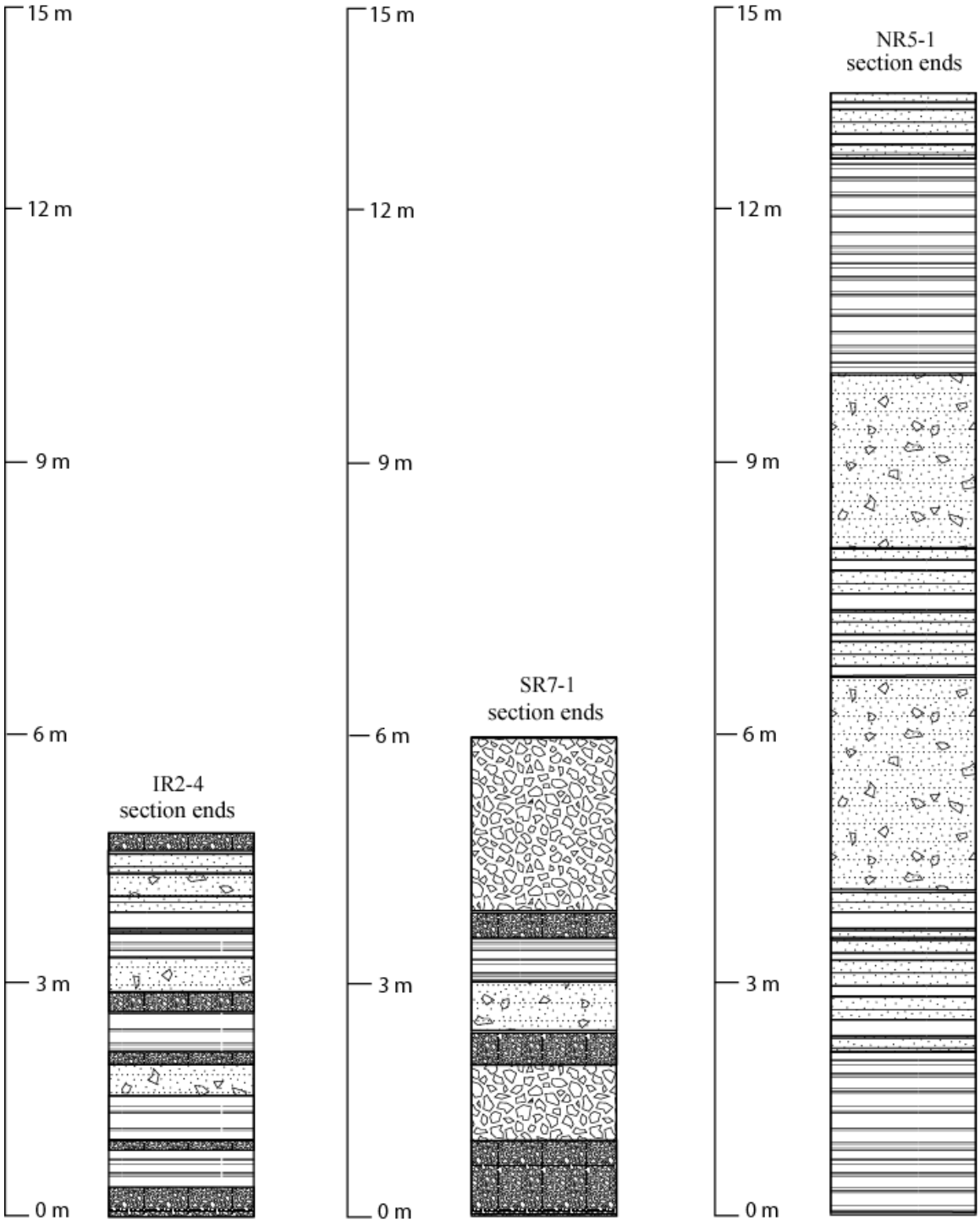
15 m
12 m
9 m
6 m
3 m
0 m
IR2-4
section ends
SR7-1
section ends
NR5-1
section ends

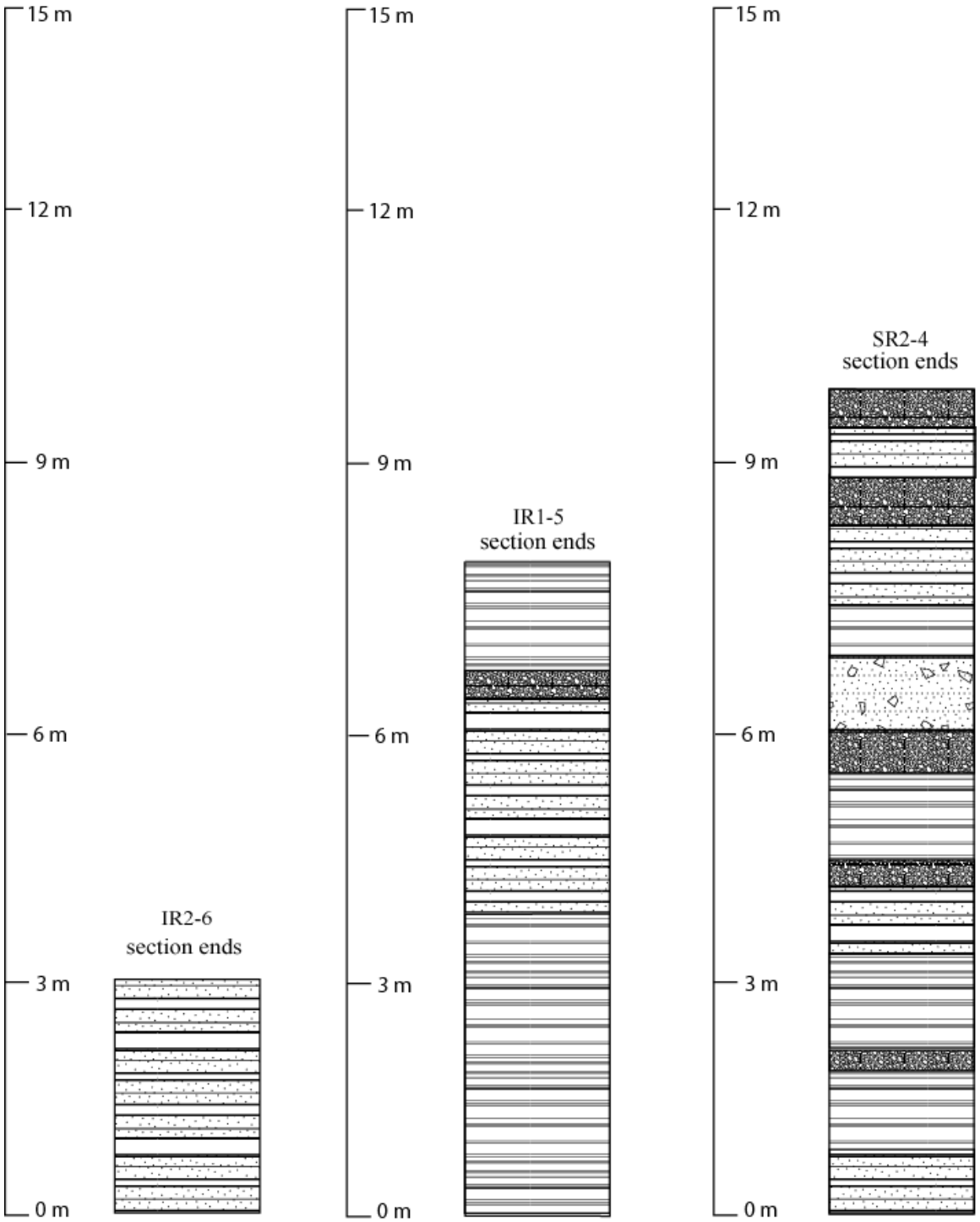
15 m
12 m
9 m
6 m
3 m
0 m
IR2-6
section ends
IR1-5
section ends
SR2-4
section ends

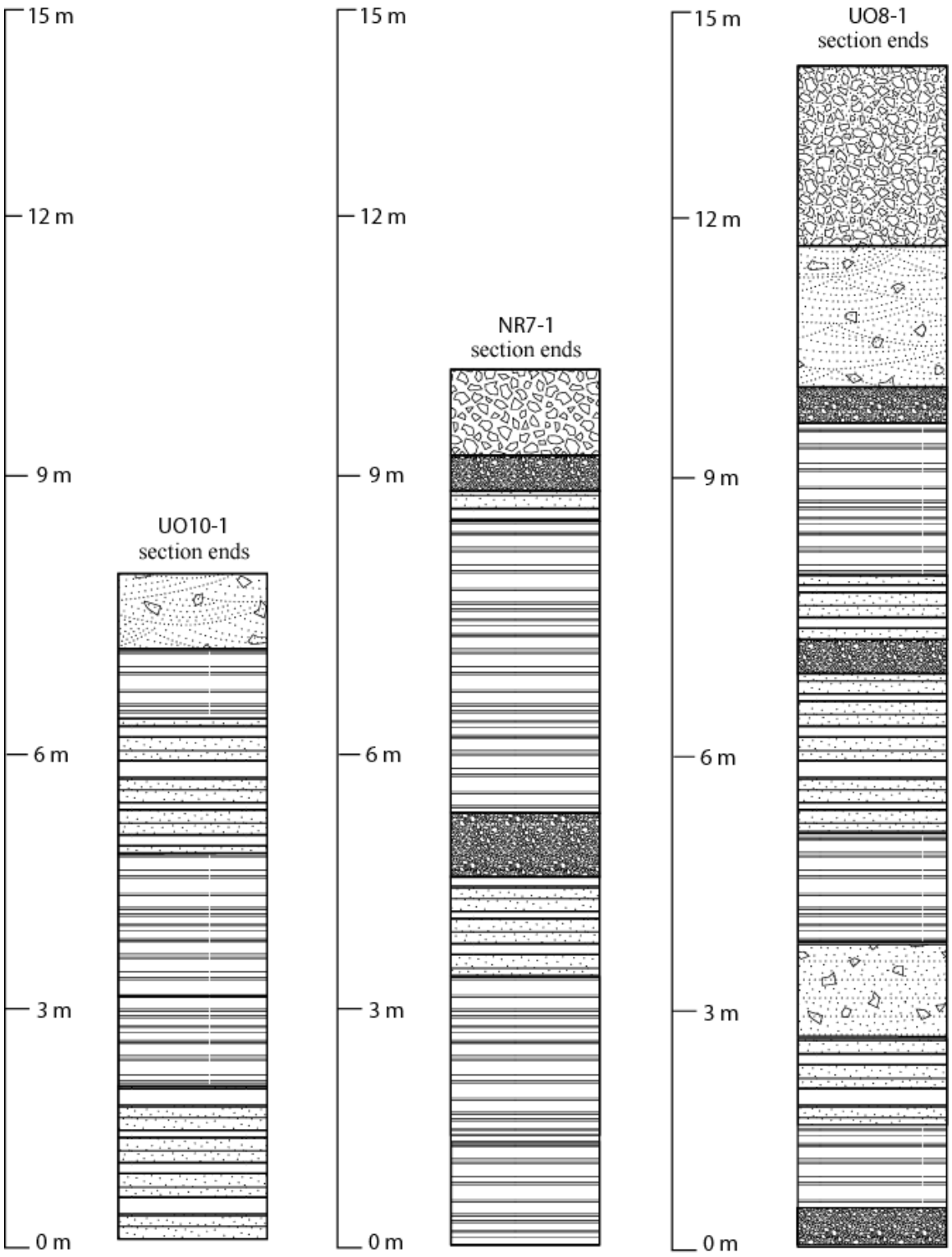
15 m
12 m
9 m
6 m
3 m
0 m
UO10-1
section ends
15 m
12 m
9 m
6 m
3 m
0 m
NR7-1
section ends
15 m
12 m
9 m
6 m
3 m
0 m
UO8-1
section ends

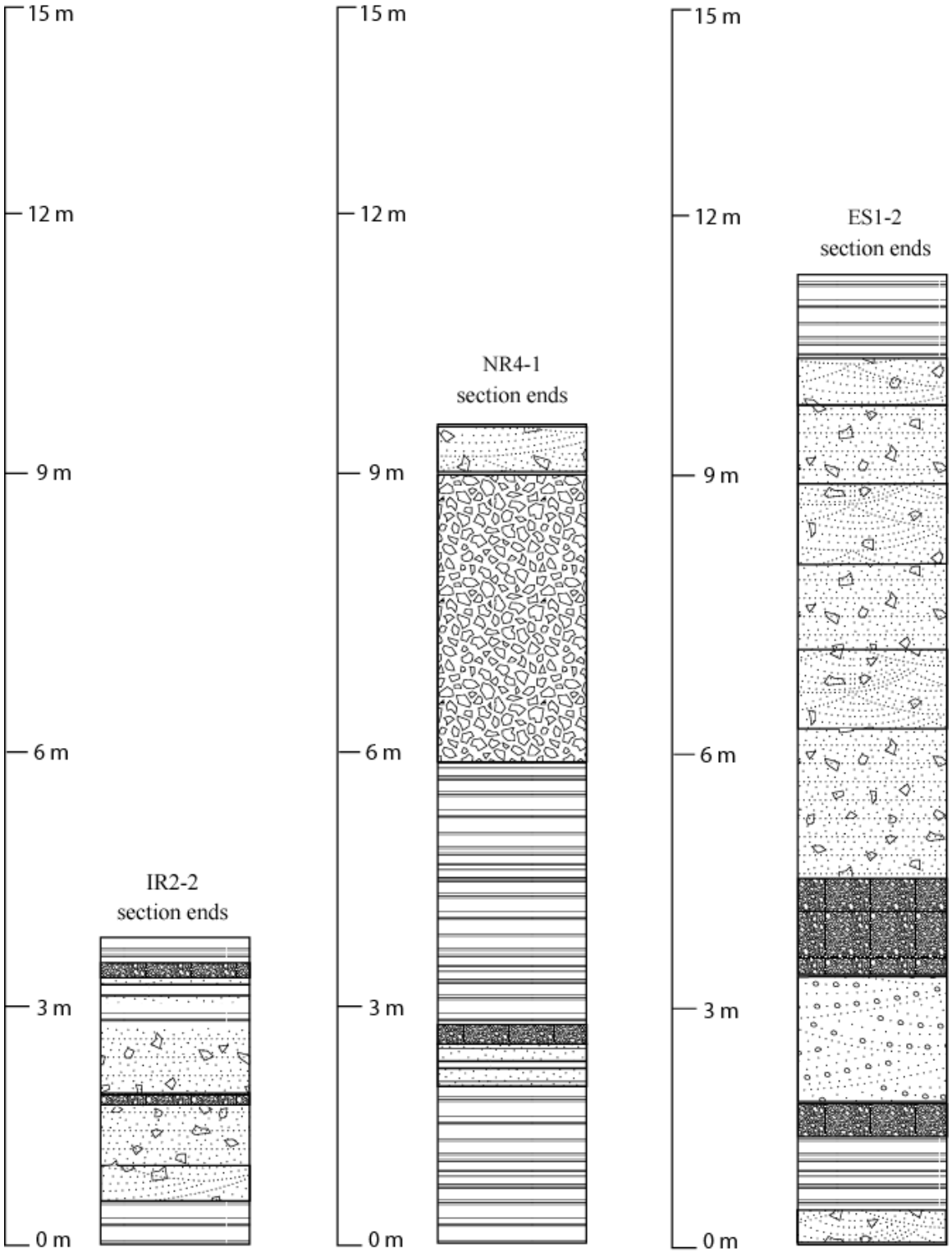
15 m
12 m
9 m
6 m
3 m
0 m
IR2-2
section ends
NR4-1
section ends
ES1-2
section ends

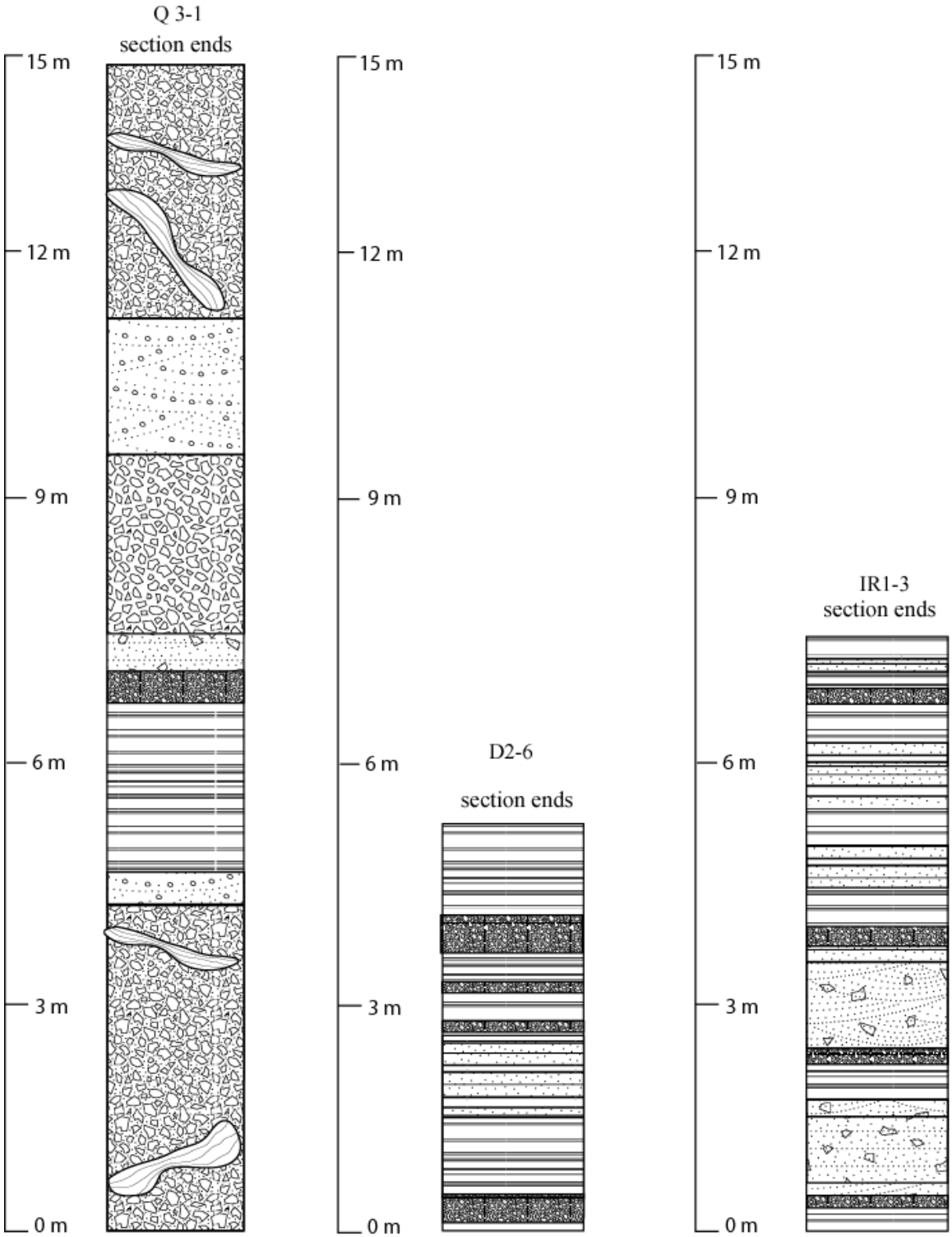
Q 3-1
section ends
15 m
12 m
9 m
6 m
3 m
0 m
D2-6
section ends
IR1-3
section ends